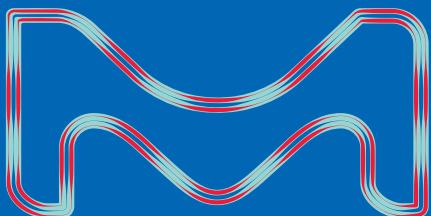


3D BIOPRINTING:

Printing a Brighter Future

- Bioink Selection
- Bioprinting of Tissue Models
- Incorporating Vascularization
- Bioprinting Protocols

Featuring contributions from
Profs. Yu Shrike Zhang, Shaochen Chen,
Yunzhi Peter Yang, and Khoon S. Lim



Preface



Megan Muroski, Ph.D
Senior Product
Manager, Energy and
3D Bioprinting

Introduction

3D bioprinting is an increasingly widespread technology with promising applications in disease modeling, drug discovery, and regenerative medicine. Successful technology bridges expertise in materials science, engineering, and cell biology, making 3D bioprinting a well-suited technology for applications in pre-clinical testing and wider disease research (Figure 1).

3D Bioprinting enables the creation of functional tissue based on additive manufacturing with improved physiological relevance, in both pre-clinical and clinical applications. In pre-clinical applications, 3D bioprinting can be used for *in-vitro* models and drug discovery, while clinical applications focus on tissue regeneration and functional organ replacement. 3D bioprinting has the potential to improve the reliability and predictive power of pre-clinical testing through the production of more realistic and reproducible *in vitro* models.

Current 2D model systems have recognized limitations, such as different genotypic and phenotypic cell responses, leading to low drug candidate predictability and pre-clinical cell-based assay results. In drug discovery and *in-vitro* testing, researchers are seeking new approaches to overcome some of the limitations of conventional cell culture. Many researchers believe that 3D bioprinting can combine the ease of use of existing cell culture methods with the physiological relevance of *in vivo* animal models and human clinical trials. 3D bioprinting can help to address some of the limitations of 3D cell culture by providing a scalable, and highly reproducible method to form complex 3D structures that can be automated.

3D bioprinting offers the potential of improved tools for disease research overcoming the current shortcomings in disease models, regenerative medicine, and drug discovery. However, in the development of new 3D bioprinting applications, three main elements must be considered: the bioink, printing method, and application.

Extrusion-based bioprinting

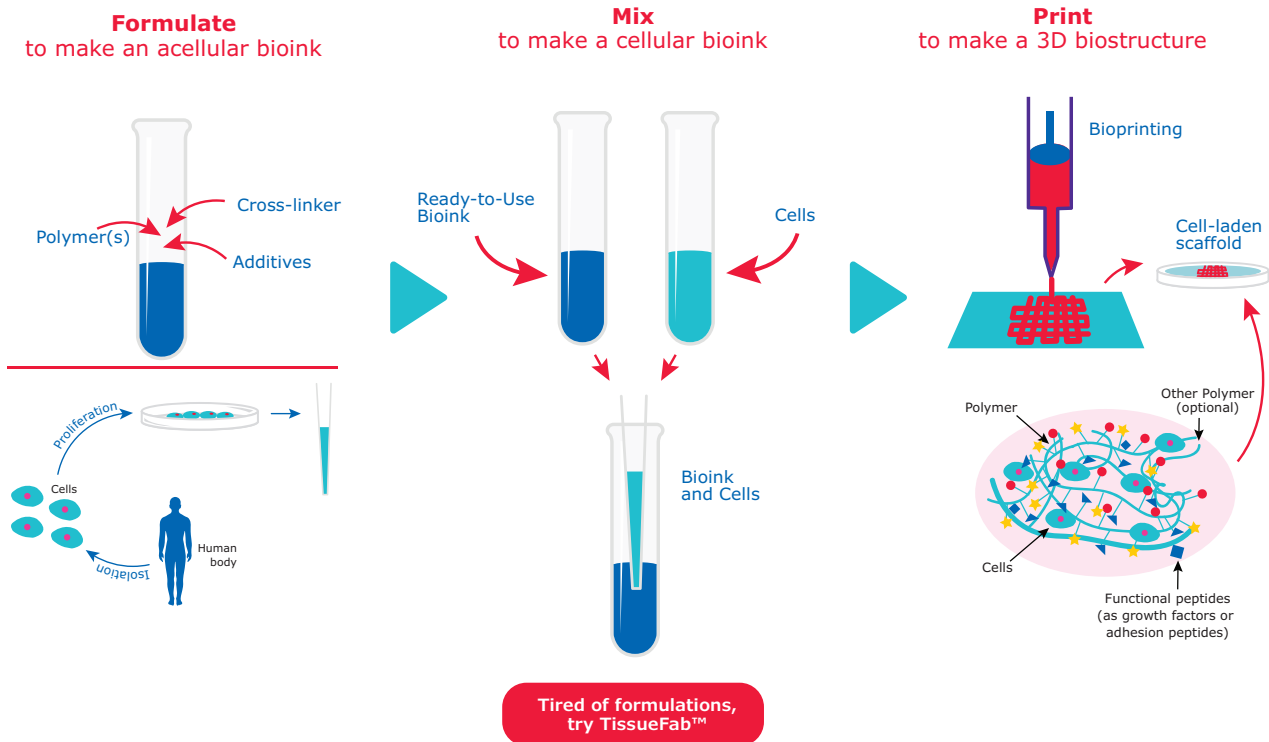
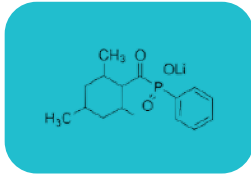
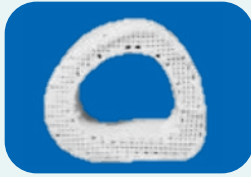




Figure 1. 3D bioprinting is an additive manufacturing process that uses cells and biomaterials to print an object layer by layer. The steps to create a 3D bioprinted structure include formulation, mixing, and printing. In formulation, polymers, cross-linkers, and additives are mixed in a matrix to form an acellular bioink. Cells are simultaneously cultured or isolated and prepared in a solution. Next, the formulated acellular bioink precursor must be mixed with cells for printing. Common techniques include using a Luer-lock coupler, a static mixer, or dish mixing. Creating the 3D structure by bioprinting is next. The bioprinter prints the mixture via syringe while following a 3D computer-generated model. After the print is complete, the structure is cured to prevent dissolution when cell culture media is added. The 3D structure now contains a scaffold and cells, which will grow to fill the 3D printed matrix. Culture media and additives are required to optimize and enhance cellular expansion.

Table 1. Types of polymers used in bioinks.

Type of Material	Examples
 <p>Initiators & Additives</p>	<p>Rapid curing, water soluble hydrogel photoinitiators for visible light polymerization</p> <ul style="list-style-type: none"> • TPO Nanoparticle • LAPw <p>Traditional photoinitiators</p> <ul style="list-style-type: none"> • Irgacure 2959
 <p>Thermally processable polymers</p>	<p>Mimics bone or stiff tissues</p> <p>Low melting point</p> <p>Biodegradable</p> <ul style="list-style-type: none"> • Polycaprolactone • Polylactide
 <p>Synthetic Polymers</p>	<p>Includes reactive end groups for hydrogel network formation and/or functionalization</p> <ul style="list-style-type: none"> • Poly(ethylene glycol) • peptides • PEG-diacrylate <p>Reversible gelation</p> <ul style="list-style-type: none"> • Pluronic® F-127
 <p>Natural polymers</p>	<p>Mimics extracellular matrix components</p> <p>Encourages cell adhesion, growth, proliferation</p> <p>Examples:</p> <ul style="list-style-type: none"> • Sodium Alginate • Low Endotoxin Gelatin • Collagen • Natural Polymer derivatives, e.g. GelMA, HAMA, AlgMA

While the application dictates the choice of cells used, the printing method should be selected based on the mechanical and physical requirements, such as shear rate, model complexity, and size. Furthermore, the biomaterial ink must have compatibility with the cell and properties type to ensure proper printing in the chosen printer system. In addition, the ink should allow maturation or differentiation of the type of cells used within the construct and be complementary with the downstream analysis.

Bioink

A bioink is a material that acts as a microenvironment for living cells. These materials can contain a variety of polymers, biomaterials, extracellular matrix components, and living cells, see **Table 1** for the type of polymers used in bioinks. The composition of biomaterial inks can vary in complexity, ranging from single to multi-component mixtures, and offers varying levels of modification and crosslinking. Furthermore, biomaterial components can come from various sources, either synthetic or natural origins, and are further modified to introduce cross-linking or functionalization sites.

Polymers provide the acellular material in 3D bioprinting that forms a scaffold and supports cellular growth. Researchers have used many different polymers to find the best approach. However, polymers alone cannot provide the physical and biochemical requirements of cell growth without modification or formulation with other materials. The most widely used biomaterials in 3D Bioprinting include gelatin, alginate, collagen, and hyaluronic acid. Alginate, the most popular material used, derived from brown algae, is biocompatible and provides mild crosslinking conditions. Disadvantages of this material include slow degradation kinetics and poor cell adhesion. Gelatin and collagen, require chemical modification for crosslinking making high-resolution printing and high fidelity printing challenging, however, these materials have shown high biological relevance (bone, skin) and are also popular choices in bioink creation. Hyaluronic acid has biological relevance in connective, epithelial, and neural tissues, but suffers from poor stability.

Even with the many tools and customized polymers now available, it can still be difficult to make an effective bioink. A good bioink formulation must balance material properties, printability, biocompatibility, and biochemical cues. On one hand, a bioink material must be sufficiently viscous for printing, but once printed, have the mechanical strength and structural integrity to maintain its shape. The printed structure must have both high water content and porosity to enable cells to receive nutrients and oxygen and remove waste and should be soft and biodegradable to allow the cells to spread, migrate, proliferate, and interact with each other.

In addition to biocompatibility, physical considerations, such as viscosity, surface tension, temperature sensitivity must also be considered. Currently, there is a need for high-quality, commercially available ready-to-use bioink formulations, such as our R&D created **TissueFab® bioinks**, to enable reproducible fabrication of synthetic tissues and organs by 3D Bioprinting.

Printing

There is a wide variety of printing techniques including micro-extrusion, SLA/DLP, LIFT, inkjet, acoustic, magnetic, and volumetric technologies; and of these methods, the most popular being extrusion-based and inkjet printing. Extrusion bioprinting, in which printing speed and structures can be highly controlled, but shear stress can impact cell viability. Inkjet-based printing is well known for fast printing speed, biological compatibility, and low cost, however, requires low viscosity materials.

Each method has specific capabilities making them straightforward for a given application while demanding careful selection of material properties from the bioink used. To this end, optimizing the various material and system properties at an early stage will result in robust and reliable methods for generating tissue and disease constructs.

In addition to the type of printing, the technology can be sorted into two categories: acellular and cellular constructs. In acellular bioprinting, the scaffold and biomaterial itself are made in the absence of cells during the printing process. The advantages of this technique offer higher accuracy and greater shape complexity, as the printing criteria can be more rigorous as cell health does not have to be considered. In cellular bioprinting, the scaffold and manufacturing are completed in the presence of cells and other biological agents to mimic living tissue constructs. Careful consideration must be taken into account as cells and

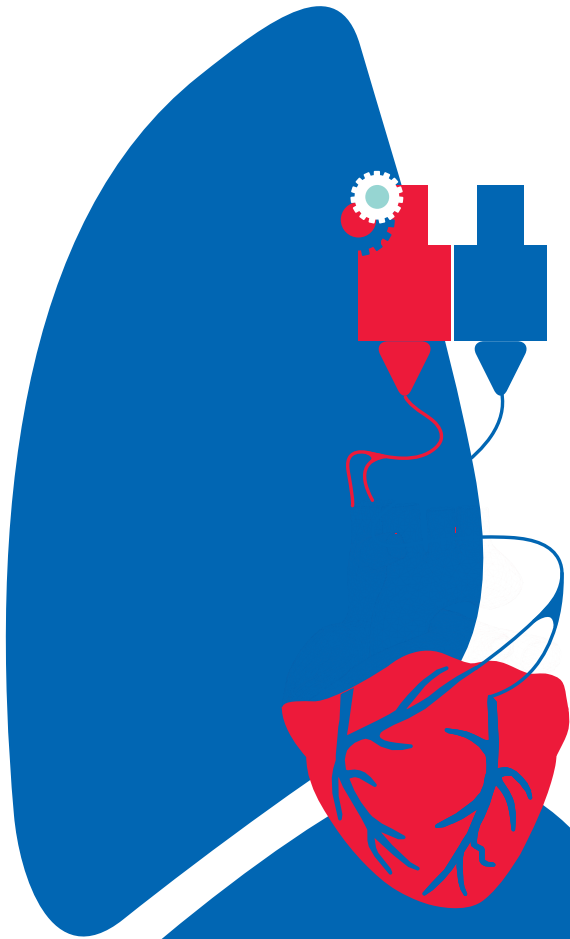
other biological entities can be sensitive to additive manufacturing techniques. Both methods offer unique advantages, and the printing parameters, biomaterials, and properties of the 3D-printed constructs will depend on the presence or absence of cells and biological substances.

Applications

3D bioprinting has the potential to improve the reliability and predictive power of pre-clinical testing through the production of more realistic and reproducible *in vitro* models. 3D bioprinting can offer reproducible fabrication of 3D cell-laden constructs to better mimic conditions *in vivo*, reducing the need for poorly predictive 2D models whether in drug discovery, *in-vitro* disease models, or regenerative medicine. Vascularization offers significant improvements in our ability to model tissues and disease states while at the same time increasing our understanding of critical disease pathologies and pathways. Understanding blood vessel formation and function will develop the field of 3D bioprinting into pre-clinical testing, broader disease research and precision medicine approaches.

Final Thoughts

3D Bioprinting is a powerful tool which is enabling the fabrication of complex tissue and structures for regenerative medicine and drug discovery. 3D Bioprinting technology is still in its early stage and several challenges remain to be addressed to move the field forward. Current approaches have had limited success for the development of the physical and functional components required for tissue regeneration due to their inherent complexity in biological, physical, chemical, mechanical attributes. Newly engineered bioink materials and compatible bioprinting applications on the horizon may provide improvements in these challenging areas. Future endeavors in this space will no doubt increase our ability to model tissues and disease states in addition to expanding our understanding of disease pathologies and offering insight into potentially druggable pathways.



About this Guide

In this guide, we explore 3D bioprinting and its great potential to improve drug discovery efforts and for implementation at various stages of the drug development pipeline. We have reviews by leading researchers along with protocols designed by leading R&D experts in Bioprinting.

The guide has been developed for both novice and experienced researchers interested in 3D Bioprinting. Our review articles discuss bioprinting and current strategies in tissue modeling and vascularization. As demonstrated in the reviews, biomaterial and bioprinting options are numerous; however, once a bioprinting application is fully established, it offers excellent reproducibility thanks to the automated aspects of the setup. To help get you started, we offer protocols covering the reconstitution of lyophilized inks, cell mixing, crosslinking, and bioprinting protocols. Furthermore, our product guide covers our ready-to-use, R&D-created, **TissueFab® bioinks** as well as popular precursors for advanced users. We hope that this publication will enable biologists, chemists, translational researchers, pharma scientists, to explore the ever-expanding research field of 3D Bioprinting.

Table of Contents

Articles

Design of Bioinks for Bioprinting Xiao Kuang, Guosheng Tang, Zeyu Luo, Yu Shrike Zhang	5
3D Bioprinting of Functional Tissue Models Min Tang, Shangting You, Jennifer Sun, Wei Zhu, Shaochen Chen	20
Hybrid printing for Engineering Vascularized Tissue Constructs Jiannan Li, Sungwoo Kim, Carolyn Kim, Yunzhi Peter Yang	26
Recent Advances in 3D Biofabrication of Blood Vessels Alessia Longoni, Tim BF Woodfield, Jelena Rnjak-Kovacina, Khoon S Lim	30

Protocols

Bioprinting Protocol with Ready-to-use TissueFab® Bioinks	36
Bioink Preparation	38
PhotoCol Methacrylated Collagen Bioink	
PhotoHA Methacrylated Hyaluronic Acid Bioink	
Lifeink® Type I Collagen Bioink	
Lifesupport™ Support Slurry	
Decellularized ECM Bioink Precursor	
INVIVO-Gel	
Cell-bioink Mixing Protocol	51
General Guide to Photo, Ionic, and Enzymatic Crosslinking	53

Products

Natural Polymers Cellulose, Chitosans, Ligans, and Hyaluronic Acids	56
Bioinks TissueFab®, GelMA, Modified Gelatins, Alginate-based Bioinks, Decellularized Bioinks, Collagen Bioinks, HA Bioinks, Ready-made Bioinks, Biodegradable Polymers, PEG and PEO	58
Bioprinting Consumables	61

we hear you

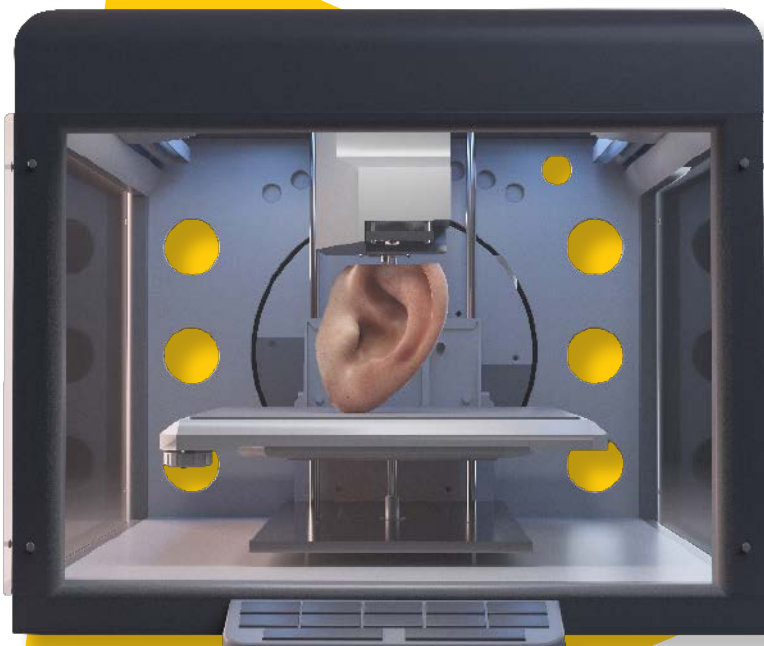
We now offer a line of low endotoxin, high-quality ready-to-print bioinks and bioink precursors.

Cut out your design time with our ready-to-print bioinks for extrusion-based bioprinting with products like:

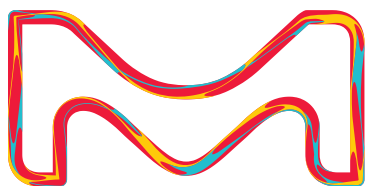
Cat. No.	Product Description
918741	TissueFab® - GelMA-Vis-LAP bioink
919926	TissueFab® - crosslinking solution

We also offer bioink precursors to create your own formulations, such as:

Cat. No.	Product Description
919373	Low endotoxin alginate
918628	Low endotoxin GelMA
918644	Low gelatin solution



To find the optimal bioinks and bioink precursors, please visit SigmaAldrich.com/bioink-selector



The life science business of Merck operates as MilliporeSigma in the U.S. and Canada.

Sigma-Aldrich®
Lab & Production Materials

Design of Bioinks for Bioprinting



Xiao Kuang, Guosheng Tang, Zeyu Luo, and Yu Shrike Zhang*

Division of Engineering in Medicine, Brigham and Women's Hospital, Department of Medicine, Harvard Medical School, Cambridge, MA 02139, United States of America

*E-mail: yszhang@research.bwh.harvard.edu

Introduction

Bioprinting has emerged as a disruptive biofabrication method for producing three-dimensional (3D) tissue constructs.¹⁻² Bioprinting potentially enables the customization of fabricated constructs to match the unique anatomical structures of a patient, providing personalized 3D representations of tissue structures for applications in tissue engineering and regenerative medicine.³⁻⁵ The typical bioprinting process involves the automated deposition of bioinks into target geometries in a layer-by-layer manner, frequently followed by selective material-solidification (i.e., crosslinking). A major feature of the 3D bioprinting technology is the use of "bioinks" composed of living cells, extracellular matrix (ECM)-like support biomaterials, and/or other bioactive components to print 3D tissue constructs.⁶⁻⁷ A prerequisite of the bioinks is their compatibility for the survival of embedded cells. Biomaterial hydrogels with a high-water-content environment similar to the physical properties of the native ECM are extensively used for bioprinting. A variety of natural polymers, including protein-based materials (e.g., collagen, gelatin, fibrin, and silk fibroin), and polysaccharide-based materials (e.g., alginate, hyaluronic acid (HA)), as well as some biocompatible synthetic polymers (e.g., poly(ethylene glycol) (PEG)), have been used to formulate bioinks.^{3,8-10} The bioinks provide different rheological properties, crosslinking behaviors, and bioactivities to accommodate successful bioprinting.

Up to date, there are several main categories of 3D bioprinting techniques, i.e., extrusion-based bioprinting,¹¹⁻¹⁶ inkjet/droplet bioprinting,¹⁷⁻¹⁹ and vat polymerization-based bioprinting.²⁰⁻²² Extrusion-based bioprinting, continuously extruding bioinks from a dispensing nozzle, is one of the most versatile bioprinting techniques. Depending on bioink deposition features, this technique can be further divided into direct extrusion, extrusion with bath, and extrusion with microfluidics.^{13,15} Microfluidics-based micro-extrusion using co-axial nozzle systems is extensively used

for bioprinting of solid microfibrinous and tubular tissues.²³⁻²⁴ Inkjet bioprinting produces droplets from a low-viscosity cell-suspended liquid in a "drop-on-demand" manner to pattern biomaterial inks. Vat (photo)polymerization-based bioprinting refers to bioprinting techniques that use light energy dispersion to manipulate the solidification of photoactive bioinks. Each bioprinting technique requires specific physical and chemical bioink properties. The bioink formulation influences the viscosity, surface tension, and crosslinking capability, which together determine printability. For example, direct extrusion-based bioprinting usually requires high viscosity and shear thinning of bioinks to facilitate shape-fixing after material deposition. *In situ* crosslinking and extrusion in a support bath allow for printing using low-viscosity bioinks.²⁵⁻²⁶ Inkjet-based bioprinting is limited to low-viscosity bioinks. By contrast, vat polymerization-based bioprinting requires use of photocurable bioinks.²¹⁻²² More recently, volumetric bioprinting, a subgroup of vat polymerization-based bioprinting, enables layerless, ultra-fast biofabrication.²⁷⁻²⁹ Besides, other bioprinting techniques, such as acoustic bioprinting³⁰ and spheroid fusion-based bioprinting,³¹ have emerged as parallel innovation tracks of both bioprinting techniques and bioink design.

The design of customizable bioinks with proper printability (viscosity and crosslinking) and cell viability is central to bioprinting method selection and achieving optimal final tissue construct properties.³²⁻³⁴ This article presents an overview of crosslinking strategies and covers the modification of common biomaterials for the design of bioinks. The advantages and limitations of widely used biomaterials are compared. In addition, bioink function improvement in terms of printability, bioactivity, and physical properties, is summarized. This review provides guidance on the bioink design for various bioprinting and biomedical applications.



Overview of Bioink Crosslinking

During most 3D bioprinting procedures, aqueous bioinks containing living cells and ECM-like support biomaterials are patterned into target shapes and transformed into solid network structures via crosslinking. The crosslinking process plays a critical role in bioprinting, influencing printing fidelity, mechanical and physicochemical properties of the bioprinted tissue constructs, and cellular behavior after printing.³⁵⁻³⁷ There are several general principles in the design of crosslinking bioinks to consider for bioprinting: *i*) biocompatible reagents and end-products for the cells, and *ii*) suitable crosslinking kinetics under physiological conditions (aqueous medium at neutral pH). Depending on the nature of crosslinking, both covalent and noncovalent bonding can be used to form a chemical and physical network in bioinks, respectively. Although some crosslinking processes are not conducted under physiological conditions, they can still be utilized in bioprinting with optimized reaction conditions to minimize the side effects on the cells. In this section, we summarize the primary crosslinking approaches used in bioprinting (Figure 1).

Physical Crosslinking

Physical crosslinking takes advantage of weak but collective intermolecular interactions, such as electrostatic interactions, hydrogen bonding, hydrophobic interaction, and host-guest interaction, to form a physical network (Table 1). The electrostatic interaction between carboxylic acid in polysaccharides, such

alginate,³⁸⁻⁴¹ gellan gum,⁴²⁻⁴³ and divalent cations (e.g., Ca^{2+} , Mg^{2+} , Ba^{2+}) are extensively used in bioprinting due to their fast curing and good biocompatibility. Besides this, electrostatic interaction between oppositely charged polymer chains, such as blends of gelatin-hyaluronate,⁴⁴ chitosan-alginate,⁴⁵ and gelatin-chitosan,⁴⁶ also enables hydrogel-gelation. Hydrogen bonding is a strong intermolecular interaction between hydrogen atoms (in amide and hydroxyl) and electronegative atoms (such as oxygen and nitrogen). The binding energy of multiple hydrogen bonds can be even stronger, which can induce polymer gelation. For example, gelatin and agarose chains can self-assemble upon cooling by forming helix complexes via collective hydrogen bonds.⁴⁷⁻⁴⁹ Hydrophobic interactions, together with hydrogen bonds, contribute to β -sheet folding of silk fibroin for gelation.⁵⁰⁻⁵¹ The charge screening of collagen upon pH change can also lead to hydrogel-gelation.⁵²⁻⁵³ In addition, host-guest interactions also help to form physically crosslinked dynamic biomaterial hydrogel.⁵⁴ Physical crosslinking is usually used to impart shearing thinning or assist shape-fixing in extrusion-based bioprinting.⁵⁵⁻⁵⁶ It is noted that physical crosslinking can also be sensitive to the physiological environment and pH levels.

Chemical Crosslinking

Chemical crosslinking is extensively used to improve the dimension stability and mechanical properties of hydrogels. Chemical crosslinking occurs within functional groups in either

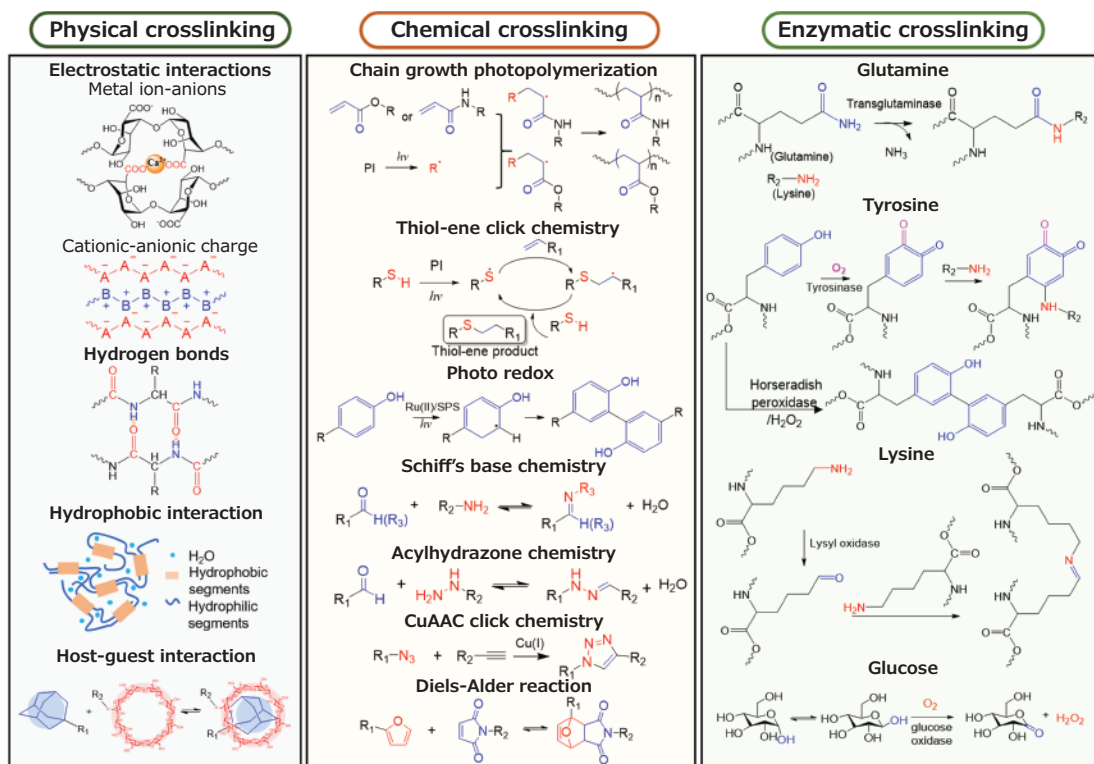


Figure 1. Three crosslinking methods and typical examples with involved interactions and reactions for bioink crosslinking. Physical crosslinking relies on intermolecular interactions, including electrostatic interactions, hydrogen bonds, hydrophobic interactions, and Host-guest interactions. Popular chemical crosslinking includes chain-growth photopolymerization of methacrylates, and step-growth polymerization using thiol-ene chemistry, photo redox, Schiff's base chemistry, acylhydrazone, CuAAC click chemistry, and Diels-Alder reaction. Enzymatic crosslinking of glutamine, tyrosine, lysine amino residues, and glucose oxidation under relevant enzymes.

Table 1. Three major crosslinking methods for common biomaterial hydrogels.

Crosslinking methods	Specific mechanism	Active species	Bioink examples	Notes	References
Physical crosslinking	Electrostatic interaction	Carboxylate/multivalent cations	Alginate, Gellan gum, Agarose	Fast (+)	38,43
				pH-sensitive (-)	
		Anionic-cationic moiety	Gelatin/hyaluronate, Chitosan/alginate, Gelatin/chitosan	Fast (+)	44–46
				pH-sensitive (-)	
	Weak (-)				
	Hydrogen bonds	Oxygen/hydrogen atoms	Gelatin Agarose	Tunable binding energy (+)	48–49
Hydrophobic interaction	β -sheet-folding	Silk fibroin	Weak (-)	50–51	
			Polymer-dependent (-)		
Charge screening	Amine	Collagen	Fast (+)	52–53	
			pH-sensitive (-)		
Host-guest interaction	Cyclodextrin/adamantane	Cyclodextrin hyaluronate/adamantane hyaluronate	Additional synthesis (-)	54	
			Weak (-)		
Chemical crosslinking	Radical photocrosslinking	(Meth)acrylates, (meth)acrylamides	Gelatin methacryloyl	Fast (+)	58–59
				Free radical (-)	
	Thiol-ene chemistry	Thiol/vinyl	Gelatin–vinyl ester/thiol	Fast (+)	62–63
				Free radical(-)	
	Photoredox	Tyrosine, tyramine	Silk fibroin	Fast (+)	64–67
				Free radical (-)	
Schiff's base chemistry	Aldehyde/amine	Gelatin/oxidized dextran	Fast (+)	72	
			pH-sensitive (-)		
Acyldiazide chemistry	Aldehyde/hydrozide	Oxidized hyaluronate/dihydrozide	Fast (+)	73	
			pH-sensitive (-)		
CuAAC Click chemistry	Azide/alkyne	Azide-modified polymers	Efficient (+)	68–70	
			Toxic copper (-)		
Enzymatic crosslinking	Transglutaminase	Glutamine/lysine	Gelatin, Fibrinogen	Cell-benign (+)	76–77
				Soft (-)	
	Horseradish peroxidase	Tyrosine, Tyramine	Silk fibroin	Slow (-)	78–79
				Residual H ₂ O ₂ (-)	
	Lysyl oxidase	Glutamine	Elastin, Fibroin	Slow (-)	81–83
Noncommercial (-)					
Copper (-)					
Glucose oxidase	Heparin, Acrylates	Heparin-based hydrogels poly(ethylene glycol)-diacrylate	Slow (-)	84	

a step-growth or chain-growth manner, forming a covalent polymer network. The typical reactions used for chemical crosslinking of biomaterials are summarized in **Table 1**. Photo-triggered chemical crosslinking is the most popular method because it is contact-free, and provides spatiotemporal controlled, on-demand, rapid curing.²¹ For example, the fast chain-growth photopolymerization reaction of vinyl double bonds is the most widely used chemical crosslinking method, particularly in vat polymerization-based bioprinting techniques.⁵⁷ Synthetic and natural hydrogel precursors can be easily modified with (meth)

acrylates/(meth)acrylamides and formulated with water-soluble photoinitiators to make photocurable bioinks.^{58–59} A variety of water-soluble visible-light triggered photoinitiators, such as lithium-acyl phosphinate (LAP), 2,2'-azobis[2-methyl-N-(2-hydroxyethyl) propionamide] (VA-086), and eosin Y have been developed for bioprinting with enhanced cellular viability.^{21,60} In the chain-growth photopolymerization, vinyl double bonds on the hydrogel-precursors polymerize into carbon-carbon chains by free radicals, forming a heterogeneous network with defects such as dangling chain, loops, and different chain lengths.⁶¹ The

chain-growth crosslinking kinetics are complicated and influenced by reactive species diffusion and radical termination, such as oxygen-inhibition.

In contrast, the photochemistry of the thiol-ene reaction between the thiol and vinyl double bonds proceed in a step-growth manner, forming more uniform networks and showing less sensitivity to oxygen.⁶²⁻⁶³ Another increasingly popular visible light-based crosslinking is the photoredox of tyrosine via di-tyrosine bond-formation in the presence of ruthenium/sodium persulfate (Ru/SPS).⁶⁴ Since many natural proteins contain amino residues of tyrosine, this crosslinking strategy can proceed in the native form of a hydrogel-processor (such as silk fibroin) without post-modification.⁶⁵⁻⁶⁶ Meanwhile, hydrogel-precursors can be chemically grafted with the tyramine groups to facilitate di-tyrosine-formation.⁶⁷ Besides this, various other biorthogonal click chemistry, including azide-alkyne cycloadditions,⁶⁸⁻⁷⁰ Diels-Alder [4+2] cycloaddition,⁷¹ Schiff's base chemistry,⁷² and acylhydrazone chemistry⁷³ can also be exploited for biopolymer crosslinking.⁷⁴ However, most of these crosslinking approaches involve the post-modification of the hydrogel-precursors.

Enzymatic Crosslinking

Besides normal curing reactions using additional chemicals or crosslinkers, enzymes are also utilized to catalyze the crosslinking of protein-based bioinks at physiological conditions.⁷⁵ Transglutaminases can catalyze the formation of isopeptide bonds between lysine ϵ -amines and glutamine sidechain amides.⁷⁶⁻⁷⁷ This reaction has been used to effectively crosslink proteins bearing rich lysine and glutamine residues, such as fibrinogen and gelatin, to produce insoluble hydrogels.⁷⁵ Another widely used enzyme system is the hydrogen peroxidase (HRP) for hydrogel crosslinking via tyramine oxidative coupling in the presence of hydrogen peroxide (H_2O_2). Tyramine-rich hydrogel-precursors, including natural silk fibroin⁷⁸⁻⁷⁹ and tyramine-functionalized HA,⁸⁰ can be effectively crosslinked by this HRP/ H_2O_2 system. Lysyl oxidase, a critical enzyme for the formation and repair of the

native ECM, has also been used for enzymatic crosslinking of peptide-based hydrogels. The reaction mechanism reduces lysine sidechain residues to form aldehydes, followed by interpeptide crosslinking with lysine via Schiff's base reaction.⁸¹⁻⁸³ In addition, glucose oxidase has been used to crosslink PEG-diacrylate (PEGDA)-based hydrogels through enzyme-mediated radical polymerization, enabling acrylate-based hydrogel-formation at ambient temperature.⁸⁴

Biomaterials as Bioinks

Protein- and Peptide-based Bioinks

Collagen is the main structural protein in the ECM of the human body and is rich in connective tissues.⁸³ The most abundant collagen protein is collagen type I. Collagen possesses tissue-matching physicochemical properties and excellent *in vitro/in vivo* biocompatibility, and is widely used in biomedical applications.⁸⁵⁻⁸⁶ Collagen is soluble at low temperatures (2–8 °C) and acidic conditions and forms a fibrous gel by changing to neutral pH. Collagen can also self-assemble at 37 °C, enabling slow gelation.⁶ Due to these reasons, pure collagen is not directly used as bioinks. Instead, it is most often used as the cell support layer in bath-based bioprinting.⁵³ Properties of collagen bioinks can be tuned by simply blending with other biomaterials, such as alginate,⁸⁷ agarose,⁸⁸ and silk,⁸⁹ to enhance the printability. In addition, collagen can be chemically modified with photosensitive groups, such as methacryloyl, for light-based crosslinking.⁹⁰⁻⁹¹ For example, a multicomponent bioink containing methacryloyl-modified collagen and thiolated hyaluronic acid was developed to print tissue models to mimic the liver microenvironment.⁹⁰ In another study, methacryloyl-modified collagen was blended with alginate to bioprint a human corneal model.⁹¹ With the combined control over pH, temperature, collagen ratios, and precursor concentration, the gelation and printing fidelity of collagen and derivatives can be tuned to facilitate successful printing.⁹²⁻⁹⁴ Collagen and typical derivative-based bioinks for bioprinting are summarized in **Table 2**.

Table 2. Summary of natural and synthetic polymers and their derivatives for bioinks using different crosslinking methods.

Primary material	Bioink	Printing approach	Crosslinking method	Notes	References
Collagen	Col	Extrusion	Neutralize	pH change	53
	Col/Fib	Extrusion	Neutralize before print	Improved printability and cell-adherence	229
	Col-MA/Alg	Extrusion	Ionic crosslinking	Increased mechanic property	91
	Col-MA/HA	Extrusion	UV irradiation after bioprinting	Light curable	90
Gelatin	Gel/Alg	Extrusion	Ionic crosslinking + glutaraldehyde	Increased mechanical properties	230
	GelMA	Extrusion	Photocrosslinking	Improved printability and cell-adherence	12,101
		Vat-polymerization			
	D-GelMA	Vat-polymerization	Photocrosslinking	Improved printability and cell-adherence	231
	GelMA/Alg	Extrusion	Ionic crosslinking + photocrosslinking	Enhanced printability	199,232
	Gel-NB	Vat-polymerization	Photocrosslinking	Low swelling ratios	233
	GelMA-Tyr	Extrusion	Photocrosslinking	Enhanced adhesion	67,234
Gel-AGE	Extrusion	Thiol-ene + photoredox	Low bioink viscosity	62,235	
	Vat-polymerization				

Primary material	Bioink	Printing approach	Crosslinking method	Notes	References
Silk fibroin	SF	Extrusion	HRP/H ₂ O ₂	Slow curing residual H ₂ O ₂	128
		Extrusion	Ru/SPS	Fast crosslinking	66
	SF-MA	Vat-polymerization	Photocrosslinking	Fast crosslinking	127,236
dECM	dECM	Extrusion	Physical crosslinking at 37 °C	Mechanically weak	131
	dECM-MA	Extrusion	Photocrosslinking	Mimicking native microenvironment	90
	dECM/Alg	Extrusion	Ionic crosslinking	Good printability	237-239
Fibrinogen	PEG monoacrylate/ Fib/Alg	Extrusion	Ionic crosslinking + photo-irradiation during bioprinting	Increased mechanical property and printability	134
Elastin	MeTro/GelMA	Extrusion	Photocrosslinking	High elasticity	138
	MeTro/CNT	Extrusion	Photocrosslinking	Enhanced conductivity	137
Alginate	Alg	Extrusion	Ionic crosslinking	Fast curing, low cell adherence	240-241
		Inkjet			
	Alg-MA	Vat-polymerization	Ionic crosslinking	Dual-crosslink	242-243
			Photocrosslinking		
	Oxi-Alg-MA	Extrusion	Ionic crosslinking	Rapidly degradable	244-245
		Vat-polymerization	photocrosslinking		
	Alg-NB	Extrusion	Ionic crosslinking	Tunable properties	147
			photocrosslinking		
Alg-Tyr	Extrusion	HRP/H ₂ O ₂	Fast curing	149	
Alg-RGD	Extrusion	Ionic crosslinking	Improve cell adhesion	153,246	
Hyaluronic acid	HA	Extrusion	-	Weak	247
	HA-MA	Extrusion	Photocrosslinking	Enhanced stability	164-166
		Vat-polymerization			
	Oxi-HA	Extrusion	Schiff's base	Extended degradation time, increased stability	170,173-174
	HA-ADH/Oxi-HA	Extrusion	Acylhydrazone chemistry	Short term stable, self-healing	171-172
	HA-Tyr	Extrusion	HRP/H ₂ O ₂	High cell viability	80,149
	HA-CD/HA-Ad	Extrusion	Host-guest interaction	Self-healing	54
PEG	PEGDA	Vat-polymerization	Photocrosslinking	Tunable properties	182-183
	PEGX	Extrusion	Photocrosslinking	Low viscosity, tunable curing chemistry	184-185
	PEGDA/Alg	Extrusion	Ionic crosslinking + Photocrosslinking	High toughness	228
Pluronic	F127	Extrusion	Thermal gelation	Temperature sensitive	189-192
	F127DA	Extrusion	Photocrosslinking	Low cell adherence, high toughness	248-249
Vat-polymerization					

Abbreviations: collagen (Col), methacryloyl-modified collagen (Col-MA), gelatin (gel), gelatin methacryloyl (GelMA), dopamine-modified gelatin methacryloyl (D-GelMA), allylated gelatin (Gel-AGE), vinyl ester modified gelatin (Gel-VE), norbornene-modified gelatin (Gel-NB), cysteine-modified gelatin (Gel-Cys), tyramide-modified gelatin (Gel-Tyr), furan-modified Gelatin (Gel-FA), furfuryl-modified gelatin (Gel-F1), silk fibroin (SF), methacrylated silk fibroin (SF-MA), decellularized extracellular matrix (dECM), methacrylated decellularized extracellular matrix (dECM-MA), fibrinogen (Fib), methacryloyl-modified tropoelastin (MeTro), alginate (Alg), methacrylated alginate (Alg-MA), norbornene-modified alginate (Alg-NB), tyramide-modified alginate (Alg-Tyr), RGD-modified alginate (Alg-RGD), oxidized alginate (Oxi-Alg), hyaluronic acid (HA), methacrylated hyaluronic acid (HA-HA), oxidized hyaluronic acid (Oxi-HA), tyramide-modified hyaluronic acid (HA-Tyr), norbornene-modified hyaluronic acid (HA-NB), azide-modified hyaluronic acid (HA-Azide), dihydrazide-modified hyaluronic acid (HA-ADH), furan-modified hyaluronic acid (HA-FA), β -cyclodextrin-modified hyaluronic acid (HA-CD), adamantine-modified hyaluronic acid (HA-Ad), polyethylene glycol-diacrylate (PEGDA), Pluronic F127 (F127), Pluronic F127-diacrylate (F127DA), ruthenium/sodium persulfate (Ru/SPS).

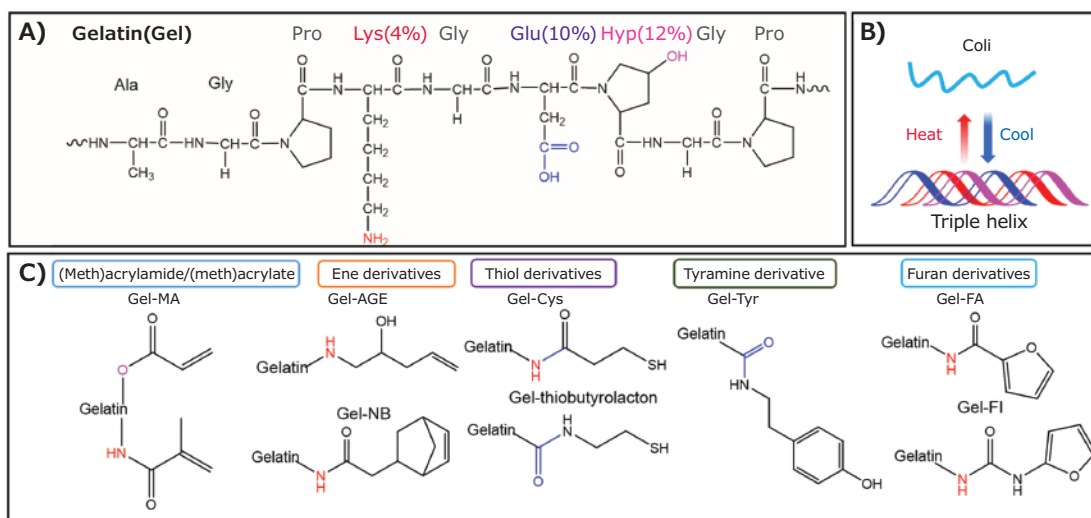


Figure 2. Gelatin and derivatives with different crosslinking for biinks. **A)** Chemical structures with major amino residues and typical reactive functional groups in gelatin. **B)** Gelatin chains reversibly transform from random coil to triple helix configuration upon heating/cooling modulated by hydrogen bonds. **C)** Major gelation derivatives: methacrylated gelatin (Gel-MA), ene-derivatives including allylated gelatin (Gel-AGE), vinyl ester-modified gelatin (Gel-VE), norbornene-modified gelatin (Gel-NB), thiol-modified gelatin including cysteine-modified gelatin (Gel-Cys), and thiobutylolacton-modified gelatin (Gel-Thiol), tyramine-modified gelatin (Gel-Try), furan/furfuryl-modified gelatin (Gel-FA, Gel-FI).

Gelatin is produced by hydrolyzing collagen from connective tissues of animals, such as the skin.⁹⁵ The primary reactive functional groups of gelatin are amine, carboxylate, and hydroxyl groups (**Figure 2A**). Similar to collagen, gelatin contains cell-adhesive peptide sequences, such as Arg-Gly-Asp (RGD) as well as protease-sensitive sites. It has been approved by the United States Food and Drug Administration (FDA) for biological and biomedical applications.⁹⁶ Due to the advantages of good bioactivity, biocompatibility, biodegradability, and low cost, as well as widely tunable properties, gelatin is one of the widely used materials in tissue engineering, and bioprinting.^{61,97} There are several methods to crosslink gelatin-based biomaterials. As shown in **Figure 2B**, gelatin displays a thermally reversible sol-gel transition upon heating and cooling due to its reversible triple helix-coil transition.⁹⁸⁻⁹⁹ To improve the structural integrity of gelatin hydrogels for *in vivo* applications, chemical crosslinking of gelatin by glutaraldehyde, genipin, and 1-ethyl-3-(3-dimethyl aminopropyl) carbodiimide (EDC) are used.¹⁰⁰ In addition, more benign enzymatic crosslinking of gelatin using transglutaminase is extensively adopted.⁷⁵⁻⁷⁶ Meanwhile, various gelatin derivatives have been developed for fast chemical crosslinking (**Figure 2C**).⁹⁶ For example, the formation of (meth)acrylamide- and (meth)acrylate-modified gelatin (GelMA, or gelatin methacryloyl) through reaction between amine (in lysine) and hydroxyl (in hydroxyproline) residues with methacrylate anhydride (MAAH) to form pending vinyl double bonds is the most widely used derivatives for chain-growth photopolymerization.^{12,58,97,101-103} Also, the carboxyl acid residues (glutamate) can be modified with tyramine for photo-reduction by the Ru/SPS system.⁶⁷ In addition, step-growth polymerization by click chemistry, including thiol-ene chemistry, Diels-Alder reaction, and Schiff's base, is widely used for crosslinking gelatin hydrogels.⁶¹ To develop thiol-ene photo-crosslinkable gelatin, 'ene' functional groups, including norbornene, vinyl esters, pentenyl, allyl ethers, or acrylates,

have been grafted on gelatin molecules.¹⁰⁴⁻¹⁰⁵ For example, pentenoate-modified gelatin,¹⁰⁴ vinyl ester-modified gelatin (Gel-VE),¹⁰⁶ norbornene-modified gelatin (Gel-NB),^{63,107} and allylated gelatin (Gel-AGE)⁶² can be modified and then photocrosslinked with multifunctional thiol crosslinkers. Thiol functionalized gelatin, including cysteine-modified gelatin (Gel-Cys),^{104,108} and gelatin thiobutylolacton,¹⁰⁴ were also used for thiol-ene chemistry or thiol-Michael reactions. Furan-modified gelatin (Gel-FA) was synthesized for Diels-Alder reaction-based crosslinking.¹⁰⁹ Besides, Gel-FA can proceed with photo-oxidation-based crosslinking in the presence of a photosensitizer, such as Rose Bengal.¹¹⁰⁻¹¹¹ Moreover, the wide use of gelatin and its derivatives to blend with other biomaterials, such as alginate and PEGDA, increases the printability and physical properties of the biinks.¹¹²⁻¹¹³

Silk fibroin is a natural protein derived from silkworms (**Figure 3A**),¹¹⁴ which has attracted increasing attention for use in bioprinting.¹¹⁵⁻¹¹⁷ The most widely used silk material is the domesticated *Bombyx mori* silk protein, which shows good biocompatibility, low inflammatory profile, and tunable mechanical properties.¹¹⁸ Silk fibroin consists of hydrophobic segments with multiple hydrogen bonds and hydrophilic segments containing reactive amino residues of tyrosine (5.2%), lysine (0.3%), and glutamate (1.0%).¹¹⁹⁻¹²⁰ To prepare silk fibroin-based bioink, silk fibroin is treated with ionic liquids or water-based salt systems to break the strong hydrogen bonds between the proteins.¹²¹ The silk fibroin hydrogels can be obtained using chemical and physical crosslinking approaches. Physical crosslinking of silk fibroin is achieved through a structural transformation from a random-coil configuration to β -sheet folding (**Figure 3B**),¹²²⁻¹²³ which can be accelerated by treatment conditions, including sonication, shear action, temperature change, pH adjusting, electrical stimulation, and addition of polar organic solvents, such as polyols or surfactants.¹²⁴ The physically crosslinked silk hydrogels with a

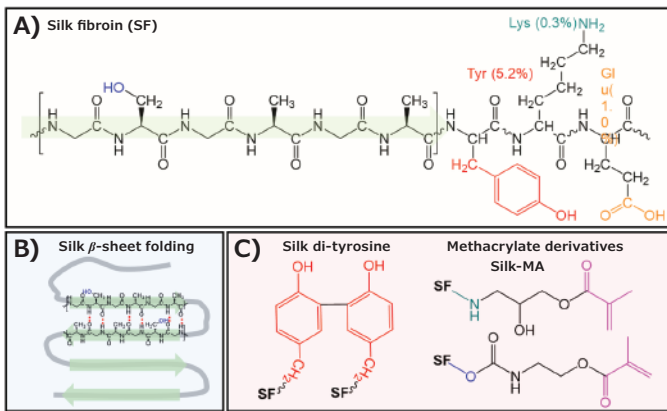


Figure 3. Silk fibroin and derivatives with different crosslinking for bioinks. **A)** Chemical structures with major amino residues and typical reactive functional groups in silk fibroin. **B)** Physical crosslinking of silk fibroin by configuration transformation from random coil to β -sheeting folding dominated by the collective hydrogen bonds in the hydrophobic segments. **C)** Chemical crosslinking of SF: native silk fibroin via di-tyrosine-formation and methacrylated silk fibroin (SF-MA) for photocrosslinking.

large amount of β -sheet folding are usually stiff and hard to be remodeled by cells. To this end, soft silk fibroin hydrogels are fabricated by chemical crosslinking. The native silk fibroin can be crosslinked by forming di-tyrosine bonds between the phenolic tyrosine residues (**Figure 3C**). The di-tyrosine-based crosslinking is realized by either photoredox-based chemical crosslinking,^{64,125} or enzymatic crosslinking approaches using HRP/H₂O₂.^{79,126} Particularly, the photoredox crosslinking using Ru/SPS system triggered by visible light is efficient and rapid,⁶⁴ and can be used in bioprinting of silk fibroin.⁶⁶ In addition, silk fibroin can also be modified with methacrylate groups for vat photopolymerization-based printing (**Figure 3C**).¹²⁷⁻¹²⁸

Other proteins, including decellularized ECM (dECM), fibrin, and elastin, are also used for bioinks. The dECM is obtained from the target tissue with all the cellular components removed while preserving the proteins, and gross architecture can also be preserved as needed.¹²⁹ The dECM hydrogels are rich in ECM components, improving cell viability and functionality by providing a natural microenvironment. The dECM pregel solutions are liquid below 10 °C and slowly gels above 37 °C.¹³⁰ Despite these advantages, the low mechanical strength of dECM limits its wide application. For this reason, dECM is frequently modified by incorporating photosensitive functional groups or mixed with other cross-linkable components when used in bioinks.¹³¹ Fibrin exhibits good biodegradability and can promote cell growth and tissue regeneration.¹³² However, the high viscosity of fibrin makes it difficult to use without modification as a bioink in extrusion-based 3D bioprinting.¹³³ As a result, fibrin is typically chemically modified and/or blended with other printable materials such as gelatin to make bioinks.^{134,135} Elastin can provide elasticity when used as a major component for printing of tissues like skin,¹³⁶ but its intrinsic crosslinking creates challenges to using it as a bioink. Therefore, its soluble precursor, such as recombinant tropoelastin, has been used to produce bioinks.¹³⁷⁻¹³⁸

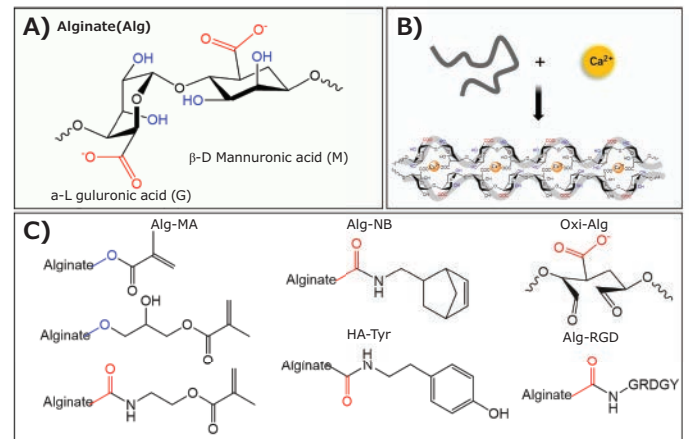


Figure 4. Alginate and derivatives with different crosslinking for bioinks. **A)** Chemical structure of alginate. **B)** Electrostatic interactions between metal ions and carboxylate for ionic crosslinking of alginate. **C)** Typical alginate derivatives: methacrylated alginate (Alg-MA), norbornene-modified alginate (Alg-NB), tyramide-modified alginate (Alg-Tyr), RGD-modified alginate (Alg-RGD), oxidized alginate (Oxi-Alg).

Polysaccharide-based Bioinks

Polysaccharides and their derivatives have attracted considerable attention as biomaterials for use in biomedical engineering and materials science. Here, we briefly introduce polysaccharides, including alginate, HA, agarose, chitosan, and their derivatives as bioinks. Alginate, also known as alginic acid, is a natural anionic polysaccharide refined from brown seaweed composed of β -D-mannuronic (M) and α -L-guluronic acids (G) (**Figure 4A**), which is similar to the glycosaminoglycans found in the native ECM of the human body. It has seen significant use in biomedicine and tissue engineering due to its biocompatibility, low cytotoxicity, mild gelation process, and low cost.¹³⁹⁻¹⁴⁰ In particular, it has been widely used as a bioink because of its rapid gelation without harmful byproducts.³ As shown in **Figure 4B**, ionic gelation of alginate can be easily achieved by rapid crosslinking of the carboxylic acid group in the G unit by divalent cations, such as calcium (Ca²⁺), to form an “egg-box” structure.¹⁴¹ Thus, bioinks based on alginate, modified alginate, or alginate blended with other biomaterials are some of the most widely used in bioprinting.⁴⁰⁻⁴¹ Unfortunately, ionic crosslinking of alginate is not stable under physiological conditions due to ionic exchange.¹⁴² Accordingly, various alginate derivatives, such as methacrylated alginate (Alg-MA), are synthesized for chemical crosslinking (**Figure 4C**). Alg-MA was obtained by reaction with MAAH,¹⁴³ glycidyl methacrylate (GMA),¹⁴⁴ or 2-aminoethyl methacrylate in the presence of EDC and *N*-hydroxysuccinimide (NHS).¹⁴⁵⁻¹⁴⁶ Rapid UV-induced thiol-ene crosslinking is used to crosslink norbornene-modified alginate (Alg-NB).¹⁴⁷⁻¹⁴⁸ Additionally, enzymatic crosslinking of tyramide-modified alginate (Alg-Tyr) by HRP/H₂O₂ is utilized for extrusion bioprinting.¹⁴⁹ Derivatives of alginate with *in-vivo* biodegradability are also highly sought after for biomedical applications.¹⁵⁰ To enhance biodegradability, oxidized alginate (Oxi-Alg) was prepared by partially breaking the ring using a strong oxidant, such as sodium periodate, and tuning the degradation rate by the oxidation degree.^{145,151} Alginate

also lacks cell adhesion sites, leading to poor cell proliferation and differentiation. To this end, cell adhesive peptides of RGD can be conjugated to alginates.¹⁵²⁻¹⁵³ Thus, alginate bioinks can be engineered with a wide variety of functionalities, including photocrosslinkability, biodegradability, and cellular attachment properties for various biomedical applications.¹⁵⁴⁻¹⁵⁵ Further, multi-component hydrogels can be created by blending alginate with other polymers, including chitosan, gelatin, and hyaluronic acid to enhance comprehensive performance.¹⁵⁶⁻¹⁵⁸

HA is a non-sulfated glycosaminoglycan that is ubiquitous in the human body, especially in skeletal structures and supporting tissues, like skin, bone, cartilage, and vascular tissue.^{59,159} HA mediates cellular signalling, and is a critical component of synovial fluid, vitreous humour, and hyaline cartilage.¹⁶⁰ Due to its excellent biocompatibility, HA hydrogels have been progressively applied in biomedical applications for decades.¹⁶¹⁻¹⁶² However, when used in bioinks HA provides limited capability for cell migration, angiogenesis, and proliferation, as well as weak mechanical properties.¹⁶³ Although high molecular-weight HA is viscous and displays shear-thinning properties, it is difficult to maintain its printed shape and is mechanically weak in an uncrosslinked HA hydrogel. To successfully use HA as a bioink, various chemical modifications must be employed to incorporate reactive functional groups for crosslinking (**Figure 5**). This is accomplished via reaction of the three major functional groups: glucuronic acid, and the primary and secondary hydroxyl groups. For example, methacrylated HA (HA-MA) can be obtained by reacting HA with MAAH or GMA for light-triggered hydrogels crosslinking.¹⁶⁴⁻¹⁶⁶ In addition, several other HA derivatives have been developed to prepare HA hydrogels by different crosslinking approaches, including thiol modified HA (HA-Thiol) for thiol-Michael addition,¹⁶⁷⁻¹⁶⁸ norbornene-modified HA (HA-NB) for thiol-ene reactions,¹⁶⁹ and tyramide-modified HA (HA-Tyr) for enzymatic crosslinking,^{80,149} furan-modified HA (HA-FA) for Diels-Alder crosslinking,⁷¹ and azide-modified HA (HA-Azide) for CuAAC click chemistry.⁷⁰ Meanwhile, HA was also modified to fabricate hydrogels containing dynamic bonds, including β -cyclodextrin-modified HA (HA-CD) and adamantane-modified HA (HA-Ad)

based hydrogels by host-guest interaction,⁵⁴ oxidized-HA and dihydrazide-modified HA (HA-ADH) dynamic hydrogel by Schiff's-base chemistry,¹⁷⁰⁻¹⁷⁴ and dynamic thiol-HA/silver composite hydrogel,¹⁷⁵ to assist the material extrusion or enable functional self-healing properties. HA can blend with gelatin components or be modified with RGD to improve cellular interaction.^{165,174} Therefore, these HA modifications enable the fabrication of mechanically stable, biodegradable hydrogels with good cell adhesion for bioprinting. Overall, derived HA with modified properties has been widely used as bioinks in tissue engineering, regeneration medicine, and biomedical applications.¹⁷⁶⁻¹⁷⁸

Besides these, other polysaccharides and derivatives are used as bioinks as well. Agarose is a biocompatible polysaccharide extracted from marine algae and seaweed. Agarose shows thermoreversible gelation at around 30–40 °C depending on the aqueous solution concentration and molecular weight, and is suitable for extrusion-based printing of structures.¹⁷⁹ Similar to other polysaccharides with poor cell adhesion, agarose can be mixed with additional components, such as gelatin or collagen, to prepare bioinks.¹⁸⁰ Besides, agarose can be chemically modified by carboxylation to soften the hydrogel by reducing the helical-helical interactions and/or graft RGD to enhance cell adhesion.¹⁸⁰ Chitin is the most naturally abundant amino-polysaccharide with biocompatible and biodegradable properties.¹⁸¹ By partial deacetylation of chitin, chitosan is obtained with amine residues that show good anti-bacterial and wound healing performance.¹⁸¹ Chitosan can be readily dissolved in dilute acids for facile processing, and further blended with other polymers to prepare multi-component bioinks.⁴⁵⁻⁴⁶

Synthetic Polymer-based Bioinks

Synthetic polymer hydrogels formed by chemical crosslinking of synthetic monomers or oligomers have also been widely used for bioprinting.⁸ Compared with natural polymer hydrogels, synthetic polymer hydrogels have stronger and more highly tailorable mechanical properties. Among them, the most widely used synthetic hydrogel is based on PEG or poly(ethylene oxide) (PEO) (high molecular weights, >10 kDa) hydrogels.

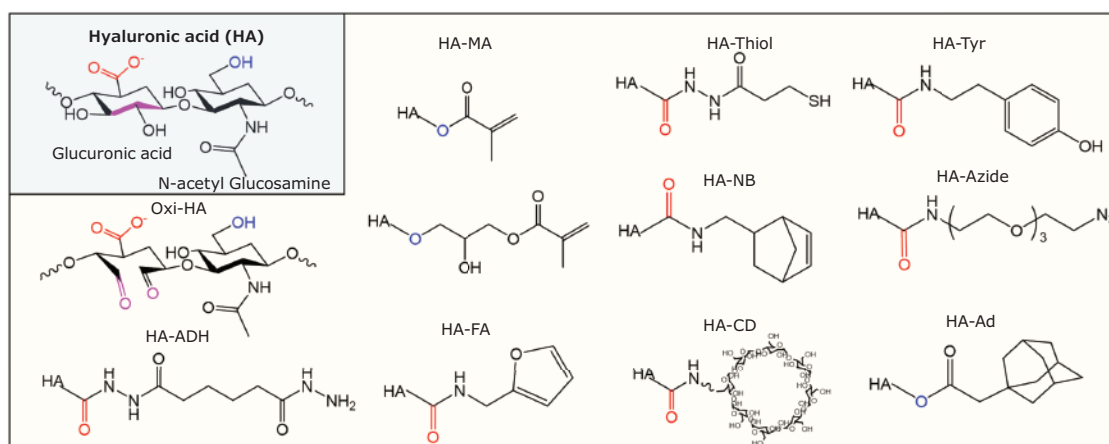


Figure 5. Chemical of hyaluronic acid and typical derivatives: methacrylated HA (HA-MA), HA-Thiol, oxidized HA (Oxi-HA), norbornene-modified HA (HA-NB), tyramide-modified HA (HA-Tyr), azide-modified HA (HA-Azide), dihydrazide-modified HA (HA-ADH), furan-modified HA (HA-FA), β -cyclodextrin-modified HA (HA-CD), and adamantane-modified HA (HA-Ad).

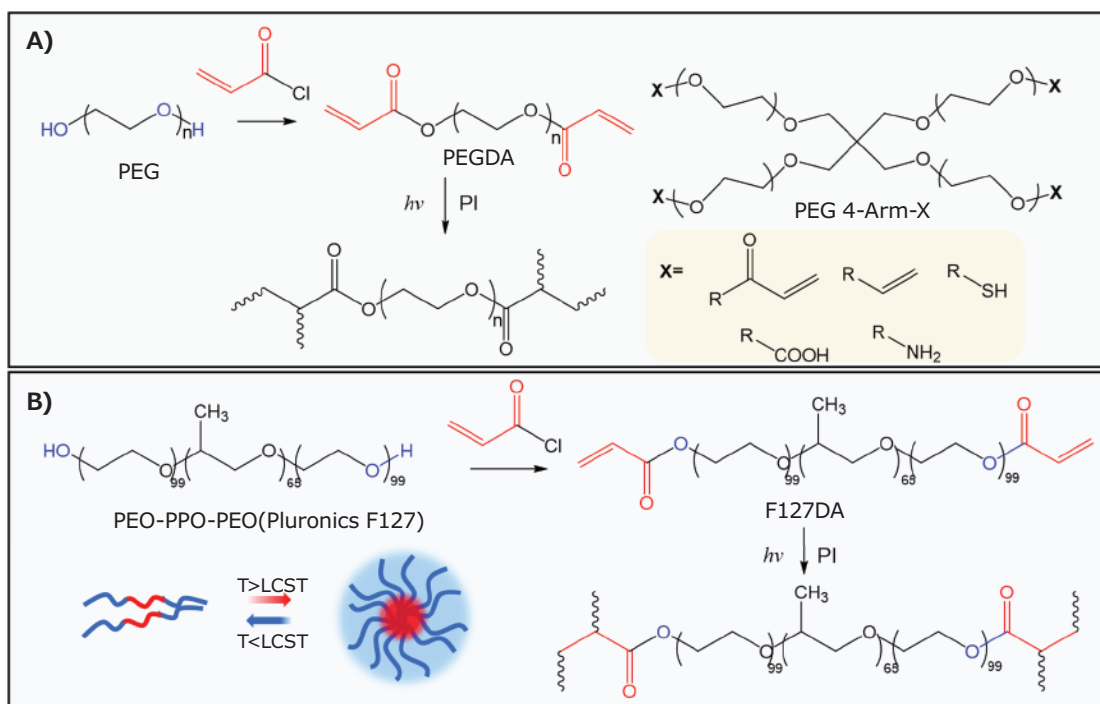


Figure 6. Chemical structure, modification of synthetic polymers to prepare crosslinked bioinks **A)** PEG and derivatives. **B)** Pluronic F127 and derivatives.

PEG contains hydrophilic ethylene oxide repeating units and hydroxyl end-groups. PEG can be tailored to have different molecular weights and chain architectures, including linear or multi-arms. To accommodate crosslinking for bioprinting, PEG can be modified with (meth)acrylate, such as PEGDA.¹⁸²⁻¹⁸³ Under light irradiation, PEGDA can proceed with chain-growth photopolymerization with the aid of various photoinitiators (**Figure 6A**). By altering the oligomer concentration and oligomer chain length, the mechanical properties of PEGDA hydrogels can be simply tuned in a wide range. PEG has also been modified with other functional groups, including carboxylic acid, vinyl, amine, and thiol groups for step-growth polymerization with click chemistry-based crosslinking.¹⁸⁴⁻¹⁸⁵ It is noted that the existence of low-molecular-weight PEGDA residual oligomers would lead to cytotoxicity in PEGDA hydrogels.¹⁸⁶

Another class of extensively studied synthetic polymer is Poloxamer (or Pluronic F127), which is a linear triblock copolymer composed of hydrophilic PEO and hydrophobic poly(propylene oxide) blocks (PEO-PPO-PEO). Pluronic F127 has been approved by FDA as a human-use cytocompatible biomaterial.¹⁸⁷ It shows polymer concentration-dependent thermoreversible sol-gel transition. Above a critical micelle concentration and a temperature in the range of 4–10 °C, Pluronic F127 reversibly forms a physical gel via micellar aggregation (**Figure 6B**). The concentration of Pluronic F127 must be as high as 14 % to form a gel in a cell culture medium, leading to low cell viability.¹⁸⁸ Therefore, Pluronic F127 is more frequently used as a sacrificial or support material in extrusion-based bioprinting.¹⁸⁹⁻¹⁹² Acrylated Pluronic F127 (F127DA) was synthesized to produce photocurable bioinks.^{188,193} Significant drawbacks of synthetic hydrogels include their biological inertness, inherently poor adhesion for cells or

proteins, and a lack of biodegradability. To this end, various active components, such as cell-adhesive peptides or growth factors, can be incorporated into synthetic hydrogels, as discussed later.

Bioink Functional Improvements

Printability

Printability of bioinks generally refers to the degree of extrudability, filament uniformity, and shape fidelity of the printed object compared to the original computer-aided design.¹⁹⁴ Printability is closely associated with multiple rheological properties (e.g., bioink viscosity and viscoelasticity), physical properties (e.g., surface tension), crosslinking strategies as well as bioprinting parameters (e.g., applied pressure). Usually, bioinks with a high viscosity and shear-thinning enable good printing fidelity in direct extrusion-based bioprinting. Various biocompatible rheological modifiers, such as agarose,¹⁷⁹ gelatin,¹⁹⁵ and laponite,¹⁹⁶⁻¹⁹⁷ are widely used to tune the rheological properties of bioinks. However, a bioink with high viscosity and a large shearing force in the dispensing nozzle can also be detrimental to living cells.¹⁹⁸ In this sense, the use of low-viscosity bioinks with *in situ* crosslinking and support bath-based extrusion are favored in specific scenarios.²⁵⁻²⁶ Another way to enhance the printability of a bioink is to include a secondary component that uses rapid physical crosslinking as a sacrifice template.¹⁴² Low-viscosity alginate is extensively mixed with GelMA,¹⁹⁹⁻²⁰⁰ collagen,¹⁴² and dECM¹¹³ and used as a sacrifice template for co-axial extrusion bioprinting. For example, we reported a general method for bioink design using alginate-templated dual-stage crosslinking for use with low-viscosity bioinks.¹⁴² These multi-component bioinks consisted of low viscosity alginate combined with bio-macromolecular components such as collagen, gelatin, or GelMA. The fast ionic crosslinking of the alginate component serves as a temporal

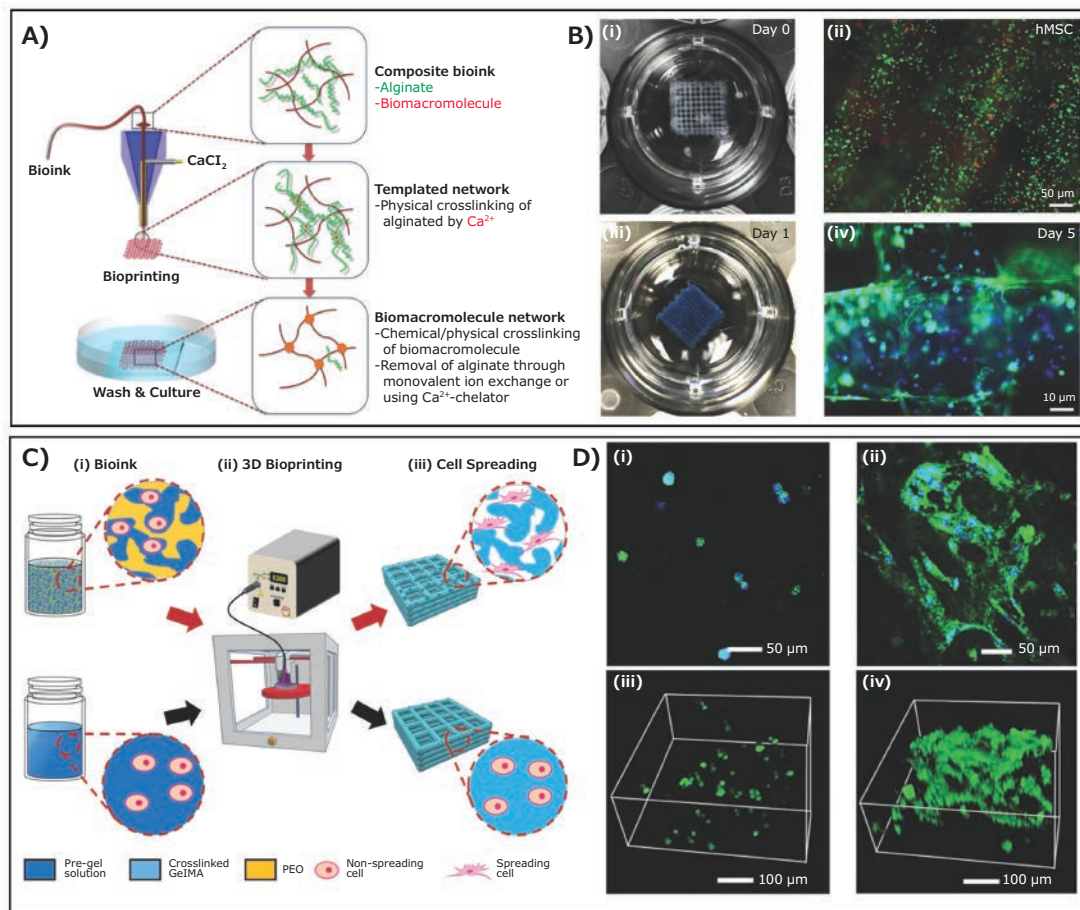


Figure 7. Typical examples of bioink-customization to improve printability, cell viability, and mechanical properties of the bioprinted constructs. **A)** Schematic showing alginate-templated dual-stage crosslinking for bioprinting. The multi-component bioink contains low-viscosity alginate with fast ionic crosslinking and biomacromolecule components with secondary crosslinking for co-axial bioprinting. **B)** Photographs of bioprinted five-layer constructs at day 0 and day 1 post-bioprinting, as well as fluorescence microscopic images of live/dead staining (live cells in green and dead in red) at day 0, and F-actin/nuclei staining (F-actin in green and nuclei in blue) at day 5 of the encapsulated hMSCs in the bioprinted constructs. **A)** and **B)** are adapted with permission from reference 142, copyright 2018 John Wiley and Sons. **C)** Schematic showing 3D bioprinting of a micropore-forming hydrogel structure using the APTe bioink and a conventional hydrogel structure. **D)** Confocal fluorescence micrographs showing morphologies of NIH/3T3 fibroblasts within i, iii) standard GelMA constructs and ii, iv) microporous GelMA constructs. The cells were stained for nuclei (blue) and F-actin (green). **C)** and **D)** are adapted with permission from reference 207, copyright 2018 John Wiley and Sons.

structural support to stabilize the construct shape during co-axial extrusion bioprinting. After chemical or physical crosslinking of the bio-macromolecular component, the alginate physical network was selectively removed to leave the desired bio-macromolecule network (**Figure 7A**), enabling good cell viability and spreading in the resultant hydrogels (**Figure 7B**).

Enhancing Cellular Behaviors

The cellular behavior of bioprinted tissue constructs can be influenced by many factors before, during, and after printing.²⁰¹ First, before printing, cell-laden bioinks containing hydrogel-precursors, initiators, or crosslinkers must be biocompatible with cells. Hydrogel systems that use toxic chemical crosslinkers or extreme pH conditions are not suitable candidates for use in cell-laden bioinks. For extrusion-based bioprinting, overly high shearing stress can cause cellular deformation, leading to cell damage or loss of function.²⁰² Use of lower shearing force, lower-viscosity bioinks, or shear-thinning bioinks can mitigate

this issue. In the case of vat polymerization-based bioprinting, exposure to light irradiation can also impact the living cells. Thus, highly efficient visible-light photoinitiators are favored to initiate crosslinking.²¹ After printing, cell growth can also be influenced by hydrogel bioactivity. Therefore, hydrogels that possess cell-attachment sites, such as gelatin and dECM, are frequently used alone or mixed with other components. To enhance the cell adhesion and bioactivity of synthetic polymer-based hydrogels, biologically active components, such as cell-adhesive RGD peptides or growth factor-sequestering heparan sulfate proteins (HSP) can be grafted onto polymer chains to prepare the bioinks. For example, Moon et al. developed PEG hydrogels with integrin-binding sites and protease-sensitive substrates to produce bioinks with good cell adhesion and biodegradability.²⁰³

Besides the cell adhesion sites, the polymer network structure can also influence cell growth. Biomaterial hydrogels with high polymer concentration or crosslinking density featuring small network mesh sizes reduce cell viability and retard cell

spreading and proliferation.^{204–205} However, increasing the mesh size to enhance cell viability sacrifices mechanical properties. To address this, micro pore-forming hydrogel biomaterials have been developed that can be applied to bioprinting.^{206–208} For example, a micro pore-forming bioink based on the aqueous two-phase emulsion (ATPE) improved cell viability and enhanced cell proliferation (**Figure 7C**).²⁰⁷ The ATPE bioink was prepared by mixing GelMA and PEO aqueous solutions, forming phase-separated PEO domains in the range of several tens of micrometers. The cell-laden ATPE bioink was used for extrusion-based bioprinting or vat polymerization-based bioprinting modalities. After photocrosslinking of the GelMA component, the PEO microphase was leached, forming microscale pores. The 3D-bioprinted porous GelMA constructs, encapsulating various cell types, showed better viability, proliferation, and metabolic activity than those bioprinted with conventional pure GelMA as the bioink (**Figure 7D**).^{101,209} Bioprinted 3D tissues with enhanced cellular behaviors such as these may soon become widespread in tissue engineering and tissue model engineering.^{210–212}

Physical Properties

Several physical properties must be considered for the clinical translation of bioprinted tissue constructs including biodegradability and mechanical properties. Human tissue has unique mechanical properties, including low modulus, viscoelasticity, high toughness, and good fatigue-resistance.²¹³ Bioprinted tissue constructs require comparable stiffness to match that of the targeted tissue and must show controllable degradation to remodel with the host tissue. It is highly demanding to have both widely tunable and good mechanical properties in bioprinted constructs. Therefore, the design and optimization of bioprinting parameters must be carefully customized. Take GelMA as an example; mechanical properties of a GelMA hydrogel can be altered by changing GelMA methacryloyl-modification degree, polymer concentration, and UV exposure time.^{58,103,214} The crosslinking density and modulus of GelMA hydrogels increases with higher GelMA concentration, longer curing time, and higher degree of methacryloyl-modification. Usually, single-component hydrogels show limited tunability in mechanical properties. To this end, multicomponent biomaterial hydrogels, including hybrid hydrogels, nanocomposite hydrogels, and double-network hydrogels, with tunable mechanical properties and enhanced toughness, are developed.^{13,34,215} For instance, Rutz et al. reported a PEGX toolkit to manipulate the properties of PEG-based bioinks.¹⁸⁵ PEG is functionalized with reactive groups (represent the “X”) on both ends and act as a crosslinker for various polymers. The chain length and architecture (linear or multi-arms) of PEGX crosslinker can be altered. Linear (e.g., gelatin), branched (e.g., four-arm PEG amine), or multifunctional (e.g., GelMA) polymer can be mixed with PEGX and cells to formulate the bioinks. The use of thiol Michael addition and tetrazine-norbornene click chemistry allows for good cell viability.¹⁸⁴ The mechanical properties of the resulting gel can be tuned depending on the concentration of PEGX and its molecular weight and functional groups. Moreover, secondary crosslinking can increase mechanical robustness after printing. Besides, various nanoparticles, including gold nanorods, laponite, and hydroxyapatite, can also be used to make composite GelMA bioinks

with tuned mechanical properties.^{216–219} In addition, multi-walled carbon nanotubes (MWCNTs) have also been added to GelMA to enhance both the mechanical and electrophysiological properties. Magnetic nanoparticles have also been added to hydrogel matrices to introduce magnetic properties.^{220–222} Interpenetrating polymer network hydrogels, specifically double-network (DN) hydrogels, have attracted attention for increasing the mechanical properties of the hydrogels, especially the toughness.^{223–224} DN hydrogels consisted of one stiff and brittle polymer network and a second soft and ductile network. This concept is also gaining popularity for fabricating tough biomaterial hydrogels. To design bioinks for tough biomaterial hydrogels, an ionically cross-linkable polysaccharide, such as alginate,^{225–227} is suitable for the stiff first network; loose chemical crosslinking is adopted for the second biopolymer network. For example, Hong et al. developed a DN hydrogel-based bioink containing high-molecular-weight PEGDA and medium-viscosity sodium alginate.²²⁸ To facilitate extrusion bioprinting, nanoclays were also added to impart shearing. After crosslinking, the hydrogel with a water content of 77.5 wt% had a fracture toughness above 1,500 J m⁻². The ionically crosslinked alginate dissipated mechanical energy under deformation, and the long-chain PEG network maintained high hydrogel elasticity. Since both PEG and alginate are biocompatible, this tough hydrogel enabled high viability of encapsulated human mesenchymal stem cells (hMSCs) for up to 7 days.

Conclusions

Bioprinting is a disruptive biofabrication technique that allows for direct fabrication of anatomical 3D tissue constructs based on individual patient needs. With the advances in bioprinting techniques and bioink design, the bioprinting of complex cell-laden tissue constructs has found broad applications in tissue modeling and regenerative medicine. Bioink design and customization plays a critical role in printability, cell viability and function, and the physical properties of the resulting tissue constructs. Natural and synthetic polymer biomaterials are physically or chemically crosslinked to form 3D networks that provide an ECM-like matrix to supporting cell growth. Bioinks composition and crosslinking methods can be customized to tune printability. Biorthogonal crosslinking approaches that use precursors and by-products with low toxicity, suitable crosslinking kinetics, and compatibility with physiological conditions are preferred in bioink design. Among these, the rapid ionic crosslinking of polysaccharides is widely used. Chain-growth photopolymerization and click chemistry-based crosslinking methods are extensively used to form biomaterial hydrogels from polysaccharides and protein derivatives with good physiological and environmental stability. Bioactivity and network topological structures of crosslinked biomaterial hydrogels are modulated to enhance cell behavior. The mechanical properties of biomaterial hydrogels are engineered using multicomponent bioinks with multiple crosslinking mechanisms, including copolymerization of hybrid hydrogels nanocomposite hydrogels, and DN hydrogels. Recently, many more natural and synthetic polymers have come into commercialization as bioinks. The wider use of these materials, and continuous innovation in bioink design will broaden bioprinting research and deepen its impact in tissue engineering and regenerative medicine.

Acknowledgment

The authors gratefully acknowledge funding from the National Institutes of Health (R00CA201603, R21EB025270, R21EB026175, R01EB028143, R01HL153857, R21EB030257), the National Science Foundation (NSF-CBET-1936105), and the Brigham Research Institute.

Conflict of Interest

Y. S. Zhang sits on the Scientific Advisory Board of Allevi, Inc., which however, did not support, participate, or influence in this work.

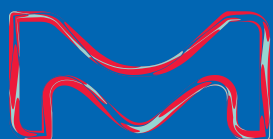
References

- Levato, R.; Jungst, T.; Scheuring, R. G.; Blunk, T.; Groll, J.; *Adv. Mater.* **2020**, 1906423.
- Zhang, Y. S.; Yue, K.; Aleman, J.; Mollazadeh-Moghaddam, K.; Bakht, S. M.; Yang, J.; Jia, W.; Dell'Erba, V.; Assawes, P.; Shin, S. R. *Ann. Biomed. Eng.* **2017**, 45, 148–163.
- Gungor-Ozkerim, P. S.; Inci, I.; Zhang, Y. S.; Khademhosseini, A.; Dokmeci, M. R. *Biomater. Sci.* **2018**, 6, 915–946.
- Vijayavenkataraman, S.; Yan, W.-C.; Lu, W. F.; Wang, C.-H.; Fuh, J. Y. H. *Adv. Drug Deliv. Rev.* **2018**, 132, 296–332.
- Fonseca, A. C.; Melchels, F. P. W.; Ferreira, M. J. S.; Moxon, S. R.; Potjewyd, G.; Dargaville, T. R.; Kimber, S. J.; Domingos, M. *Chem. Rev.* **2020**, 120, 11093–11139.
- Gopinathan, J.; Noh, I. *Biomater. Res.* **2018**, 22, 11.
- Groll, J.; Burdick, J. A.; Cho, D. W.; Derby, B.; Gelinsky, M.; Heilshorn, S. C.; Jungst, T.; Malda, J.; Mironov, V. A.; Nakayama, K.; Ovsianikov, A.; Sun, W.; Takeuchi, S.; Yoo, J. J.; Woodfield, T. B. F. *Biofabrication* **2018**, 11, 013001.
- Bedell, M. L.; Navara, A. M.; Du, Y.; Zhang, S.; Mikos, A. G. *Chem. Rev.* **2020**, 120, 10744–10792.
- Natural and Synthetic Biomedical Polymers*, 1st ed.; Kumbar, S.; Cato, L.; Meng, D.; Eds.; Elsevier, 2014.
- Hospodiuk, M.; Dey, M.; Sosnoski, D.; Ozbolat, I. T. *Biotechnol. Adv.* **2017**, 35, 217–239.
- Gong, J.; Schuurmans, C. C. L.; Genderen, A. M. v.; Cao, X.; Li, W.; Cheng, F.; He, J. J.; López, A.; Huerta, V.; Manriquez, J.; Li, R.; Li, H.; Delavaux, C.; Sebastian, S.; Capendale, P. E.; Wang, H.; Xie, J.; Yu, M.; Masereeuw, R.; Vermonden, T.; Zhang, Y. S. *Nat. Commun.* **2020**, 11, 1267.
- Ying, G. L.; Jiang, N.; Maharjan, S.; Yin, Y. X.; Chai, R. R.; Cao, X.; Yang, J. Z.; Miri, A. K.; Hassan, S.; Zhang, Y. *Aqueous Adv. Mater.* **2018**, 30(50), e1805460.
- Cui, X.; Li, J.; Hartanto, Y.; Durham, M.; Tang, J.; Zhang, H.; Hooper, G.; Lim, K.; Woodfield, T. *Adv. Healthc. Mater.* **2020**, 9, 1901648.
- Jiang, T.; Munguia-Lopez, J. G.; Flores-Torres, S.; Kort-Mascort, J.; Kinsella, J. M. *Appl. Phys. Rev.* **2019**, 6, 011310.
- Ning, L.; Chen, X. *Biotechnol. J.* **2017**, 12, 1600671.
- Ozbolat, I. T.; Hospodiuk, M. *Biomaterials* **2016**, 76, 321–343.
- Pereira, R. F.; Bártolo, P. J. *J. Appl. Polym. Sci.* **2015**, 132, 42458.
- Tuan, R. S.; Boland, G.; Tuli, R. *Arthritis Res. Ther.* **2003**, 5, 32–45.
- Li, X.; Liu, B.; Pei, B.; Chen, J.; Zhou, D.; Peng, J.; Zhang, X.; Jia, W.; Xu, T. *Chem. Rev.* **2020**, 120, 10793–10833.
- Lim, K. S.; Levato, R.; Costa, P. F.; Castilho, M. D.; Alcalá-Orozco, C. R.; Van Doremalen, K. M.; Melchels, F. P.; Gawlitta, D.; Hooper, G. J.; Malda, J. J. B. *Biofabrication* **2018**, 10, 034101.
- Lee, M.; Rizzo, R.; Surman, F.; Zenobi-Wong, M. *Chem. Rev.* **2020**, 120, 10950–11027.
- Lim, K. S.; Galarraga, J. H.; Cui, X.; Lindberg, G. C. J.; Burdick, J. A.; Woodfield, T. B. F. *Chem. Rev.* **2020**, 120, 10662–10694.
- Hasan, A.; Paul, A.; Vrana, N. E.; Zhao, X.; Memic, A.; Hwang, Y.-S.; Dokmeci, M. R.; Khademhosseini, A. *Biomaterials* **2014**, 35, 7308–7325.
- Costantini, M.; Colosi, C.; Świączkowski, W.; Barbetta, A. *Biofabrication* **2018**, 11, 012001.
- Quyung, L.; Highley, C. B.; Sun, W.; Burdick, J. A. *Adv. Mater.* **2017**, 29, 1604983.
- Hinton, T. J.; Jallerat, Q.; Palchesko, R. N.; Park, J. H.; Grodzicki, M. S.; Shue, H.-J.; Ramadan, M. H.; Hudson, A. R.; Feinberg, A. W. *Sci. Adv.* **2015**, 1, 1–10.
- Bernal, P. N.; Delrot, P.; Loterie, D.; Li, Y.; Malda, J.; Moser, C.; Levato, R. *Adv. Mater.* **2019**, 31, 1904209.
- Regehy, M.; Garmshausen, Y.; Reuter, M.; König, N. F.; Israel, E.; Kelly, D. P.; Chou, C.-Y.; Koch, K.; Asfari, B.; Hecht, S. *Nature* **2020**, 588, 620–624.
- Kelly, B. E.; Bhattacharya, I.; Heidari, H.; Shusteff, M.; Spadaccini, C. M.; Taylor, H. K. *Science* **2019**, 363, eaau7114.
- Armstrong, J. P. K.; Puetzer, J. L.; Serio, A.; Guex, A. G.; Kapnisi, M.; Breant, A.; Zong, Y.; Assal, V.; Skaalure, S. C.; King, O.; Murty, T.; Meinert, C.; Franklin, A. C.; Bassindale, P. G.; Nichols, M. K.; Terracciano, C. M.; Huttmacher, D. W.; Drinkwater, B. W.; Klein, T. J.; Perriman, A. W.; Stevens, M. M. *Adv. Mater.* **2018**, 30, 1802649.
- Daly, A. C.; Davidson, M. D.; Burdick, J. A. *Nat. Commun.* **2021**, 12, 753.
- Valot, L.; Martinez, J.; Mehdi, A.; Subra, G. *Chem. Soc. Rev.* **2019**, 48, 4049–4086.
- Malda, J.; Visser, J.; Melchels, F. P.; Jungst, T.; Hennink, W. E.; Dhert, W. J.; Groll, J.; Huttmacher, D. W. *Adv. Mater.* **2013**, 25, 5011–5028.
- Chimene, D.; Kaunas, R.; Gaharwar, A. K. *Adv. Mater.* **2020**, 32, 1902026.
- GhavamiNejad, A.; Ashammakhi, N.; Wu, X. Y.; Khademhosseini, A. *Small* **2020**, 16, 2002931.
- Nele, V.; Wojciechowski, J. P.; Armstrong, J. P.; Stevens, M. M. *Adv. Funct. Mater.* **2020**, 30, 2002759.
- Gao, Y.; Peng, K.; Mitrugotri, S. *Adv. Mater.* **2021**, 33, 2006362.
- Grant, G. T.; Morris, E. R.; Rees, D. A.; Smith, P. J.; Thom, D. *FEBS Lett.* **1973**, 32, 195–198.
- Yang, C. H.; Wang, M. X.; Haider, H.; Yang, J. H.; Sun, J.-Y.; Chen, Y. M.; Zhou, J.; Suo, Z. *ACS Appl. Mater. Interfaces* **2013**, 5, 10418–10422.
- Axpe, E.; Oyen, M. L. *Int. J. Mol. Sci.* **2016**, 17, 1976.
- Jia, J.; Richards, D. J.; Pollard, S.; Tan, Y.; Rodriguez, J.; Visconti, R. P.; Trusk, T. C.; Yost, M. J.; Yao, H.; Markwald, R. R. *Acta Biomaterialia* **2014**, 10, 4323–4331.
- Kesti, M.; Eberhardt, C.; Pagliccia, G.; Kenkel, D.; Grande, D.; Boss, A.; Zenobi-Wong, M. *Adv. Funct. Mater.* **2015**, 25, 7406–7417.
- Morris, E. R.; Nishinari, K.; Rinaudo, M. *Food Hydrocoll.* **2012**, 28, 373–411.
- Shi, R.; Sun, T. L.; Luo, F.; Nakajima, T.; Kurokawa, T.; Bin, Y. Z.; Rubinstein, M.; Gong, J. P. *Macromolecules* **2018**, 51, 8887–8898.
- Khong, T. T.; Aarstad, O. A.; Skjåk-Bræk, G.; Drageit, K. I.; Vårum, K. M. *Biomacromolecules* **2013**, 14, 2765–2771.
- Ng, W. L.; Yeong, W. Y.; Naing, M. W. *Int. J. Bioprinting* **2016**, 2, 53–62.
- Hayashi, A.; Oh, S.-C. *Agric. Biol. Chem.* **1983**, 47, 1711–1716.
- Fernández, E.; López, D.; Mijangos, C.; Duskova-Smrckova, M.; Ilavsky, M.; Dusek, K. J. *Poly. Sci. B: Polym. Phys.* **2008**, 46, 322–328.
- Kramer, R. Z.; Bella, J.; Mayville, P.; Brodsky, B.; Berman, H. M. *Nat. Struct. Biol.* **1999**, 6, 454–457.
- Lu, S.; Li, J.; Zhang, S.; Yin, Z.; Xing, T.; Kaplan, D. L. *J. Mater. Chem. B* **2015**, 3, 2599–2606.
- Zheng, Z.; Wu, J.; Liu, M.; Wang, H.; Li, C.; Rodriguez, M. J.; Li, G.; Wang, X.; Kaplan, D. L. *Adv. Healthc. Mater.* **2018**, 7, e1701026.
- Achilli, M.; Mantovani, D. *Polymers* **2010**, 2, 664–680.
- Lee, A.; Hudson, A.; Shiwardski, D.; Tashman, J.; Hinton, T.; Yerneni, S.; Billely, J.; Campbell, P.; Feinberg, A. *Science* **2019**, 365, 482–487.
- Highley, C. B.; Rodell, C. B.; Burdick, J. A. *Adv. Mater.* **2015**, 27, 5075–5079.
- Yin, J.; Yan, M.; Wang, Y.; Fu, J.; Suo, H. *ACS Appl. Mater. Interfaces* **2018**, 10, 6849–6857.
- Liu, W.; Heinrich, M. A.; Zhou, Y.; Akpek, A.; Hu, N.; Liu, X.; Guan, X.; Zhong, Z.; Jin, X.; Khademhosseini, A. *Adv. Healthc. Mater.* **2017**, 6, 1601451.
- Yu, C.; Schimelman, J.; Wang, P.; Miller, K. L.; Ma, X.; You, S.; Guan, J.; Sun, B.; Zhu, W.; Chen, S. *Chem. Rev.* **2020**, 19, 10695–10742.
- Billiet, T.; Gevaert, E.; De Schryver, T.; Cornelissen, M.; Dubruel, P. *Biomaterials* **2014**, 35, 49–62.
- Allison, D. D.; Grande-Allen, K. J. *Tissue Eng.* **2006**, 12, 2131–2140.
- Zheng, Z.; Eglin, D.; Alini, M.; Richards, G. R.; Qin, L.; Lai, Y. *Engineering* **2020**, 7, 966–978.
- Van Hooricx, J.; Tytgat, L.; Dobos, A.; Ottevaere, H.; Van Erps, J.; Thienpont, H.; Ovsianikov, A.; Dubruel, P.; Van Vlierberghe, S. *Acta Biomater.* **2019**, 97, 46–73.
- Bertlein, S.; Brown, G.; Lim, K. S.; Jungst, T.; Boeck, T.; Blunk, T.; Tessmar, J.; Hooper, G. J.; Woodfield, T. B.; Groll, J. *Adv. Mater.* **2017**, 29, 1703404.
- Van Hooricx, J.; Gruber, P.; Markovic, M.; Rollet, M.; Graulus, G. J.; Vagenende, M.; Tromayer, M.; Van Erps, J.; Thienpont, H.; Martins, J. C. *Macromol. Rapid. Comm.* **2018**, 39, 1800181.
- Fancy, D. A.; Kodadek, T. *Proc. Natl. Acad. Sci. U. S. A.* **1999**, 96, 6020–6024.
- Partlow, B. P.; Applegate, M. B.; Omenetto, F. G.; Kaplan, D. L. *ACS Biomater. Sci. Eng.* **2016**, 2, 2108–2121.
- Cui, X.; Soliman, B. G.; Alcalá-Orozco, C. R.; Li, J.; Vis, M. A. M.; Santos, M.; Wise, S. G.; Levato, R.; Malda, J.; Woodfield, T. B. F.; Rnjak-Kovacina, J.; Lim, K. S. *Adv. Healthc. Mater.* **2020**, 9, 1901667.
- Lim, K. S.; Abinzano, F.; Bernal, P. N.; Albillos Sanchez, A.; Atienza-Roca, P.; Otto, I. A.; Peiffer, Q. C.; Matsusaki, M.; Woodfield, T. B. F.; Malda, J.; Levato, R. *Adv. Healthc. Mater.* **2020**, 9, 1901792.
- Liu, S. Q.; Ee, P. L. R.; Ke, C. Y.; Hedrick, J. L.; Yang, Y. Y. *Biomaterials* **2009**, 30, 1453–1461.
- Breger, J. C.; Fisher, B.; Samy, R.; Pollack, S.; Wang, N. S.; Isayeva, I. *J. Biomed. Mater. Res. B: Appl. Biomater.* **2015**, 103, 1120–1132.
- Hu, X.; Li, D.; Zhou, F.; Gao, C. *Acta Biomater.* **2011**, 7, 1618–1626.
- Nimmo, C. M.; Owen, S. C.; Shoichet, M. S. *Biomacromolecules* **2011**, 12, 824–830.
- Du, Z.; Li, N.; Hua, Y.; Shi, Y.; Bao, C.; Zhang, H.; Yang, Y.; Lin, Q.; Zhu, L. *Chem. Commun.* **2017**, 53, 13023–13026.
- Kim, S. W.; Kim, D. Y.; Roh, H. H.; Kim, H. S.; Lee, J. W.; Lee, K. Y. *Biomacromolecules* **2019**, 20, 1860–1866.
- Gopinathan, J.; Noh, I. *Tissue Eng. Regen. Med.* **2018**, 15, 531–546.

- (75) Teixeira, L. S. M.; Feijen, J.; van Blitterswijk, C. A.; Dijkstra, P. J.; Karperien, M. *Biomaterials* **2012**, *33*, 1281–1290.
- (76) Liu, Y.; Weng, R.; Wang, W.; Wei, X.; Li, J.; Chen, X.; Liu, Y.; Lu, F.; Li, Y. *Int. J. Biol. Macromol.* **2020**, *162*, 405–413.
- (77) Schöneberg, J.; De Lorenzi, F.; Theek, B.; Blaeser, A.; Rommel, D.; Kuehne, A. J.; Kießling, F.; Fischer, H. *Sci. Rep.* **2018**, *8*, 1–13.
- (78) Partlow, B. P.; Hanna, C. W.; Rnjak Kovacina, J.; Moreau, J. E.; Applegate, M. B.; Burke, K. A.; Marelli, B.; Mitropoulos, A. N.; Omenetto, F. G.; Kaplan, D. L. *Adv. Funct. Mater.* **2014**, *24*, 4615–4624.
- (79) Raia, N. R.; Partlow, B. P.; McGill, M.; Kimmerling, E. P.; Ghezzi, C. E.; Kaplan, D. L. *Biomaterials* **2017**, *131*, 58–67.
- (80) Darr, A.; Calabro, A. J. *Mater. Sci.: Mater. Med.* **2009**, *20*, 33–44.
- (81) Bakota, E. L.; Aulisa, L.; Galler, K. M.; Hartgerink, J. D. *Biomacromolecules* **2011**, *12*, 82–87.
- (82) Kothapalli, C. R.; Ramamurthi, A. J. *Tissue Eng. Regen. Med.* **2009**, *3*, 655–661.
- (83) Kagan, H. M.; Li, W. J. *Cell. Biochem.* **2003**, *88*, 660–672.
- (84) Su, T.; Tang, Z.; He, H.; Li, W.; Wang, X.; Liao, C.; Sun, Y.; Wang, Q. *Chem. Sci.* **2014**, *5*, 4204–4209.
- (85) Lee, J. M.; Suen, S. K. Q.; Ng, W. L.; Ma, W. C.; Yeong, W. Y. *Macromol. Biosci.* **2021**, *21*, e2000280.
- (86) Marques, C. F.; Diogo, G. S.; Pina, S.; Oliveira, J. M.; Silva, T. H.; Reis, R. L. J. *Mater. Sci.: Mater. Med.* **2019**, *30*, 32.
- (87) Attalla, R.; Ling, C. S. N.; Selvaganapathy, P. R. *Adv. Healthc. Mater.* **2018**, *7*, 1870023.
- (88) Duarte Campos, D. F.; Blaeser, A.; Korsten, A.; Neuss, S.; Jakel, J.; Vogt, M.; Fischer, H. *Tissue Eng. Part A* **2015**, *21*, 740–576.
- (89) Lee, H.; Yang, G. H.; Kim, M.; Lee, J.; Huh, J.; Kim, G. *Mater. Sci. Eng. C* **2018**, *84*, 140–147.
- (90) Mazzocchi, A.; Devarasetty, M.; Huntwork, R.; Soker, S.; Skardal, A. *Biofabrication* **2018**, *11*, 015003.
- (91) Isaacson, A.; Swioklo, S.; Connon, C. J. *Exp. Eye. Res.* **2018**, *173*, 188–193.
- (92) Drzewiecki, K. E.; Parmar, A. S.; Gaudet, I. D.; Branch, J. R.; Pike, D. H.; Nanda, V.; Shreiber, D. I. *Langmuir* **2014**, *30*, 11204–11211.
- (93) Rhee, S.; Puetzer, J. L.; Mason, B. N.; Reinhart-King, C. A.; Bonassar, L. J. *ACS Biomater. Sci. Eng.* **2016**, *2*, 1800–1805.
- (94) Diamantides, N.; Wang, L.; Pruiksma, T.; Siemiatkoski, J.; Dugopolski, C.; Shortkroff, S.; Kennedy, S.; Bonassar, L. J. *Biofabrication* **2017**, *9*, 034102.
- (95) Gómez-Guillén, M. C.; Turnay, J.; Fernández-Díaz, M. D.; Ulmo, N.; Lizarbe, M. A.; Montero, P. *Food Hydrocoll.* **2002**, *16*, 25–34.
- (96) Van Hoorick, J.; Tytgat, L.; Dobos, A.; Ottevaere, H.; Van Erps, J.; Thienpont, H.; Ovsianikov, A.; Dubruel, P.; Van Vlierberghe, S. *Acta Biomater.* **2019**, *97*, 46–73.
- (97) Ying, G.; Jiang, N.; Yu, C.; Zhang, Y. S. *Bio-Des. Manuf.* **2018**, *1*, 215–224.
- (98) Zhu, M.; Wang, Y.; Ferracci, G.; Zheng, J.; Cho, N. J.; Lee, B. H. *Sci. Rep.* **2019**, *9*, 6863.
- (99) Gornall, J. L.; Terentjev, E. M. *Soft Matter* **2008**, *4*, 544–549.
- (100) Yang, G.; Xiao, Z.; Long, H.; Ma, K.; Zhang, J.; Ren, X.; Zhang, J. *Sci. Rep.* **2018**, *8*, 1616.
- (101) Ying, G.; Jiang, N.; Parra, C.; Tang, G.; Zhang, J.; Wang, H.; Chen, S.; Huang, N. P.; Xie, J.; Zhang, Y. S. *Adv. Funct. Mater.* **2020**, *30*, 2003740.
- (102) Van Den Bulcke, A. I.; Bogdanov, B.; De Rooze, N.; Schacht, E. H.; Cornelissen, M.; Berghmans, H. *Biomacromolecules* **2000**, *1*, 31–38.
- (103) Yue, K.; Trujillo-de Santiago, G.; Alvarez, M. M.; Tamayol, A.; Annabi, N.; Khademhosseini, A. *Biomaterials* **2015**, *73*, 254–271.
- (104) Russo, L.; Sgambato, A.; Visone, R.; Occhetta, P.; Moretti, M.; Rasponi, M.; Nicotra, F.; Cipolla, L. *Monatsh. Chem.* **2016**, *147*, 587–592.
- (105) Van Hoorick, J.; Ovsianikov, A.; Dubruel, P.; Van Vlierberghe, S. *Material Matters* **2018**, *13*, 75–82.
- (106) Qin, X. H.; Torgersen, J.; Saf, R.; Mühleder, S.; Pucher, N.; Ligon, S. C.; Holthöner, W.; Redl, H.; Ovsianikov, A.; Stampfl, J. J. *Polym. Sci., Part A: Polym. Chem.* **2013**, *51*, 4799–4810.
- (107) Muñoz, Z.; Shih, H.; Lin, C.-C. *Biomater. Sci.* **2014**, *2*, 1063–1072.
- (108) Fu, Y.; Xu, K.; Zheng, X.; Giacomini, A. J.; Mix, A. W.; Kao, W. J. *Biomaterials* **2012**, *33*, 48–58.
- (109) García-Astrain, C.; Gandini, A.; Peña, C.; Algar, I.; Eceiza, A.; Corcuera, M.; Gabilondo, N. *RSC Adv.* **2014**, *4*, 35578–35587.
- (110) Son, T. I.; Sakuragi, M.; Takahashi, S.; Obuse, S.; Kang, J.; Fujishiro, M.; Matsushita, H.; Gong, J.; Shimizu, S.; Tajima, Y. *Acta Biomater.* **2010**, *6*, 4005–4010.
- (111) Mazaki, T.; Shiozaki, Y.; Yamane, K.; Yoshida, A.; Nakamura, M.; Yoshida, Y.; Zhou, D.; Kitajima, T.; Tanaka, M.; Ito, Y.; Ozaki, T.; Matsukawa, A. *Sci. Rep.* **2014**, *4*, 4457.
- (112) Cao, X.; Ashfaq, R.; Cheng, F.; Maharjan, S.; Li, J.; Ying, G.; Hassan, S.; Xiao, H.; Yue, K.; Zhang, Y. S. *Adv. Funct. Mater.* **2019**, *29*, 1807173.
- (113) Pi, Q.; Maharjan, S.; Yan, X.; Liu, X.; Singh, B.; van Genderen, A. M.; Robledo-Padilla, F.; Parra-Saldivar, R.; Hu, N.; Jia, W.; Xu, C.; Kang, J.; Hassan, S.; Cheng, H.; Hou, X.; Khademhosseini, A.; Zhang, Y. S. *Adv. Mater.* **2018**, *30*, e1706913.
- (114) Vepari, C.; Kaplan, D. L. *Prog. Polym. Sci.* **2007**, *32*, 991–1007.
- (115) Mu, X.; Fitzpatrick, V.; Kaplan, D. L. *Adv. Healthc. Mater.* **2020**, *9*, 1901552.
- (116) Mu, X.; Sahoo, J. K.; Cebe, P.; Kaplan, D. L. *Polymers* **2020**, *12*, 2936.
- (117) Mu, X.; Agostinacchio, F.; Xiang, N.; Pei, Y.; Khan, Y.; Guo, C.; Cebe, P.; Motta, A.; Kaplan, D. L. *Prog. Polym. Sci.* **2021**, *115*, 101375.
- (118) Mu, X.; Wang, Y.; Guo, C.; Li, Y.; Ling, S.; Huang, W.; Cebe, P.; Hsu, H.-H.; De Ferrari, F.; Jiang, X.; Xu, Q.; Balduini, A.; Omenetto, F. G.; Kaplan, D. L. *Macromol. Biosci.* **2020**, *20*, 1900191.
- (119) Mondal, M.; Trivedy, K.; NIRMAL, K. S. *Caspian J. Env. Sci.* **2007**, *2*, 63–76.
- (120) Jin, H.-J.; Kaplan, D. L. *Nature* **2003**, *424*, 1057–1061.
- (121) Rockwood, D. N.; Preda, R. C.; Yücel, T.; Wang, X.; Lovett, M. L.; Kaplan, D. L. *Nat. Protoc.* **2011**, *6*, 1612.
- (122) Kim, U.-J.; Park, J.; Li, C.; Jin, H.-J.; Valluzzi, R.; Kaplan, D. L. *Biomacromolecules* **2004**, *5*, 786–792.
- (123) Matsumoto, A.; Chen, J.; Collette, A. L.; Kim, U.-J.; Altman, G. H.; Cebe, P.; Kaplan, D. L. *J. Phys. Chem. B* **2006**, *110*, 21630–21638.
- (124) Zheng, H.; Zuo, B. J. *J. Phys. Chem. B* **2021**, *9*, 1238–1258.
- (125) Piluso, S.; Gomez, D. F.; Dokter, I.; Teixeira, L. M.; Li, Y.; Leijten, J.; Van Weeren, R.; Vermonden, T.; Karperien, M.; Malda, J. J. *Mater. Chem. B* **2020**, *8*, 9566–9575.
- (126) Hu, W.; Wang, Z.; Xiao, Y.; Zhang, S.; Wang, J. *Biomater. Sci.* **2019**, *7*, 843–855.
- (127) Kim, S. H.; Yeon, Y. K.; Lee, J. M.; Chao, J. R.; Lee, Y. J.; Seo, Y. B.; Sultan, M. T.; Lee, O. J.; Lee, J. S.; Yoon, S.-i. *Nat. Commun.* **2018**, *9*, 1–14.
- (128) Kim, S. H.; Yeon, Y. K.; Lee, J. M.; Chao, J. R.; Lee, Y. J.; Seo, Y. B.; Sultan, M. T.; Lee, O. J.; Lee, J. S.; Yoon, S. I.; Hong, I. S.; Khang, G.; Lee, S. J.; Yoo, J. J.; Park, C. H. *Nat. Commun.* **2018**, *9*, 1620.
- (129) Kabirian, F.; Mozafari, M. *Methods* **2020**, *171*, 108–118.
- (130) Kim, B. S.; Das, S.; Jang, J.; Cho, D.-W. *Chem. Rev.* **2020**, *120*, 10608–10661.
- (131) Pati, F.; Jang, J.; Ha, D. H.; Won Kim, S.; Rhie, J. W.; Shim, J. H.; Kim, D. H.; Cho, D. W. *Nat. Commun.* **2014**, *5*, 3935.
- (132) Li, Y.; Meng, H.; Liu, Y.; Lee, B. P. *Sci. World J.* **2015**, *2015*, 685690.
- (133) De Melo, B. A. G.; Jodat, Y. A.; Cruz, E. M.; Benincasa, J. C.; Shin, S. R.; Porcionatto, M. A. *Acta Biomater.* **2020**, *117*, 60–76.
- (134) Maiullari, F.; Costantini, M.; Milan, M.; Pace, V.; Chirivi, M.; Maiullari, S.; Rainer, A.; Baci, D.; Marei, H. E.-S.; Seliktar, D.; Gargioli, C.; Bearzi, C.; Rizzi, R. *Sci. Rep.* **2018**, *8*, 13532.
- (135) Freeman, S.; Ramos, R.; Alexis Chando, P.; Zhou, L.; Reeser, K.; Jin, S.; Soman, P.; Ye, K. *Acta Biomater.* **2019**, *95*, 152–164.
- (136) Baldock, C.; Oberhauser, A. F.; Ma, L.; Lammie, D.; Siegler, V.; Mithieux, S. M.; Tu, Y.; Chow, J. Y. H.; Suleman, F.; Malfois, M. *Proc. Natl. Acad. Sci. U. S. A.* **2011**, *108*, 4322–4327.
- (137) Annabi, N.; Shin, S. R.; Tamayol, A.; Miscuglio, M.; Bakooshli, M. A.; Assmann, A.; Mostafalu, P.; Sun, J. Y.; Mithieux, S.; Cheung, L. *Adv. Mater.* **2016**, *28*, 40–49.
- (138) Lee, S.; Sani, E. S.; Spencer, A. R.; Guan, Y.; Weiss, A. S.; Annabi, N. *Adv. Mater.* **2020**, *32*, 2003915.
- (139) Zhang, Y.; Yu, Y.; Akkouch, A.; Dababneh, A.; Dolati, F.; Ozbolat, I. *Biomater. Sci.* **2014**, *3*, 134–143.
- (140) Tang, G.; Xiong, R.; Lv, D.; Xu, R. X.; Braeckmans, K.; Huang, C.; De Smedt, S. C. *Adv. Sci.* **2019**, *6*, 1802342.
- (141) Mørch, Y. A.; Qi, M.; Gundersen, P. O. M.; Formo, K.; Lacik, I.; Skjåk Bræk, G.; Oberholzer, J.; Strand, B. L. J. *Biomed. Mater. Res. A* **2012**, *100*, 2939–2947.
- (142) Zhu, K.; Chen, N.; Liu, X.; Mu, X.; Zhang, W.; Wang, C.; Zhang, Y. S. *Macromol. Biosci.* **2018**, *18*, 1800127.
- (143) Smeds, K. A.; Grinstaff, M. W. *J. Biomed. Mater. Res.* **2001**, *54*, 115–121.
- (144) Araiza-Verduzco, F.; Rodríguez-Velázquez, E.; Cruz, H.; Rivero, I. A.; Acosta-Martinez, D. R.; Pina-Luis, G.; Alatorre-Meda, M. *Materials* **2020**, *13*, 534.
- (145) Jeon, O.; Bouhadir, K. H.; Mansour, J. M.; Alsberg, E. *Biomaterials* **2009**, *30*, 2724–2734.
- (146) Jeon, O.; Lee, Y. B.; Jeong, H.; Lee, S. J.; Wells, D.; Alsberg, E. *Mater. Horiz.* **2019**, *6*, 1625–1631.
- (147) Ooi, H. W.; Mota, C.; ten Cate, A. T.; Calore, A.; Moroni, L.; Baker, M. B. *Biomacromolecules* **2018**, *19*, 3390–3400.
- (148) Wang, G.; Zhu, J.; Chen, X.; Dong, H.; Li, Q.; Zeng, L.; Cao, X. *RSC Adv.* **2018**, *8*, 11036–11042.
- (149) Sakai, S.; Mochizuki, K.; Qu, Y.; Mail, M.; Nakahata, M.; Taya, M. *Biofabrication* **2018**, *10*, 045007.
- (150) Kong, H. J.; Kaigler, D.; Kim, K.; Mooney, D. J. *Biomacromolecules* **2004**, *5*, 1720–1727.
- (151) Bouhadir, K. H.; Lee, K. Y.; Alsberg, E.; Damm, K. L.; Anderson, K. W.; Mooney, D. J. *Biotechnol. Prog.* **2001**, *17*, 945–950.
- (152) Rowley, J. A.; Madlambayan, G.; Mooney, D. J. *Biomaterials* **1999**, *20*, 45–53.
- (153) Yu, J.; Gu, Y.; Du, K. T.; Mihardja, S.; Sievers, R. E.; Lee, R. J. *Biomaterials* **2009**, *30*, 751–756.
- (154) Jeon, O.; Bouhadir, K. H.; Mansour, J. M.; Alsberg, E. *Biomaterials* **2009**, *30*, 2724–2734.

- (155) Jeon, O.; Powell, C.; Ahmed, S. M.; Alsberg, E. *Tissue Eng. A* **2010**, *16*, 2915–2925.
- (156) Chen, X.; Fan, M.; Tan, H.; Ren, B.; Yuan, G.; Jia, Y.; Li, J.; Xiong, D.; Xing, X.; Niu, X. *Mater. Sci. Eng. C* **2019**, *101*, 619–629.
- (157) Gao, T.; Gillispie, G. J.; Copus, J. S.; Pr, A. K.; Seol, Y.-J.; Atala, A.; Yoo, J. J.; Lee, S. J. *Biofabrication* **2018**, *10*, 034106.
- (158) Kim, Y. M.; Oh, S. H.; Choi, J. S.; Lee, S.; Ra, J. C.; Lee, J. H.; Lim, J. Y. *The Laryngoscope* **2014**, *124*, E64–E72.
- (159) Reitingner, S.; Lepperdinger, G. *Gerontology* **2013**, *59*, 71–76.
- (160) Asahara, T.; Murohara, T.; Sullivan, A.; Silver, M.; van der Zee, R.; Li, T.; Witzenbichler, B.; Schatteman, G.; Isner, J. M. *Science* **1997**, *275*, 964–966.
- (161) Xu, X.; Jha, A. K.; Harrington, D. A.; Farach-Carson, M. C.; Jia, X. *Soft Matter* **2012**, *8*, 3280–3294.
- (162) Highley, C. B.; Prestwich, G. D.; Burdick, J. A. *Curr. Opin. Biotechnol.* **2016**, *40*, 35–40.
- (163) Abatangelo, G.; Vindigni, V.; Avruscio, G.; Pandis, L.; Brun, P. *Cells* **2020**, *9*, 1743.
- (164) Poldervaart, M. T.; Goversen, B.; De Ruijter, M.; Abbadessa, A.; Melchels, F. P.; Oner, F. C.; Dhert, W. J.; Vermonden, T.; Alblas, J. *PLoS One* **2017**, *12*, e0177628.
- (165) Skardal, A.; Zhang, J.; McCoard, L.; Xu, X.; Ootamasathien, S.; Prestwich, G. D. *Tissue Eng. A* **2010**, *16*, 2675–2685.
- (166) Skardal, A.; Zhang, J.; Prestwich, G. D. *Biomaterials* **2010**, *31*, 6173–6181.
- (167) Shu, X. Z.; Liu, Y.; Palumbo, F. S.; Luo, Y.; Prestwich, G. D. *Biomaterials* **2004**, *25*, 1339–1348.
- (168) Shu, X. Z.; Ahmad, S.; Liu, Y.; Prestwich, G. D. *J. Biomed. Mater. Res. A* **2006**, *79*, 902–912.
- (169) Galarraga, J. H.; Kwon, M. Y.; Burdick, J. A. *Sci. Rep.* **2019**, *9*, 19987.
- (170) Li, S.; Pei, M.; Wan, T.; Yang, H.; Gu, S.; Tao, Y.; Liu, X.; Zhou, Y.; Xu, W.; Xiao, P. *Carbohydr. Polym.* **2020**, *250*, 116922.
- (171) Weis, M.; Shan, J.; Kuhlmann, M.; Jungst, T.; Tessmar, J.; Groll, J. *Gels* **2018**, *4*, 82.
- (172) Su, W.-Y.; Chen, K.-H.; Chen, Y.-C.; Lee, Y.-H.; Tseng, C.-L.; Lin, F.-H. *J. Biomater. Sci., Poly. Ed.* **2011**, *22*, 1777–1797.
- (173) Su, W.-Y.; Chen, Y.-C.; Lin, F.-H. *Acta Biomater.* **2010**, *6*, 3044–3055.
- (174) Chen, F.; Ni, Y.; Liu, B.; Zhou, T.; Yu, C.; Su, Y.; Zhu, X.; Yu, X.; Zhou, Y. *Carbohydr. Polym.* **2017**, *166*, 31–44.
- (175) Skardal, A.; Zhang, J.; McCoard, L.; Ootamasathien, S.; Prestwich, G. D. *Adv. Mater.* **2010**, *22*, 4736–4740.
- (176) Burdick, J. A.; Prestwich, G. D. *Adv. Mater.* **2011**, *23*, H41–H56.
- (177) Ahmadian, E.; Dizaj, S. M.; Eftekhari, A.; Dalir, E.; Vahedi, P.; Hasanzadeh, A.; Samiei, M. *Drug Res.* **2020**, *70*, 6–11.
- (178) Tiwari, S.; Bahadur, P. *Int. J. Biol. Macromol.* **2019**, *121*, 556–571.
- (179) López-Marcial, G. R.; Zeng, A. Y.; Osuna, C.; Dennis, J.; García, J. M.; O'Connell, G. D. *ACS Biomater. Sci. Eng.* **2018**, *4*, 3610–3616.
- (180) Salati, M. A.; Khazai, J.; Tahmuri, A. M.; Samadi, A.; Taghizadeh, A.; Taghizadeh, M.; Zarrintaj, P.; Ramsey, J. D.; Habibzadeh, S.; Seidi, F. *Polymers* **2020**, *12*, 1150.
- (181) Chitosan: Derivatives, Composites and Applications. Ahmed, S.; Ikram, S., Ed: John Wiley & Sons: 2017.
- (182) Warr, C.; Valdoz, J. C.; Bickham, B. P.; Knight, C. J.; Franks, N. A.; Chartrand, N.; Van Ry, P. M.; Christensen, K. A.; Nordin, G. P.; Cook, A. D. *ACS Appl. Bio. Mater.* **2020**, *3*, 2239–2244.
- (183) Nemir, S.; Hayenga, H. N.; West, J. L. *Biotechnol. Bioeng.* **2010**, *105*, 636–644.
- (184) Rutz, A. L.; Gargus, E. S.; Hyland, K. E.; Lewis, P. L.; Setty, A.; Burghardt, W. R.; Shah, R. N. *Acta Biomater.* **2019**, *99*, 121–132.
- (185) Rutz, A. L.; Hyland, K. E.; Jakus, A. E.; Burghardt, W. R.; Shah, R. N. *Adv. Mater.* **2015**, *27*, 1607–1614.
- (186) Fairbanks, B. D.; Schwartz, M. P.; Bowman, C. N.; Anseth, K. S. *Biomaterials* **2009**, *30*, 6702–6707.
- (187) Pitto-Barry, A.; Barry, N. P. E. *Polym. Chem.* **2014**, *5*, 3291–3297.
- (188) Wu, W.; DeConinck, A.; Lewis, J. A. *Adv. Mater.* **2011**, *23*, H178–H183.
- (189) Kolesky, D. B.; Homan, K. A.; Skylar-Scott, M. A.; Lewis, J. A. *Proc. Natl. Acad. Sci. U. S. A.* **2016**, *113*, 3179–3184.
- (190) Lin, N. Y.; Homan, K. A.; Robinson, S. S.; Kolesky, D. B.; Duarte, N.; Moisan, A.; Lewis, J. A. *Proc. Natl. Acad. Sci. U. S. A.* **2019**, *116*, 5399–5404.
- (191) Skylar-Scott, M. A.; Uzel, S. G.; Nam, L. L.; Ahrens, J. H.; Truby, R. L.; Damaraju, S.; Lewis, J. A. *Sci. Adv.* **2019**, *5*, eaaw2459.
- (192) Homan, K. A.; Kolesky, D. B.; Skylar-Scott, M. A.; Herrmann, J.; Obuobi, H.; Moisan, A.; Lewis, J. A. *Sci. Rep.* **2016**, *6*, 34845.
- (193) Millik, S. C.; Dostie, A. M.; Karis, D. G.; Smith, P. T.; McKenna, M.; Chan, N.; Curtis, C. D.; Nance, E.; Theberge, A. B.; Nelson, A. *Biofabrication* **2019**, *11*, 045009.
- (194) Fu, Z.; Naghieh, S.; Xu, C.; Wang, C.; Sun, W.; Chen, X. *Biofabrication* **2021**, *13*, 033001.
- (195) Duan, B.; Hockaday, L. A.; Kang, K. H.; Butcher, J. T. *J. Biomed. Mater. Res. A* **2013**, *101*, 1255–1264.
- (196) Jin, Y.; Chai, W.; Huang, Y. *ACS Appl. Mater. Interfaces* **2018**, *10*, 28361–28371.
- (197) Jin, Y.; Liu, C.; Chai, W.; Compaan, A.; Huang, Y. *ACS Appl. Mater. Interfaces* **2017**, *9*, 17456–17465.
- (198) Yu, Y.; Zhang, Y.; Martin, J. A.; Ozbolat, I. T. *J. Biomech. Eng.* **2013**, *135*, 0910111–0910119.
- (199) Colosi, C.; Shin, S. R.; Manoharan, V.; Massa, S.; Costantini, M.; Barbetta, A.; Dokmeci, M. R.; Dentini, M.; Khademhosseini, A. *Adv. Mater.* **2016**, *28*, 677–684.
- (200) Pi, Q.; Maharjan, S.; Yan, X.; Liu, X.; Singh, B.; van Genderen, A. M.; Robledo-Padilla, F.; Parra-Saldivar, R.; Hu, N.; Jia, W.; Xu, C.; Kang, J.; Hassan, S.; Cheng, H.; Hou, X.; Khademhosseini, A.; Zhang, Y. S. *Adv. Mater.* **2018**, *30*, 1706913.
- (201) Hözl, K.; Lin, S.; Tytgat, L.; Van Vlierberghe, S.; Gu, L.; Ovsianikov, A. *Biofabrication* **2016**, *8*, 032002.
- (202) Ning, L.; Betancourt, N.; Schreyer, D. J.; Chen, X. *ACS Biomater. Sci. Eng.* **2018**, *4*, 3906–3918.
- (203) Moon, J. J.; Saik, J. E.; Poché, R. A.; Leslie-Barbick, J. E.; Lee, S.-H.; Smith, A. A.; Dickinson, M. E.; West, J. L. *Biomaterials* **2010**, *31*, 3840–3847.
- (204) Nichol, J. W.; Koshy, S. T.; Bae, H.; Hwang, C. M.; Yamanlar, S.; Khademhosseini, A. *Biomaterials* **2010**, *31*, 5536–5544.
- (205) Lin, S.; Sangaj, N.; Razafiarison, T.; Zhang, C.; Varghese, S. *Pharm. Res.* **2011**, *28*, 1422–1430.
- (206) Hori, A.; Watabe, Y.; Yamada, M.; Yajima, Y.; Utoh, R.; Seki, M. *ACS Appl. Bio. Mater.* **2019**, *2*, 2237–2245.
- (207) Ying, G. L.; Jiang, N.; Maharjan, S.; Yin, Y. X.; Chai, R. R.; Cao, X.; Yang, J. Z.; Miri, A. K.; Hassan, S.; Zhang, Y. S. *Adv. Mater.* **2018**, *30*, 1805460.
- (208) Bao, G.; Jiang, T.; Ravanbakhsh, H.; Reyes, A.; Ma, Z.; Strong, M.; Wang, H.; Kinsella, J. M.; Li, J.; Mongeau, L. *Mater. Horiz.* **2020**, *7*, 2336–2347.
- (209) Ying, G. L.; Jiang, N.; Maharjan, S.; Yin, Y. X.; Chai, R. R.; Cao, X.; Yang, J. Z.; Miri, A. K.; Hassan, S.; Zhang, Y. S. *Adv. Mater.* **2018**, *30*, 1805460.
- (210) Nagarajan, N.; Dupret-Bories, A.; Karabulut, E.; Zorlutuna, P.; Vrana, N. E. *Biotechnol. Adv.* **2018**, *36*, 521–533.
- (211) Noor, N.; Shapira, A.; Edri, R.; Gal, I.; Wertheim, L.; Dvir, T. *Adv. Sci.* **2019**, *6*, 1900344.
- (212) Qiu, K.; Haghighatiani, G.; McAlpine, M. C. *Annu. Rev. Anal. Chem.* **2018**, *11*, 287–306.
- (213) Chaudhuri, O.; Cooper-White, J.; Janmey, P. A.; Mooney, D. J.; Shenoy, V. B. *Nature* **2020**, *584*, 535–546.
- (214) O'Connell, C. D.; Zhang, B.; Onofriolo, C.; Duchi, S.; Blanchard, R.; Quigley, A.; Bourke, J.; Gambhir, S.; Kapsa, R.; Di Bella, C.; Choong, P.; Wallace, G. G. *Soft Matter* **2018**, *14*, 2142–2151.
- (215) Ravanbakhsh, H.; Bao, G.; Luo, Z.; Mongeau, L. G.; Zhang, Y. S. *ACS Biomater. Sci. Eng.* **2020**, *7*, 4009–4026.
- (216) Zhu, K.; Shin, S. R.; van Kempen, T.; Li, Y. C.; Ponraj, V.; Nasajpour, A.; Mandla, S.; Hu, N.; Liu, X.; Leijten, J. *Adv. Funct. Mater.* **2017**, *27*, 1605352.
- (217) Cidonio, G.; Alcalá-Orozco, C. R.; Lim, K. S.; Glinka, M.; Mutreja, I.; Kim, Y.-H.; Dawson, J. I.; Woodfield, T. B.; Oreffo, R. O. *Biofabrication* **2019**, *11*, 035027.
- (218) Cui, H.; Esworthy, T.; Zhou, X.; Hann, S. Y.; Glazer, R. I.; Li, R.; Zhang, L. G. *Adv. Healthc. Mater.* **2020**, *9*, 1900924.
- (219) Zhu, W.; Cui, H.; Boualam, B.; Masood, F.; Flynn, E.; Rao, R. D.; Zhang, Z.-Y.; Zhang, L. G. *Nanotechnology* **2018**, *29*, 185101.
- (220) Lee, Y.-W.; Ceylan, H.; Yasa, I. C.; Kilic, U.; Sitti, M. *ACS Appl. Mater. Interfaces* **2021**, *13*, 12759–12766.
- (221) Qin, J.; Asempah, I.; Laurent, S.; Fornara, A.; Muller, R. N.; Muhammed, M. *Adv. Mater.* **2009**, *21*, 1354–1357.
- (222) Tottori, S.; Zhang, L.; Qiu, F.; Krawczyk, K. K.; Franco-Obregón, A.; Nelson, B. J. *Adv. Mater.* **2012**, *24*, 811–816.
- (223) Gong, J. P.; Katsuyama, Y.; Kurokawa, T.; Osada, Y. *Adv. Mater.* **2003**, *15*, 1155–1158.
- (224) Sun, J.-Y.; Zhao, X.; Illeperuma, W. R.; Chaudhuri, O.; Oh, K. H.; Mooney, D. J.; Vlassak, J. J.; Suo, Z. *Nature* **2012**, *489*, 133.
- (225) Fuchs, S.; Shariati, K.; Ma, M. *Adv. Healthc. Mater.* **2020**, *9*, 1901396.
- (226) Oveissi, F.; Fletcher, D. F.; Dehghani, F.; Naficy, S. *Mater. Des.* **2021**, 109609.
- (227) Dubbin, K.; Hori, Y.; Lewis, K. K.; Heilshorn, S. C. *Adv. Healthc. Mater.* **2016**, *5*, 2488–2492.
- (228) Hong, S.; Sycks, D.; Chan, H. F.; Lin, S.; Lopez, G. P.; Guilak, F.; Leong, K. W.; Zhao, X. *Adv. Mater.* **2015**, *27*, 4035–4040.
- (229) Skardal, A.; Mack, D.; Kapetanovic, E.; Atala, A.; Jackson, J. D.; Yoo, J.; Soker, S. *Stem Cells Transl. Med.* **2012**, *1*, 792–802.
- (230) Sultan, S.; Mathew, A. P. *Nanoscale* **2018**, *10*, 4421–4431.
- (231) Zhou, X.; Cui, H.; Nowicki, M.; Miao, S.; Lee, S.-J.; Masood, F.; Harris, B. T.; Zhang, L. G. *ACS Appl. Mater. Interfaces* **2018**, *10*, 8993–9001.
- (232) Jia, W.; Gungor-Ozkerim, P. S.; Zhang, Y. S.; Yue, K.; Zhu, K.; Liu, W.; Pi, Q.; Byambaa, B.; Dokmeci, M. R.; Shin, S. R.; Khademhosseini, A. *Biomaterials* **2016**, *106*, 58–68.
- (233) Dobos, A.; Van Hoorick, J.; Steiger, P.; Gruber, P.; Markovic, M.; Andriotis, O. G.; Rohatschek, A.; Dubrue, P.; Thurner, P. J.; Van Vlierberghe, S.; Baudis, S.; Ovsianikov, A. *Adv. Healthc. Mater.* **2020**, *9*, e1900752.

- (234) Hong, S.; Kim, J. S.; Jung, B.; Won, C.; Hwang, C. *Biomater. Sci.* **2019**, *7*, 4578–4587.
- (235) Soliman, B. G.; Lindberg, G. C. J.; Jungst, T.; Hooper, G. J.; Groll, J.; Woodfield, T. B. F.; Lim, K. S. *Adv. Healthc. Mater.* **2020**, *9*, 1901544.
- (236) Ju, J.; Hu, N.; Cairns, D. M.; Liu, H.; Timko, B. P. *Proc. Natl. Acad. Sci. U. S. A.* **2020**, *117*, 15482–15489.
- (237) Gao, G.; Park, W.; Kim, B. S.; Ahn, M.; Chae, S.; Cho, W. W.; Kim, J.; Lee, J. Y.; Jang, J.; Cho, D. W. *Adv. Funct. Mater.* **2021**, *31*, 2008878.
- (238) Gao, G.; Park, J. Y.; Kim, B. S.; Jang, J.; Cho, D. W. *Adv. Healthc. Mater.* **2018**, *7*, 1801102.
- (239) Gao, G.; Kim, H.; Kim, B. S.; Kong, J. S.; Lee, J. Y.; Park, B. W.; Chae, S.; Kim, J.; Ban, K.; Jang, J. *Appl. Phys. Rev.* **2019**, *6*, 041402.
- (240) Hiller, T.; Berg, J.; Elomaa, L.; Röhrs, V.; Ullah, I.; Schaar, K.; Dietrich, A.-C.; Al-Zeer, M. A.; Kurtz, A.; Hocke, A. C. *Int. J. Mol. Sci.* **2018**, *19*, 3129.
- (241) Kim, M. H.; Nam, S. Y. *Bioprinting* **2020**, *20*, e00092.
- (242) Gao, Y.; Jin, X. *Mar. Drugs* **2019**, *17*, 557.
- (243) Aldana, A. A.; Valente, F.; Dilley, R.; Doyle, B. *Bioprinting* **2021**, *21*, e00105.
- (244) Reakasame, S.; Boccaccini, A. R. *Biomacromolecules* **2018**, *19*, 3–21.
- (245) Gao, C.; Liu, M.; Chen, J.; Zhang, X. *Polym. Degrad. Stab.* **2009**, *94*, 1405–1410.
- (246) Choe, G.; Park, J.; Jo, H.; Kim, Y. S.; Ahn, Y.; Lee, J. Y. *Int. J. Biol. Macromol.* **2019**, *123*, 512–520.
- (247) Petta, D.; D'Amora, U.; Ambrosio, L.; Grijpma, D.; Eglin, D.; D'Este, M. *Biofabrication* **2020**, *12*, 032001.
- (248) Müller, M.; Becher, J.; Schnabelrauch, M.; Zenobi-Wong, M. *Biofabrication* **2015**, *7*, 035006.
- (249) Ren, P.; Zhang, H.; Dai, Z.; Ren, F.; Wu, Y.; Hou, R.; Zhu, Y.; Fu, J. *J. Mater. Chem. B* **2019**, *7*, 5490–5501.
- (250) Sakai, S.; Komatani, K.; Taya, M. *RSC Adv.* **2012**, *2*, 1502–1507.
- (251) Shriky, B.; Kelly, A.; Isreb, M.; Babenko, M.; Mahmoudi, N.; Rogers, S.; Shebanova, O.; Snow, T.; Gough, T. *J. Colloid Interface Sci.* **2020**, *565*, 119–130.
- (252) Chatterjee, S.; Hui, P. C.-I.; Kan, C.-w.; Wang, W. *Sci. Rep.* **2019**, *9*, 11658.



subscribe today

Don't miss another
topically focused technical review.

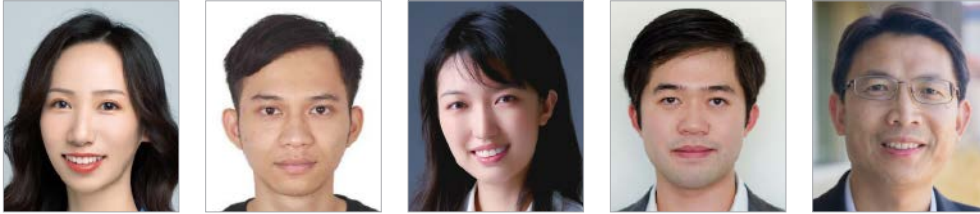
It's **free** to sign up for a print or digital
subscription of *Material Matters*™.

- Advances in cutting-edge materials
- Technical reviews on emerging technology from leading scientists
- Peer-recommended materials with application notes
- Product and service recommendations



To view the library of past issues
or to subscribe, visit
SigmaAldrich.com/mm

3D Bioprinting of Functional Tissue Models



Min Tang,¹ Shangting You,¹ Jennifer Sun,² Wei Zhu,² Shaochen Chen^{1*}

¹ Department of NanoEngineering, University of California, San Diego, 9500 Gilman Drive, La Jolla, California, 92093, USA.

² Allegro 3D, Inc, 6868 Nancy Ridge Drive, San Diego, California, 92121, USA.

* Email: chen168@eng.ucsd.edu

Introduction

The emergence of new technologies in tissue engineering and regenerative medicine promises to make a number of previously impossible applications a reality, such as personalized functional human tissues and organ replacement. Among currently available strategies and techniques, 3D bioprinting is creating a paradigm shift in how to build a wide range of complex tissues that recapitulate the *in vivo* cellular heterogeneity, microarchitectures, biophysical properties, and biochemical constituents. More specifically, 3D bioprinting enables precise control over the patterning of cells and biomaterials to mimic and ultimately replace the native arrangement of tissues. To date, numerous tissues have been fabricated using 3D bioprinting technology, including but not limited to liver, heart, lung, kidney, blood vessels, cartilage, and placenta.¹⁻⁷ These bioprinted tissues have essential applications in various biological and medical areas, serving as physiologically relevant models to elucidate biological mechanisms and screen drug compounds, lab-on-chip devices when integrated with biosensors and microfluidics, or transplantable tissues and regenerative medicines. This article reviews the current state of 3D bioprinting, highlights current work on 3D bioprinted tissue models, and discusses advanced bioinks such as gelatin methacrylate (GelMA) and decellularized extracellular matrix (dECM) that can facilitate the development of physiologically-relevant tissues.

3D Bioprinting Technologies

Several different 3D bioprinting technologies (Figure 1) are currently capable of processing cell-laden biomaterials and directly constructing complex 3D structures. These technologies include inkjet-based 3D printing, light-based 3D printing, and extrusion-based 3D printing, with each varying in terms of print resolution, speed, and biocompatibility.^{8,9}

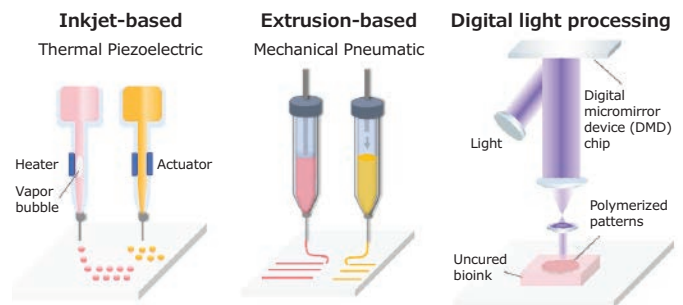


Figure 1. Different modes of 3D bioprinting technologies. Adapted with permission from reference 75, copyright 2021 Wiley.

Inkjet-based bioprinting

The 3D inkjet printer, first adopted from common desktop ink-based paper printers, deposits biomaterials and cells in a raster-like manner.¹⁰ Inkjet-based printing methods include continuous inkjet printing and drop-on-demand inkjet printing. In continuous inkjet printing,¹¹ droplets are formed by the capillary-driven Rayleigh-Plateau instability of the liquid column. Then, these droplets are charged and can be deflected by an electric field, allowing them to be controlled to either deposit on the build platform or enter a recycling collector. In drop-on-demand inkjet printing,¹² droplets are only generated when the inkjet head is aligned with the desired area, directly depositing on the build platform. The deposited bioink is then thermally, photochemically, or ionic-interactionally crosslinked. These printers are capable of ~50 μm typical printing resolutions but can only be used with low viscosity materials.^{13,14}

Extrusion-based bioprinting

Extrusion-based bioprinters are based on the widely used fused deposition modeling (FDM) 3D printers.¹⁵ Generally, biomaterials are extruded through a nozzle tip using pneumatic or mechanical pressure and deposited on the build platform in a raster-like manner. The deposited bioink is then thermally, photochemically, or ionic-interactionally crosslinked. These printers are relatively low cost, have ~50 μm typical resolution, and can accommodate a larger range of material viscosities than inkjet printers.^{16,17} Extrusion-based 3D bioprinting techniques are capable of high cell density or cell spheroid printing.¹⁸ However, the shearing force applied to the extruded biomaterials during extrusion can decrease cell viability.⁸

Light-based bioprinting

The concept of light-based 3D printing is inspired by photolithography. The liquid state printing materials can be photochemically polymerized and solidified upon light exposure; thus, a 3D structure is made by selectively delivering light energy to the desired location. Light can be delivered via scanning fashion, such as in stereolithography,¹⁹ or through imaging projection such as DLP-based bioprinting.^{20,21} Scanning stereolithography induces photopolymerization at the focal spot of the focusing light and creates 3D structures by scanning. Microstructures can be produced with a micron-scale resolution;^{19,22} even sub-micron scale resolution is possible when a two-photon photopolymerization is used.^{23,24}

DLP-based 3D bioprinting has emerged as a promising technique. Unlike inkjet-based, extrusion-based, or scanning stereolithography, where construction of a 3D structure occurs in a point scanning method, DLP-based 3D printing projects a 2D pattern and polymerizes the entire plane simultaneously, achieving much faster printing speed. In general, the 3D model is sliced into a series of 2D cross-sections and projected on the printing material to polymerize one layer of the 3D structure. The motorized stage controls the vertical position of the printed part and allows printing of the subsequent layer in a discrete layer-by-layer fashion^{25,26} or a continuous layer-less fashion.^{27,28} The typical fabrication resolution of DLP-based 3D bioprinting is a few microns where a de-magnification lens is used.²⁸

Compared to inkjet-based and extrusion-based 3D printing, light-based 3D printing can achieve better fabrication resolution (micron and sub-micron scale) due to the precise manipulation of light. Also, DLP-based 3D printing can achieve a printing speed that is a thousand times faster than an extrusion-based printing method. Furthermore, light-based 3D printing has demonstrated suitability for cell encapsulation to form biomimetic tissue constructs^{1,5,27,29} where higher cell viability is achieved as the shearing force or heating is absent. However, the light-based method requires photopolymerizable materials, which limits the range of material choices.

To date, new bioprinting techniques with improved performance and novel features are being actively researched and developed. Each technique has its advantages and disadvantages, and it is essential to select the most suitable bioprinter for the specific bioapplication carefully.

Bioinks

3D bioprinting techniques now utilize a growing variety of natural biomaterials and synthetic materials for biomedical applications. Natural materials, such as gelatin, hyaluronic acid, collagen, and derivatives, possess good biocompatibility and innate bioactive features that are ideal for cell growth. Synthetic materials lack the inherent biochemical cues of natural materials but have tunable mechanical properties suitable for bioprinting purposes. Composite materials or chemical modifications to materials are standard methods that improve the biomimicry or printability of bioinks.

Gelatin and GelMA

Gelatin, a partial hydrolysis product of collagen, is widely used in extrusion-based bioprinting due to its good rheological properties and thermal responsiveness. It possesses good biocompatibility and intrinsic bioactivity, including integrin-binding and MMP digestion sites. Gelatin is used for many tissue printing models, including skin tissues and liver tissues, due to the presence of collagen in many organs. Hepatocytes encapsulated in 3D-bioprinted gelatin hydrogel can remain functional over two months of culture.³⁰ When mixed with synthetic materials to form composite bioinks, gelatin-based biomaterials exhibit higher resolution and printability while maintaining cell viability and proliferation.³¹ GelMA is one of the most widely used biomaterials for light-based bioprinting due to its photo-sensitivity and gelatin-derived biological features. GelMA is synthesized from gelatin by substituting the lysine and hydroxyl groups with methacrylamide and methacrylate side groups;³² the rate of substitution impacts the mechanical properties of the bioprinted GelMA constructs. Various tissue models such as liver models, heart models, conjunctiva models, as well as disease models, including glioblastoma models and liver cirrhosis, have been developed using GelMA.³³⁻³⁶ GelMA has also been combined with synthetic materials such as PEGDA to generate a cardiac patch to treat myocardial infarction or regenerative construct for spinal cord injury.^{37,38}

GMHA, HAMA

Hyaluronic acid (HA) is another ubiquitous extracellular matrix (ECM) component. It is comprised of linear polysaccharides with alternating d-glucuronic acid and N-acetyl-d-glucosamine.³⁹ The negatively charged HA can attract a large volume of water, making it ideal for regulating the hydration state, porosity, and various other mechanical properties of many tissues. HA also plays a critical role in regulating physiological processes and is involved in various pathological events through interaction with cells and other ECM components. Unmodified HA lacks good printability, but it can be combined with various printable biomaterials to generate 3D tissue models for mechanistic studies and phenotypic analyses.⁴⁰⁻⁴³ For example, bioprinted brain tumor models demonstrate higher invasiveness in HA-GelMA hydrogel consisting of low molecular weight HAs than in high molecular weight HA models.⁴¹ HA-based biomaterials with different molecular weights are appropriate for modeling brain tissue and many tumor tissues.⁴⁴ Chemical modifications to improve printability of HA generally target the carboxylate group, the N-acetyl group, or the hydroxyl groups on both moieties.

Glycidyl methacrylate functionalized HA (GMHA), or methacrylic anhydride functionalized HA (HAMA) are popular bioinks for light-based bioprinting, especially DLP-based bioprinting, due to their photo-responsiveness once chemically modified. Brain tumor models and liver tissue models have been developed with GMHA using DLP-based bioprinting techniques.^{33,34} Unlike gelatin-based biomaterials, HA-based materials do not possess innate Arg-Gly-Asp (RGD) sites; thus, HAMA functionalized RGD peptides have been bioprinted to facilitate cell adhesion.⁴⁵ HA-based constructs can also be developed using extrusion-based or inkjet-based bioprinting techniques through addition and condensation reactions. For example, HA-thiol biomaterials can spontaneously polymerize through the formation of disulfide bonds.⁴⁶

dECM

dECM has emerged as a popular next-generation bioink due to its ability to preserve the complexity of native ECM composition. The biochemical cues of dECM can support tissue-specific cell growth and behaviors.³⁶ After removing cellular components, dECM derived from patient brain tissue shows that significant ECM components, including glycosaminoglycans, HA, collagen, laminin, and fibronectin, are preserved.⁴⁷ Similarly, dECM derived from liver tissue shows native ECM components such as collagen I, collagen IV, laminin, and fibronectin.³⁶ dECM is often mixed with other printable biomaterials for tissue modeling for bioprinting purposes due to its relatively slow gelation kinetics. Recently, dECM has also been independently printed through thermal gelation.⁴⁸⁻⁵⁰ Liver dECM mixed with GelMA has been used to fabricate the liver cancer model through DLP-based bioprinting with different stiffness matching the healthy and cirrhosis states.³⁶ Patient brain dECM mixed with collagen has been used to generate brain cancer models with improved printability on extrusion-based bioprinters.⁴⁷ dECM enhanced the heterogeneity of tumor cell morphology and the expression of matrix remodeling protein tumor cells compared to a pure collagen hydrogel. Various other tissues, including heart, adipose, and cartilage, have been bioprinted using dECM-based bioinks.^{36,49-52} Despite the potential downside of batch variation due to the diversity present from its primary sources, dECM has opened an avenue of precision medicine applications.

Alginate

Alginates are derivatives of alginic acid from brown algae. Alginate bioinks are commonly employed in extrusion-based bioprinting because of their adept gelation and their good mechanical properties. Various chemical modifications to alginate, such as methacrylation and norbornene functionalization, enable their use in light-based bioprinting or improve their polymerization and degradation kinetics.^{53,54} Alginate hydrogels have demonstrated good biocompatibility and have been used to develop different tissue engineering applications and tissue types, such as cardiac tissue, cornea, bone, and cartilage.⁵⁵

PEGDA

Various synthetic materials have been explored for 3D printing purposes. Polyethylene glycol (PEG) is a biocompatible and bio-inert synthetic polymer that can be combined with other bioinks or peptides to improve biomimicry for tissue modeling.⁵⁶⁻⁵⁸ Brain tumor models fabricated with PEG-HA hydrogel functionalized with RGD peptides and MMP degradation crosslinkers display different cell morphologies at different stiffness states.⁵⁹ A derivative of PEG, polyethylene glycol diacrylate (PEGDA), is light-responsive material suitable for light-based printing methods with good biocompatibility and tunable mechanical properties.³⁸ PEGDA combined with GelMA has been used to fabricate regenerative constructs through DLP-based bioprinting for spinal cord injury, exhibiting good biocompatibility and long-term integrity when implanted.^{60,61}

3D Bioprinted Functional Healthy/Diseased Tissue Models

Multiple cell types co-exist *in vivo* and communicate with each other through paracrine signaling and interactions with the surrounding ECM microenvironment to form a functional tissue unit.⁶² Creating truly biomimetic tissues *in vitro* requires the recapitulation of heterogeneous cell populations and their proper spatial arrangement within a relevant ECM microenvironment. As such, 3D bioprinting technologies offer a precise way to pattern various cell types and biomaterials. The source of cells is also of great importance in the context of creating physiologically relevant tissue models. The majority of printed tissues produced to date use established cell lines or animal cells, but these cells cannot fully reflect the behavior and function of human primary cells.⁶³ Human stem cells (hSCs), including embryonic stem cells (hESCs) and induced pluripotent stem cells (hiPSCs), with the proliferation capacity and potential to differentiate into various cell types such as cardiac cells, liver cells, and neuronal cells, have promising applications in 3D bioprinting.⁶⁴ Primary human cells derived from healthy individuals or patients are also desirable for biomimetic *in vitro* tissue modeling.

Biomimetic Human Healthy Tissue Models Based on hSCs

Diseases associated with liver and heart are significant contributors to mortality in the United States.^{65,66} Additionally, the liver is involved in xenobiotic and drug metabolism, making the investigation of hepatotoxicity essential to drug studies. Another critical factor for evaluating novel drugs is cardiotoxicity, which is the primary reason for drug retraction from the market.⁶⁷ Various 3D bioprinting approaches combined with human iPSCs have been explored to create *in vitro* liver or cardiac tissues for use in these applications.

Human iPSC and ESC-derived hepatocyte-like cells have been encapsulated by inkjet-based bioprinting in alginate hydrogels to create 3D liver constructs.⁶⁸ Hepatic cells in these 3D-printed constructs showed good viability and functionality such as albumin secretion. A more complex and biomimetic hepatic model has been developed using DLP-based bioprinting, with the

encapsulation of iPSC-derived hepatic progenitor cells (hiPSC-HPCs), human umbilical vascular endothelial cells (HUVECs), and human adipose-derived stem cells (ADSCs). GelMA was mixed with hiPSC-HPCs for the hepatic region, and GelMA-GMHA was mixed with HUVECs and ADSCs for the vascular region. Patterning of the hepatic and vascular regions via a two-step printing process mimicked tissue-scale anatomical features and dimensions of the actual liver (**Figure 2**).

Immunohistochemical staining of albumin and E-cadherin in 3D hepatic tri-culture constructs revealed more extensive aggregation and spheroid formation than hiPSC-HPC only 3D controls, suggesting a higher degree of cell junction formation, maturation, and functionality. Tri-cultured hepatic cells also expressed a higher level of crucial liver markers, including albumin, hepatocyte nuclear factor 4 alpha (HNF4a), transthyretin (TTR), and alpha fetal protein (AFP), compared to the 3D hiPSC-HPC only control and the 2D monolayer control. The 3D hepatic tri-culture model could also serve as a platform for drug screening. Assessment of anabolic and catabolic functions of hepatic cells in 3D printed constructs occurred by examining the expression of crucial cytochrome P450 (CYP) enzymes involved in liver drug metabolism.⁶⁹ Baseline CYP levels without drug treatment showed that the 3D tri-culture model expressed elevated levels of CYP3A4, CYP1A2, CYP2B6, CYP2C9, and CYP2C19 compared to the 3D hiPSC-HPC only and 2D control. Upon introducing rifampicin, a known bactericidal antibiotic drug to induce hepatotoxicity,⁷⁰ the 3D tri-culture model exhibited increased CYP3A4, CYP2C9, and CYP2C19 expression, while no significant change in CYP expressions was observed in the 3D hiPSC-HPC only or 2D controls.

Cardiac tissues have also been bioprinted using iPSC-derived cardiomyocytes (iPSC-CMs) and various bioinks. An

extrusion-based approach encapsulated iPSC-CMs and HUVECs in alginate and PEG-fibrinogen hydrogel to produce an implantable, pre-vascularized cardiac patch.⁷¹ Patient-derived iPSCs can be differentiated into iPSC-CM and iPSC-derived endothelial cells as cell sources for a personalized cardiac patch fabricated by extrusion-based bioprinting.⁷² A DLP-based bioprinting approach has been used to generate cardiac arrays for high throughput drug screening.³⁵ Different orientations of iPSC-CMs were printed on force gauge arrays, and the iPSC-CMs exhibited the highest expression of cardiac-related markers and enhanced contractile forces under drug treatment. A recent study used freeform reversible embedding of suspended hydrogels (FRESH), an extrusion-based technique, to fabricate human heart tissues using hESC-derived cardiomyocytes (hESC-CM) and chemically unmodified collagen (**Figure 3A**).⁷³ Spontaneous contraction of the bioprinted cardiac ventricle was observed after 4 days of culture, and synchronous wave propagation was confirmed after 7 days (**Figure 3B,C**). Mechanical integrity of the collagen constructs was confirmed using a tri-leaflet heart valve model. Lastly, a neonatal-scale heart consisting of internal structures such as trabeculae and blood vessels was printed using this technique as a proof-of-concept for full-scale heart printing (**Figure 3D**).

3D bioprinting can produce functional hepatic and cardiac models that recapitulate both the native tissue architecture and cellular diversity. Incorporating hSC-derived cells in the tissue models enables their potential applications as patient-specific models to study various pathophysiological disease mechanisms and serve as drug screening and discovery platforms.

Biomimetic Human Diseased Tissue Model

In addition to healthy tissue models, patient-derived disease models and cancer models are essential tools for investigating disease mechanisms and drug development. Due to the flexibility

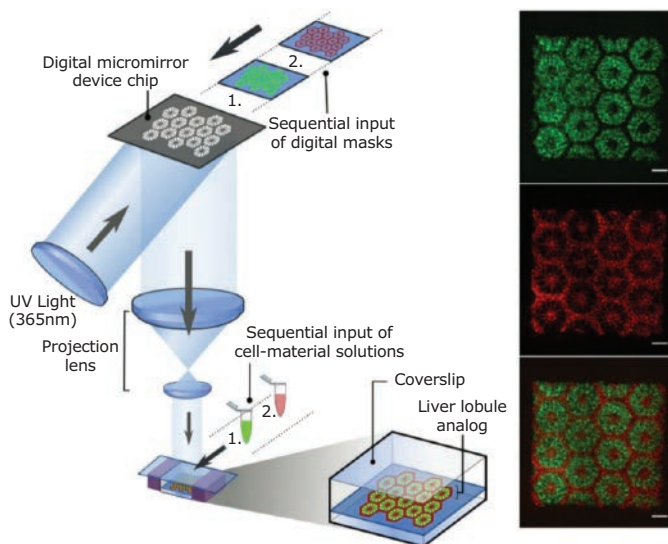


Figure 2. Human hepatic constructs by DLP-based 3D bioprinting. The construct was fabricated through a two-step printing process in which hiPSC-HPCs were patterned as hexagonal shapes (green) first, followed by the patterning of supporting cells (red): scale bars, 500 μ m. Adapted with permission from reference 1, copyright 2016 National Academy of Sciences.

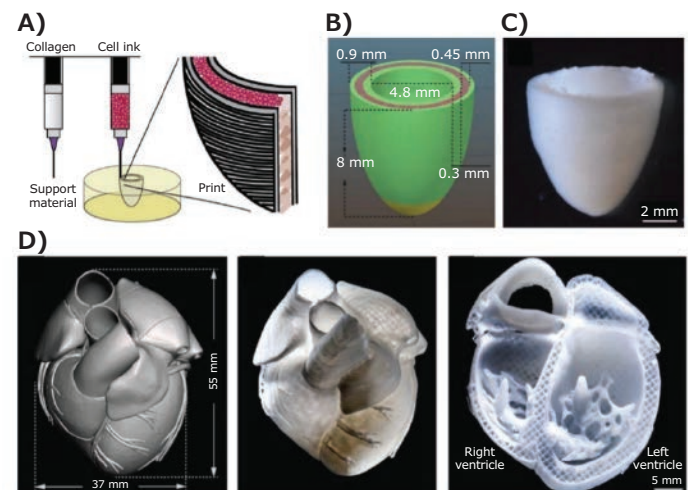


Figure 3. Human cardiac constructs by FRESH 3D bioprinting. **A)** Schematic of dual-material FRESH printing. **B)** The ventricle model has a central section of cardiac cells (pink) and a collagen shell (green and yellow). **C)** Image of the bioprinted ventricle. **D)** Neonatal-scale human heart printed based on a human heart MRI scan using FRESH. Adapted with permission from reference 73, copyright 2019 Springer.

and customizability of 3D bioprinting technology, it is especially suitable for precision medicine cancer models and recapitulation of the tumor heterogeneity to facilitate novel drug development.

A regionally patterned liver cancer model has been developed using a DLP-based bioprinter with liver dECM, collagen, GelMA, and HepG2 liver cancer cells.³⁶ Here, the stiffness of the printed hydrogel was tuned to mimic the stiffness of liver cirrhosis and normal tissue, while the dECM provided biomimetic ECM cues for cell growth. It was observed that HepG2 cells demonstrated enhanced invasion markers in the liver cirrhosis model compared to healthy controls. The work demonstrated the potential of DLP printing in recapitulating specific mechanical properties of native tissue while preserving the biochemical feature using natural biomaterials.

Brain tumor models have also been generated using different bioprinting techniques. An extrusion-based bioprinting method utilized brain dECM, patient-derived glioblastoma cells, and endothelial cells to investigate patient-specific responses to chemotherapy (Figure 4A).⁷⁴ The glioblastoma-on-a-chip consisted of a tumor region, an endothelial region, an empty chamber for medium, and a silicon wall to create oxygen gradient in the tissue. Various drug combinations were tested using a bioprinted chip to identify treatment plans with superior tumor killing ability. A multicellular glioblastoma model was also developed using DLP-based bioprinting and GelMA and GMHA as bioinks to encapsulate patient-derived glioblastoma stem cells (GSCs), macrophages, astrocytes, and neural progenitor cells (NPCs) in a tumor-parenchyma structure (Figure 4B).³⁴ Macrophages were co-printed with GSCs to form the tumor core, which mimicked the actual cellular composition of glioblastoma tumor mass (Figure 3C). Astrocytes and NPCs were printed on the periphery to encompass the tumor core. GSCs in the tetra-cellular model

demonstrated enhanced invasion and resistance to chemotherapy, while macrophages in the tetra-cellular model exhibited spontaneous polarization towards pro-tumor M2 phenotype. The model could be used as a drug screening platform to predict therapeutic outcomes or a CRISPR-Cas9 screening platform to identify novel drug targets (Figure 4D). Genes identified as essential in 3D-printed models were critical to cell viability *in vitro* and involved in a shorter survival time of experimental animals.

Conclusions

3D bioprinting technology has led to many breakthrough developments of *in vitro* tissue models and disease models for applications in mechanistic studies, drug screening, tissue engineering, and regenerative medicine. DLP-based 3D bioprinting enables rapid fabrication of complex cell-encapsulated architecture with microscale resolution and physiologically relevant structures. The human biomimetic 3D hepatic triculture and cardiac models developed by DLP-based printing composed of human iPSC-derived hepatic progenitor cells or iPSC-derived cardiac cells have enhanced functionality compared to traditional culture methods. They can provide reliable evaluation of drugs and compounds. Extrusion-based printing has the advantage of simplified scale-up to the size of the printed constructs using unmodified natural materials, but with relatively limited printing resolution compared to light-based printing. In conclusion, the future direction of 3D bioprinting for *in vitro* tissues and organs will involve multiple facets, namely, heterogeneous cell populations, proper biomaterials, relevant architecture mimicking native structures, as well as intricate vascular and neuronal networks to maintain long term growth and maturation of the tissues, to provide a tissue-specific microenvironment for enhanced functionality and biomimicry.

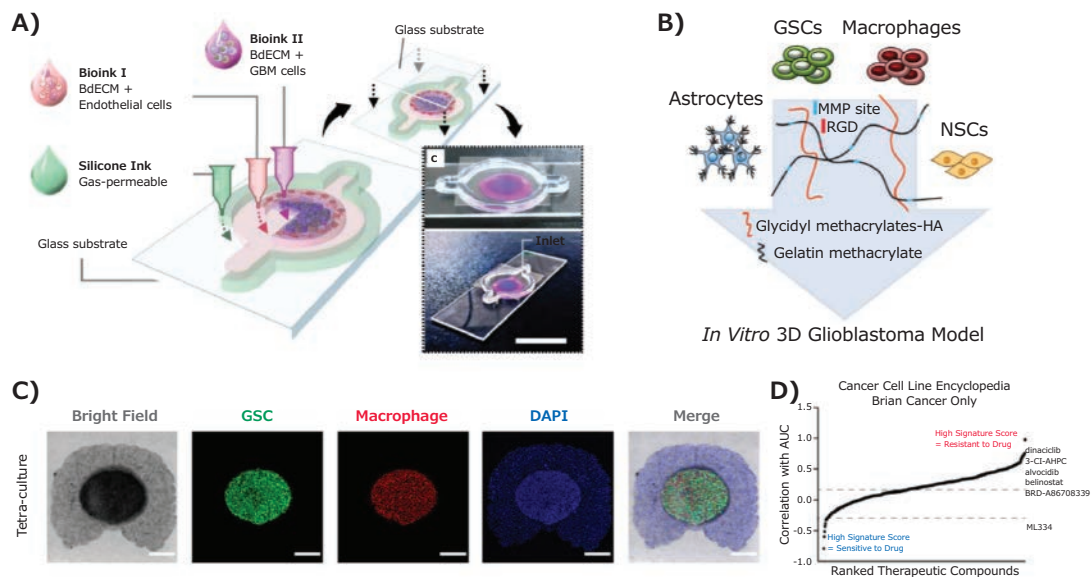


Figure 4. Human glioblastoma models by 3D bioprinting. **A)** Glioblastoma-on-a-chip using extrusion-based bioprinting. **B)** Illustration of components of a multicellular glioblastoma model using DLP-based bioprinting. Figures A and B adapted with permission from reference 74, copyright 2019 Springer. **C)** Image of the bioprinted glioblastoma model. GSC (green), macrophage (red), NPC and astrocyte (blue). Scale bar, 500 μm . **D)** Prediction of drug sensitivity based on the transcriptional profile of GSCs in the 3D bioprinted model. Figures C and D adapted with permission from reference 34, copyright 2020 Nature.

References

- (1) Ma, X.; Qu, X.; Zhu, W.; Li, Y.-S.; Yuan, S.; Zhang, H.; Liu, J.; Wang, P.; Lai, C. S. E.; Zanella, F.; Feng, G.-S.; Sheikh, F.; Chien, S.; Chen, S. *PNAS* **2016**, *113*, 2206.
- (2) Lind, J. U.; Busbee, T. A.; Valentine, A. D.; Pasqualini, F. S.; Yuan, H.; Yacid, M.; Park, S.-J.; Kotikian, A.; Nesmith, A. P.; Campbell, P. H.; Vlissak, J. J.; Lewis, J. A.; Parker, K. K. *Nat. Mater.* **2016**, *16*, 303.
- (3) Eisenstein, M. *Nature* **2015**, *519*, S16.
- (4) Homan, K. A.; Kolesky, D. B.; Skylar-Scott, M. A.; Herrmann, J.; Obuobi, H.; Moisan, A.; Lewis, J. A. *Sci. Rep.* **2016**, *6*, 34845.
- (5) Zhu, W.; Qu, X.; Zhu, J.; Ma, X.; Patel, S.; Liu, J.; Wang, P.; Sun, C.; Lai, E.; Gou, M.; Xu, Y.; Zhang, K.; Chen, S. *Biomaterials* **2017**, *124*, 106.
- (6) Nguyen, D.; Hägg, D. A.; Forsman, A.; Ekholm, J.; Nimkingratana, P.; Brantsing, C.; Kalogeropoulos, T.; Zauunz, S.; Concaro, S.; Brittlberg, M.; Lindahl, A.; Gatenholm, P.; Enejder, A.; Simonsson, S. *Sci. Rep.* **2017**, *7*, 658.
- (7) Kuo, C.-Y.; Eranki, A.; Placone, J. K.; Rhodes, K. R.; Aranda-Espinoza, H.; Fernandes, R.; Fisher, J. P.; Kim, P. C. W. *ACS Biomater. Sci. Eng.* **2016**, *2*, 1817.
- (8) Unagolla, J. M.; Jayasuriya, A. C. *Appl. Mater. Today* **2020**, *18*, 100479.
- (9) Zhou, L.; Fu, J.; He, Y. *Adv. Funct. Mater.* **2020**, *30*, 2000187.
- (10) Wilson, W. C.; Boland, T. *Anat.* **2003**, *272A*, 491.
- (11) Rosello, M.; Maîtrejean, G.; Roux, D. C. D.; Jay, P.; Barbet, B.; Xing, J. J. *Fluids Eng.* **2018**, *140*, 031202.
- (12) Calvert, P. *Chem. Mater.* **2001**, *13*, 3299.
- (13) Xu, T.; Zhao, W.; Zhu, J.-M.; Albanna, M. Z.; Yoo, J. J.; Atala, A. *Biomaterials* **2013**, *34*, 130.
- (14) Zhu, W.; Ma, X.; Gou, M.; Mei, D.; Zhang, K.; Chen, S. *Curr. Opin. Biotechnol.* **2016**, *40*, 103.
- (15) Turner, B. N.; Strong, R.; Gold, S. A. *Rapid Prototyp. J.* **2014**, *20*, 192.
- (16) Blaeser, A.; Duarte Campos, D. F.; Puster, U.; Richtering, W.; Stevens, M. M.; Fischer, H. *Adv. Healthc. Mater.* **2016**, *5*, 326.
- (17) Murphy, S. V.; Atala, A. *Nat. Biotechnol.* **2014**, *32*, 773.
- (18) Mironov, V.; Visconti, R. P.; Kasyanov, V.; Forgacs, G.; Drake, C. J.; Markwald, R. R. *Biomaterials* **2009**, *30*, 2164.
- (19) Lu, Y.; Chen, S. C. *Adv. Drug Deliv. Rev.* **2004**, *56*, 1621.
- (20) Ge, Q.; Li, Z.; Wang, Z.; Kowsari, K.; Zhang, W.; He, X.; Zhou, J.; Fang, N. X. *Int. J. Extrem. Manuf.* **2020**, *2*, 022004.
- (21) Lu, Y.; Mapili, G.; Suhali, G.; Chen, S.; Roy, K. J. *Biomed. Mater. Res. A* **2006**, *77*, 396.
- (22) Mapili, G.; Lu, Y.; Chen, S.; Roy, K. J. *Biomed. Mater. Res. B Appl. Biomater.* **2005**, *75*, 414.
- (23) Paz, V. F.; Emons, M.; Obata, K.; Ovsianikov, A.; Peterhansel, S.; Frenner, K.; Reinhardt, C.; Chichkov, B.; Morgner, U.; Osten, W. *J. Laser Appl.* **2012**, *24*, 042004.
- (24) You, S.; Li, J.; Zhu, W.; Yu, C.; Mei, D.; Chen, S. *J. Mater. Chem. B* **2018**, *6*, 2187.
- (25) Sun, C.; Fang, N.; Wu, D. M.; Zhang, X. *Sens. Actuators A: Phys.* **2005**, *121*, 113.
- (26) Han, L.-H.; Suri, S.; Schmidt, C. E.; Chen, S. *Biomed. Microdevices* **2010**, *12*, 721.
- (27) Tumbleston, J. R.; Shirvanyants, D.; Ermoshkin, N.; Januszewicz, R.; Johnson, A. R.; Kelly, D.; Chen, K.; Pinschmidt, R.; Rolland, J. P.; Ermoshkin, A.; Samulski, E. T.; DeSimone, J. M. *Science* **2015**, *347*, 1349.
- (28) Zhang, A. P.; Qu, X.; Soman, P.; Hribar, K. C.; Lee, J. W.; Chen, S.; He, S. *Adv. Mater.* **2012**, *24*, 4266.
- (29) Zhang, W.; Han, L.-H.; Chen, S. *J. Manuf. Sci. Eng.* **2010**, *132*, 030907.
- (30) Wang, X.; Yan, Y.; Pan, Y.; Xiong, Z.; Liu, H.; Cheng, J.; Liu, F.; Lin, F.; Wu, R.; Zhang, R.; Lu, Q. *Tissue Eng.* **2006**, *12*, 83.
- (31) Hsieh, C.-T.; Hsu, S.-H. *ACS Appl. Mater. Interfaces* **2019**, *11*, 32746.
- (32) Van Den Bulcke, A. I.; Bogdanov, B.; De Rooze, N.; Schacht, E. H.; Cornelissen, M.; Berghmans, H. *Biomacromolecules* **2000**, *1*, 31.
- (33) Ma, X.; Qu, X.; Zhu, W.; Li, Y.-S.; Yuan, S.; Zhang, H.; Liu, J.; Wang, P.; Lai, C. S. E.; Zanella, F.; Feng, G.-S.; Sheikh, F.; Chien, S.; Chen, S. *Proc. Natl. Acad. Sci. U.S.A.* **2016**, *113*, 2206.
- (34) Tang, M.; et al. *Cell Res.* **2020**, *10*, 833.
- (35) Ma, X.; Dewan, S.; Liu, J.; Tang, M.; Miller, K. L.; Yu, C.; Lawrence, N.; McCulloch, A. D.; Chen, S. *Acta Biomater.* **2019**, *95*, 319.
- (36) Ma, X.; Yu, C.; Wang, P.; Xu, X.; Wan, W.; Lai, C. S. E.; Liu, J.; Koroleva-Maharajh, A.; Chen, S. *Biomaterials* **2018**, *185*, 310.
- (37) Cui, H.; Liu, C.; Esworthy, T.; Huang, Y.; Yu, Z.; Zhou, X.; San, H.; Lee, S.; Hann, S. Y.; Boehm, M.; Mohiuddin, M.; Fisher, J. P.; Zhang, L. G. *Sci. Adv.* **2020**, *6*, eabb5067.
- (38) Koffler, J.; Zhu, W.; Qu, X.; Platoshyn, O.; Dulin, J. N.; Brock, J.; Graham, L.; Lu, P.; Sakamoto, J.; Marsala, M.; Chen, S.; Tuszynski, M. H. *Nat. Med.* **2019**, *25*, 263.
- (39) Perkins, K. L.; Arranz, A. M.; Yamaguchi, Y.; Hrabetova, S. *Rev. Neurosci.* **2017**, *28*, 869.
- (40) Herrera-Perez, R. M.; Voytik-Harbin, S. L.; Sarkaria, J. N.; Pollok, K. E.; Fishel, M. L.; Rickus, J. L. *PLoS ONE* **2018**, *13*, e0194183.
- (41) Chen, J.-W. E.; Pedron, S.; Shyu, P.; Hu, Y.; Sarkaria, J. N.; Harley, B. A. C. *Front. Mater.* **2018**, *5*, DOI 10.3389/fmats.2018.00039.
- (42) Florczyk, S. J.; Wang, K.; Jana, S.; Wood, D. L.; Sytsma, S. K.; Sham, J.; Kievit, F. M.; Zhang, M. *Biomaterials* **2013**, *34*, 10143.
- (43) Arulmoli, J.; Wright, H. J.; Phan, D. T. T.; Sheth, U.; Que, R. A.; Botten, G. A.; Keating, M.; Botvinick, E. L.; Pathak, M. M.; Zarebinski, T. I.; Yanni, D. S.; Razorenova, O. V.; Hughes, C. C. W.; Flanagan, L. A. *Acta Biomater.* **2016**, *43*, 122.
- (44) Burdick, J. A.; Prestwich, G. D. *Adv. Mater.* **2011**, *23*, H41.
- (45) Ananthanarayanan, B.; Kim, Y.; Kumar, S. *Biomaterials* **2011**, *32*, 7913.
- (46) Shu, X. Z.; Liu, Y.; Palumbo, F.; Prestwich, G. D. *Biomaterials* **2003**, *24*, 3825.
- (47) Koh, I.; Cha, J.; Park, J.; Choi, J.; Kang, S.-G.; Kim, P. *Sci. Rep.* **2018**, *8*, 4608.
- (48) Yu, C.; Ma, X.; Zhu, W.; Wang, P.; Miller, K. L.; Stupin, J.; Koroleva-Maharajh, A.; Hairabedian, A.; Chen, S. *Biomaterials* **2019**, *194*, 1.
- (49) Toprakhisar, B.; Nadermezah, A.; Bakirci, E.; Khani, N.; Skvortsov, G. A.; Koc, B. *Macromol. Biosci.* **2018**, *18*, e1800024.
- (50) Kim, B. S.; Kim, H.; Gao, G.; Jang, J.; Cho, D.-W. *Biofabrication* **2017**, *9*, 034104.
- (51) Nam, S. Y.; Park, S.-H. *Adv. Exp. Med. Biol.* **2018**, *1064*, 335.
- (52) Lee, H.; Han, W.; Kim, H.; Ha, D.-H.; Jang, J.; Kim, B. S.; Cho, D.-W. *Biomacromolecules* **2017**, *18*, 1229.
- (53) Ooi, H. W.; Mota, C.; Ten Cate, A. T.; Calore, A.; Moroni, L.; Baker, M. B. *Biomacromolecules* **2018**, *19*, 3390.
- (54) Jeon, O.; Bouhadir, K. H.; Mansour, J. M.; Alsberg, E. *Biomaterials* **2009**, *30*, 2724.
- (55) Rastogi, P.; Kandasubramanian, B. *Biofabrication* **2019**, *11*, 042001.
- (56) Soman, P.; Fozdar, D. Y.; Lee, J. W.; Phadke, A.; Varghese, S.; Chen, S. *Soft Matter* **2012**, *8*, 4946.
- (57) Soman, P.; Lee, J. W.; Phadke, A.; Varghese, S. Chen, S. *Acta Biomater.* **2012**, *8*, 2587.
- (58) Soman, P.; Tobe, B. T. D.; Lee, J. W.; Winkquist, A. M.; Singec, I.; Vecchio, K. S.; Snyder, E. Y.; Chen, S. *Biomed. Microdevices* **2012**, *14*, 829.
- (59) Wang, C.; Tong, X.; Yang, F. *Mol. Pharm.* **2014**, *11*, 2115.
- (60) Avci, N. G.; Fan, Y.; Dragomir, A.; Akay, Y. M.; Akay, M. *IEEE T. NanoBiosci.* **2015**, *14*, 790.
- (61) Fan, Y.; Nguyen, D. T.; Akay, Y.; Xu, F.; Akay, M. *Sci. Rep.* **2016**, *6*, DOI 10.1038/srep25062.
- (62) Thorne, J. T.; Segal, T. R.; Chang, S.; Jorge, S.; Segars, J. H.; Leppert, P. C. *Biol. Reprod.* **2015**, *92*, DOI 10.1095/biolreprod.114.121368.
- (63) Kaur, G.; Dufour, J. M. *Spermatogenesis* **2012**, *2*, 1.
- (64) Martins-Taylor, K.; Xu, R.-H. *Stem Cells* **2012**, *30*, 22.
- (65) Scaglione, S.; Kliethermes, S.; Cao, G.; Shoham, D.; Durazo, R.; Luke, A.; Volk, M. L. *J. Clin. Gastroenterol.* **2015**, *49*, 690.
- (66) Sidney, S.; Go, A. S.; Jaffe, M. G.; Solomon, M. D.; Ambrosy, A. P.; Rana, J. S. *JAMA Cardiol.* **2019**, *4*, 1280.
- (67) Dariush, M.; et al. *Circulation* **2015**, *131*, e29.
- (68) Faulkner-Jones, A.; Fyfe, C.; Cornelissen, D.-J.; Gardner, J.; King, J.; Courtney, A.; Shu, W. *Biofabrication* **2015**, *7*, 044102.
- (69) Guengerich, F. P. *Annu. Rev. Pharmacol. Toxicol.* **1999**, *39*, 1.
- (70) Faucette, S. R.; Wang, H.; Hamilton, G. A.; Jolley, S. L.; Gilbert, D.; Lindley, C.; Yan, B.; Negishi, M.; LeCluyse, E. L. *Drug Metab. Dispos.* **2004**, *32*, 348.
- (71) Maiullari, F.; Costantini, M.; Milan, M.; Pace, V.; Chirivi, M.; Maiullari, S.; Rainer, A.; Baci, D.; Marei, H. E.-S.; Seliktar, D.; Gargioli, C.; Bearzi, C.; Rizzi, R. *Sci. Rep.* **2018**, *8*, 13532.
- (72) Noor, N.; Shapira, A.; Edri, R.; Gal, I.; Wertheim, L.; Dvir, T. *Adv. Sci.* **2019**, *6*, DOI 10.1002/adv.201900344.
- (73) Lee, A.; Hudson, A. R.; Shiwarski, D. J.; Tashman, J. W.; Hinton, T. J.; Yermeni, S.; Bliley, J. M.; Campbell, P. G.; Feinberg, A. W. *Science* **2019**, *365*, 482.
- (74) Yi, H.-G.; Jeong, Y. H.; Kim, Y.; Choi, Y.-J.; Moon, H. E.; Park, S. H.; Kang, K. S.; Bae, M.; Jang, J.; Youn, H.; Paek, S. H.; Cho, D.-W. *Nat. Biomed. Eng.* **2019**, *3*, 509.
- (75) Tang, M.; Rich, J. N.; Chen, S. *Adv. Mater.* **2021**, *33* (5), e2004776. doi.

Hybrid printing for Engineering Vascularized Tissue Constructs



Jiannan Li,¹ Sungwoo Kim,¹ Carolyn Kim,^{1,2} Yunzhi Peter Yang^{1,3,4*}

¹ Department of Orthopaedic Surgery, Stanford University, 240 Pasteur Drive, Stanford, CA 94304, USA

² Department of Mechanical Engineering, Stanford University, 440 Escondido Mall, Stanford, CA 94305, USA

³ Department of Materials Science and Engineering, Stanford University, 496 Lomita Mall, Stanford, CA 94305, USA

⁴ Department of Bioengineering, Stanford University, 443 Via Ortega, Stanford, CA 94305, USA

* E-mail: ypyang@stanford.edu

Introduction

The development of three-dimensional (3D) printing¹ provides a powerful tool for tissue engineering, due to its unprecedented capability to reproduce the spatial features of native tissues by printing cell-laden constructs.² However, vascularization arguably remains the most difficult yet most crucial challenge in tissue engineering, even with 3D printing techniques. To engineer large and complex functioning tissue constructs, the development of proper vascular networks is required to ensure every individual cell is within 100–300 μm from the nearest capillary to avoid cell death.³ Despite numerous breakthroughs to significantly improve the resolution of 3D printing,⁴ the current printing resolution is still not good enough to reconstruct the required capillary networks, many of which have features smaller than 100 μm .⁵ More importantly, the engineering of thick vascularized tissue is far more complicated than simply reconstructing a vascular network. It usually involves spatially controlled distribution of multiple phenotypes of cells and different extracellular matrices with distinct properties. Additionally, to engineer a vascularized musculoskeletal composite tissue, one needs to combine bone, cartilage, muscle, and tendon, which all possess different cell compositions, mechanical properties, and biological functionalities with their own vascular networks. The engineering and seamless integration of such multi-cell, multi-material tissue constructs remain a major challenge. Various 3D printing mechanisms have been developed to target specific material types, such as fused deposition modeling (FDM) or molten material extrusion (MME) for rigid polymeric materials,⁶ and stereolithography (SLA) and syringe extrusion for soft hydrogel materials.^{7,8} However, no single

printing mechanism can engineer multiple materials with the required distinct properties. Therefore, we envision integrating multiple printing mechanisms, to engineer the desired complex multi-cell, multi-material tissue constructs as the most promising solution. This is referred to as hybrid printing or Hybprinting for short. By integrating different printing mechanisms, Hybprinting provides unprecedented coverage of material range and thus the flexibility and capability to engineer complex, customizable biomimicking vascularized scaffolds. This review focuses on using the Hybprinting approach for complex tissue engineering. Specifically, in our envisioned strategy for engineering vascularized construct, either FDM or MME can be used to generate structural support and provide the desired mechanical properties for the targeting tissue, SLA is used to print sophisticated patterns and to generate major vessel branches of vascular tree complexity. Last, syringe extrusion can be used to expand the selection of bioinks for fabrication of cell-laden tissue-specific scaffolds.

The approach can be combined with the localized distribution of growth factors for guided angiogenesis, forming microvasculature networks. We believe this approach shows great potential for engineering thick vascularized tissues (**Figure 1**). To break down the approach, we introduce each single printing mechanism, including FDM, syringe extrusion, and SLA. Meanwhile, we briefly describe their roles in the proposed Hybprinting strategy for vascularization and potential applications. We hope this provides insights into novel approaches in bioprinted vascularized tissue constructs and contributes to various tissue engineering applications.



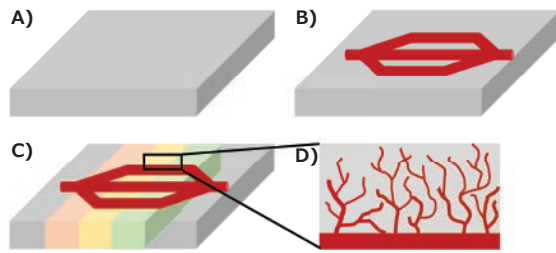


Figure 1. Envisioned strategy for engineering vascularized tissues: **A)** FDM for generating structural support with rigid polymeric materials; **B)** SLA for printing major vessels with hydrogel materials; **C)** syringe extrusion for printing cell-laden, tissue-specific scaffolds. Different colors could represent various growth factors or material compositions enabled by different syringe printing nozzles; **D)** Microvascular network are then formed by guided angiogenesis.

FDM for Structural Supports

FDM is one of the most extensively used 3D printing techniques. First developed in 1989, the FDM technique expanded rapidly and quickly showed the potential to revolutionize the prototyping and manufacturing industry. Due to its low cost and modular, customizable design, it has been widely applied to many fields, including aerospace, automobile, art, and biomedical applications.^{6,9-11} The base material, usually filament or pellets, is first heated in a barrel to melting temperature in a standard FDM process. The melted material is then extruded through a hot nozzle. Once extruded, the material cools and solidifies. The desired pattern can be formed by coordinating the extruded material with a translation system. In this process, the materials used are usually thermal plastic polymers, such as acrylonitrile butadiene styrene (ABS), polycarbonates, polylactic acid (PLA), polycaprolactone (PCL), poly(lactic-co-glycolic acid) (PLGA), etc. Many of these materials are food-grade, non-toxic materials, and some of them even show excellent biocompatibility and biodegradability, making them great candidates for tissue constructs. For example, PLGA has already been approved by the FDA for therapeutic purposes, while PLA and PCL have also been extensively used in engineering tissue scaffolds. Scaffolds fabricated with these materials are usually mechanically strong and therefore they are widely used in bone tissue engineering.¹²⁻¹⁴ However, their application is not only limited to bone engineering, as the mechanical property of the scaffold can be manipulated by geometrical design. In Hybprinting, FDM serves as one module for printing thermoplastic scaffolds that act as structural supports while maintaining proper porosity to allow for other components.

SLA for Major Vessel Branches

SLA printing is well-known in the field of manufacturing for its ultra-high resolution. Using light-curable material, SLA printing forms the desired shape in a layer-by-layer format by controlling the light pattern for each layer.^{15,16} Traditional SLA printing suffered from low throughput and high cost due to discontinuity in between layers and the high expense of custom, high-resolution photomasks or laser scanners. However, with the advancement of digital light processing (DLP)¹⁷ as well as controlled oxygen-permeable optics,¹⁸

the throughput and the cost-efficiency has improved significantly. Moreover, SLA printing resolution has also been enhanced by orders of magnitude with the development of two-photon lithography or multi-photon lithography techniques.¹⁹ SLA printing can now achieve resolution of several micrometers and even reach the sub-micron resolution. This capability to generate high-resolution patterns makes SLA an excellent fit for printing sophisticated vascular networks. For example, B. Huber et al. reported using SLA printing to fabricate photo-curable cytocompatible polyacrylate (PA) material for the generation of vessels.²⁰

Nevertheless, the resolution of SLA printing is still not sufficient enough to reproduce microvascular networks, since microvasculature dimensions are so small. In our envisioned strategy for vascularized tissue printing, SLA is to be mainly used for printing major vessels, while microvascular networks would need to be generated through guided angiogenesis. By perfusing through the major vessels and incorporating proper cells and growth factors in the surrounding scaffold, vascular sprouting can be induced from the major vessels into surrounding cell-laden hydrogels to spontaneously anastomose with microvasculature within the surrounding cell-laden hydrogel to establish a perfusable vascular bed. Our group has implemented this strategy by developing a dual hydrogel system that sequentially integrates a slower degradable hydrogel for long term sustained perfusion with a faster degradable hydrogel for microvasculature. We demonstrated this induced vascularization approach using a gelatin methacrylate/poly(ethylene glycol) dimethacrylate (GelMA/PEGDMA) dual-hydrogel system loaded with human umbilical vein endothelial cells (HUVEC)²¹ (Figure 2). We expect that combining such a technique with SLA bioprinting will lead to better reproduction of sophisticated vascular networks.

Syringe Extrusion for Tissue-specific Scaffold

Syringe extrusion is one of the most cost-effective printing techniques and has also been used extensively in bioprinting and tissue engineering.²² A syringe extrusion process is straightforward; it includes loading a prepared bioink into a syringe, then extruding it via a nozzle by applying pressure to the bioink. The key to bioprinting with syringe extrusion lies within the design of the bioink, as it must meet many criteria, including good printability, biocompatibility while possessing the desired mechanical property. Many different bioink formulations have been developed using all kinds of base materials, such as GelMA,²³ alginate,²⁴ and PEG,²⁵ for example. These bioinks have demonstrated excellent cytocompatibility as they can be used for cell encapsulation and long-term *in vitro* culture. Other advantages of syringe extrusion are its low-cost and simple setup, which allow for easy customization of multiple printer heads in a single platform. This capability facilitates simultaneous co-printing of multiple bioinks, with each bioink specifically designed for different tissues by changing the material composition and growth factors. This makes syringe extrusion optimal for printing cell-laden, tissue-specific scaffolds. For example, syringe extrusion

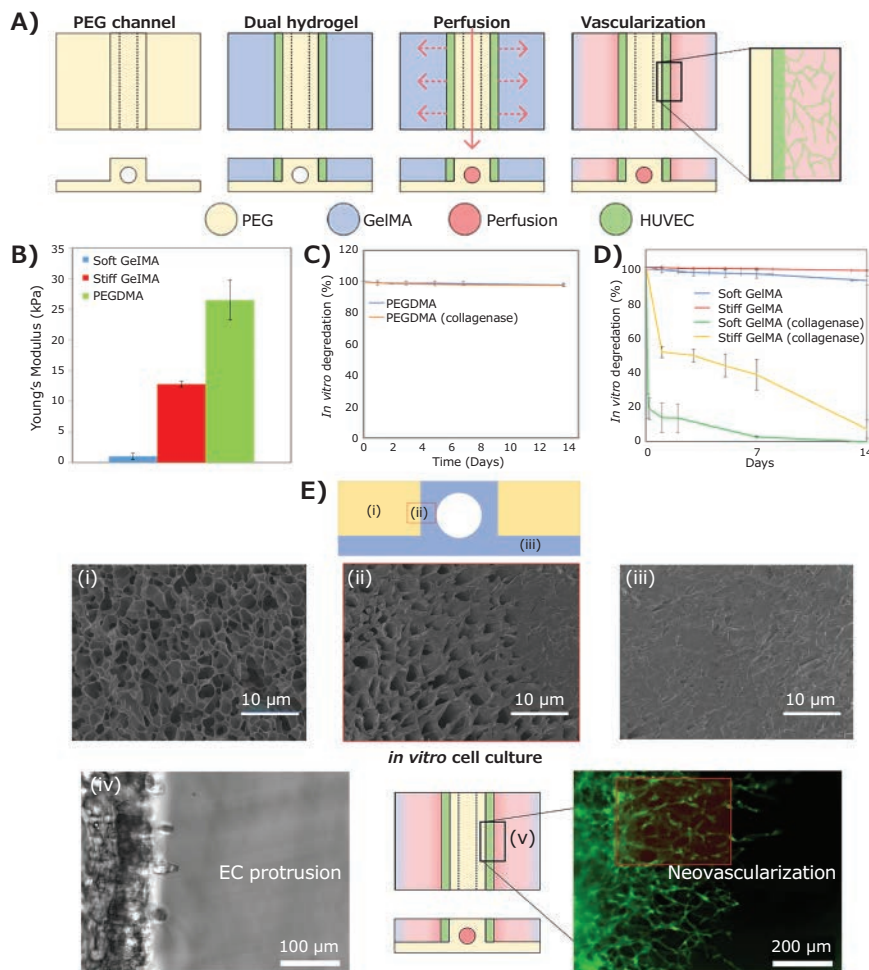


Figure 2. Development and characterization of an *in vitro* co-culture model for angiogenesis and vascularization. **A)** The manufacturing process of the dual hydrogel system; **B)** Compressive modulus; *in vitro* degradation of **C)** PEGDMA and **D)** GelMA; **E)** Representative SEM images and microvessel formation in an *in vitro* model system. (i) GelMA, (ii) Interpenetrating network (IPN) between the PEGDMA channel and the GelMA, (iii) PEGDMA, (iv) HUVEC protrusion into GelMA at day 1, (v) microvessel formation in the dual hydrogel system at two weeks.

has been used for printing tendon,²⁶ cartilage,^{27,28} muscle,²⁹ or nerve³⁰ tissues. Notably, syringe extrusion has also been used to generate major vessels;³¹ however, syringe extrusion is less effective when printing a complex structure containing bifurcating or manifold branch transition and hanging structures. In the future, syringe extrusion may be used to print sacrificial materials that are later removed to form blood vessels.

Biopink preparation is one of the most challenging steps of syringe extrusion printing, as the biopink is usually a composition of viscous materials that requires proper mixing. Various efforts have been made for optimizing the preparation of biopinks, including passive mixing³¹ or manual active mixing.³² Recently, our group has developed an automated active mixing platform (AAMP), which allows for fast, cost-effective, precisely controlled mixing and preparation of hydrogel biopinks.³³ We believe the improved biopink preparation will have great potential and a broad range of applications for bioprinting and tissue engineering.

Hybprinting for Engineering Vascularized Tissue

Each of the aforementioned printing techniques has its unique pros and cons and works for specific types of materials. We envision a platform that integrates these techniques will contribute significantly to the engineering of complex tissues, including thick vascularized tissues. Such a platform can utilize the advantages of multiple printing methods, allow for automated fabrication of multi-material constructs with mechanical and biological gradients, and better mimic native tissues. In 2015, our group developed a prototype of this bioprinting platform that integrated FDM and SLA for the very first time (**Figure 3**). The platform achieved seamless integration of rigid and soft scaffolds³⁴ and helped to pioneer the Hybprinting strategy for printing complex tissues. In the future, multiple FDM and syringe extrusion units can be integrated into a single Hybprinting platform under a single algorithm or human-machine interface.

Meanwhile, several groups have been working on integrating FDM and syringe extrusion. For example, Malda and co-workers developed a printing system using FDM to generate rigid supporting structures and syringe extrusion to print cell-laden hydrogels.³⁵ The Cho group proposed similar ideas at almost the same time.³⁶ Additionally, the Atala group used integrated FDM and syringe extrusion printing to generate anatomical scale bioscaffolds with the help of sacrificial materials.³⁷ In the future, more and more different printing techniques can be integrated, expanding the capability of Hybprinting, and allowing for the fabrication of more complicated and sophisticated tissue constructs. For example, in our envisioned strategy, growth factors can be patterned with either multi-syringe extrusion or the introduction of an inkjet printing mechanism, resulting in a growth factor gradient in the engineered scaffold. According to our previous study, the graded growth factor distribution can be specifically designed for guided angiogenesis, which will lead to the formation of microvascular networks, achieving the last step of engineering thick vascularized tissues.

Conclusion

This mini review focuses on bioprinting strategies for engineering thick vascularized tissue constructs. We reviewed different printing mechanisms, including FDM, SLA, and syringe extrusion, and their applications in printing vasculatures. Due to the complexity in engineering multi-cell, multi-material vascularized tissue constructs, we envision that future strategies will need to integrate multiple printing mechanisms in a single platform to fabricate different complex tissues in a single step. We reviewed this strategy for the printing of thick vascularized tissues, where FDM is used for printing structural supports, SLA for major vessels, syringe extrusion for cell-laden tissue-specific scaffolds, and inkjet for guided angiogenesis to create microvascular networks. Moreover, other printing mechanisms may also be integrated to further broaden the range of capabilities. We believe Hybprinting has shown great potential in engineering thick vascularized tissues due to its superior capability for handling complex cases and will have a promising future in tissue engineering applications.

Acknowledgments

This research was partially funded through financial support from NIH grants U01AR069395, R01AR072613, and R01AR074458 from NIAMS, and DoD grant W81XWH-20-1-0343, the Stanford Woods Institute for the Environment, Boswell Foundation, and Tad and Diane Taube Family Foundation.

References:

- (1) Ngo, T.; Kashani, A.; Imbalzano, G.; Nguyen, K.; Hui, D. *Compos. B-Eng.* **2018**, *143*, 172–196.
- (2) Li, J.; Chen, M.; Fan, X.; Zhou, H. *J. Transl. Med.* **2016**, *14*, 271.
- (3) Mercado-Pagán, Á.; Stahl, A. M.; Shanjan, Y.; Yang, Y. *Ann. Biomed. Eng.* **2015**, *43* (3), 718–729.
- (4) Miri, A.; Mirzaee, I.; Hassan, S.; Oskui, S.; Nieto, D.; Khademhosseini, A.; Zhang, Y. *Lab Chip* **2019**, *19* (11), 2019–2037.
- (5) Pries, A.; Schonfeld, D.; Gaehtgens, P.; Kiani, M.; Cokelet, G. *Am. J. Physiol. Heart Circ.* **1997**, *272* (6), H2716–H2725.
- (6) Dhinakaran, V.; Kumar, K.; Ram, P.; Ravichandran, M.; Vinayagamoorthy, M. *Mater. Today: Proc.* **2020**, *27*, 752–756.
- (7) Melchels, F.; Feijen, J.; Grijpma, D. *Biomaterials* **2012**, *31* (24), 6121–6130.

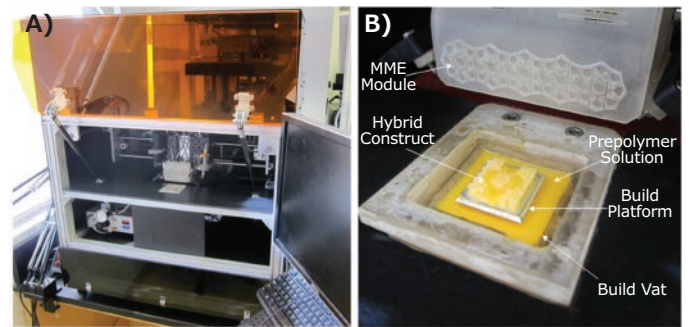


Figure 3. In-house-developed combinatory bioprinting technology: (A) view of the Hybprinter machine, (B) FDM module and SLA vat of Hybprinter and a typical scaffold-hydrogel part during the built process.

- (8) You, F.; Eames, B.; Chen, X. *Int. J. Mol. Sci.* **2017**, *18* (7), 1597.
- (9) Boparai, K.; Singh, R.; Singh, H. *Rapid Prototyp. J.* **2016**, *22* (2), 281–299.
- (10) Klippstein, H.; Sanchez, A.; Hassanin, H.; Zweiri, Y.; Seneviratne, L. *Adv. Eng. Mater.* **2018**, *20* (2), 1700552.
- (11) Liu, Z.; Wang, Y.; Wu, B.; Cui, C.; Guo, Y.; Yan, C. *Int. J. Adv. Manuf. Technol.* **2019**, *102* (9–12), 2877–2889.
- (12) Zein, I.; Huttmacher, D.; Tan, K.; Teoh, S. *Biomaterials* **2002**, *23* (4), 1169–1185.
- (13) Chen, G.; Chen, N.; Wang, Q. *Compos. Sci. Technol.* **2019**, *172*, 17–28.
- (14) Khodaei, M.; Amini, K.; Valanezhad, A. *J. Wuhan Univ. Technol. Mater. Sci. Ed.* **2020**, *35* (1), 248–251.
- (15) Ge, Q.; Li, Z.; Wang, Z.; Kowsari, K.; Zhang, W.; He, X.; Zhou, J.; Fang, N. *Int. J. Extrem. Manuf.* **2020**, *2* (2), 022004.
- (16) Deshmane, S.; Kendre, P.; Mahajan, H.; Jain, S. *Drug Dev. Ind. Pharm.* **2021**, <https://doi.org/10.1080/03639045.2021.1994990>.
- (17) Maines, E.; Porwal, M.; Ellison, C.; Reineke, T. *Green Chem.* **2021**, *23* (18), 6863–6897.
- (18) Tumbleston, J.; Shirvanyants, D.; Ermoshkin, N.; Januszewicz, R.; Johnson, A.; Kelly, D.; Chen, K.; Pinschmidt, R.; Rolland, J.; Ermoshkin, A.; Samulski, E.; DeSimone, J. *Science* **2015**, *347* (6228), 1349–1352.
- (19) Park, S.; Yang, D.; Lee, K. *Laser Photonics Rev.* **2009**, *3* (1–2), 1–11.
- (20) Huber, B.; Engelhardt, S.; Meyer, W.; Kruger, H.; Wenz, A.; Schonhaar, V.; Tovar, G.; Kluger, P.; Borchers, K. *J. Funct. Biomater.* **2016**, *7* (2), 11.
- (21) Kim, S.; Pan, C. C.; Yang, Y. P. *Macromol. Biosci.* **2020**, *20* (10), e2000204.
- (22) Jang, T.; Jung, H.; Pan, H.; Han, W.; Chen, S.; Song, J. *Int. J. Bioprinting* **2018**, *4* (1), 126.
- (23) Du, M.; Chen, B.; Meng, Q.; Liu, S.; Zheng, X.; Zhang, C.; Wang, H.; Li, H.; Wang, N.; Dai, J. *Biofabrication* **2015**, *7* (4), 044104.
- (24) Chung, J.; Naficy, S.; Yue, Z.; Kapsa, R.; Quigley, A.; Moulton, S.; Wallace, G. *Biomater. Sci.* **2013**, *1* (7), 763–773.
- (25) Gao, G.; Schilling, A.; Hubbell, K.; Yonezawa, T.; Truong, D.; Hong, Y.; Dai, G.; Cui, X. *Biotechnol. Lett.* **2015**, *37* (11), 2349–2355.
- (26) Jiang, X.; Wu, S.; Kuss, M.; Kong, Y.; Shi, W.; Streubel, P.; Li, T.; Duan, B. *Bioact. Mater.* **2020**, *5* (3), 636–643.
- (27) Kundu, J.; Shim, J.; Jang, J.; Kim, S.; Cho, D. *J. Tissue Eng. Regen. Med.* **2015**, *9* (11), 1286–1297.
- (28) Izadifar, Z.; Chang, T.; Kulyk, W.; Chen, X.; Eames, B. *Tissue Eng. Part C Methods* **2016**, *22* (3), 173–188.
- (29) Distler, T.; Solisito, A.; Schneidereit, D.; Friedrich, O.; Detsch, R.; Boccaccini, A. *Biofabrication* **2020**, *12* (4), 045005.
- (30) Gu, Q.; Tomaskovic-Crook, E.; Lozano, R.; Chen, Y.; Kapsa, R.; Zhou, Q.; Wallace, G.; Crook, J. *Adv. Healthc. Mater.* **2016**, *5* (12), 1429–1438.
- (31) Müller, M.; Öztürk, E.; Arlov, Ø.; Gatenholm, P.; Zenobi-Wong, M. *Ann. Biomed. Eng.* **2017**, *45* (1), 210–223.
- (32) Cohen, D.; Lo, W.; Tsavaris, A.; Peng, D.; Lipson, H.; Bonassar, L. *Tissue Eng. Part C Methods* **2011**, *17* (2), 239–248.
- (33) Shelby, T.; Li, J.; Alizadeh, H. V.; Yang, Y. P. Development and Characterization of an Automated Active Mixing Platform (AAMP) for Hydrogel Bioink Preparation, **2021**.
- (34) Shanjan, Y.; Pan, C.; Elomaa, L.; Yang, Y. *Biofabrication* **2015**, *7* (4), 045008.
- (35) Schuurman, W.; Khristov, V.; Pot, M.; van Weeren, P.; Dhert, W.; Malda, J. *Biofabrication* **2011**, *3* (2), 021001.
- (36) Shim, J.; Kim, J.; Park, M.; Park, J.; Cho, D. *Biofabrication* **2011**, *3* (3), 034102.
- (37) Kang, H.; Lee, S.; Ko, I.; Kengla, C.; Yoo, J.; Atala, A. *Nat. Biotechnol.* **2016**, *34* (3), 312–319.

Recent Advances in 3D Biofabrication of Blood Vessels



Alessia Longoni,¹ Tim BF Woodfield,² Jelena Rnjak-Kovacina,³ Khoon S Lim^{1,2*}

¹ Light Activated Biomaterials (LAB) Group, University of Otago Christchurch, New Zealand

² Christchurch Regenerative Medicine and Tissue Engineering (CReaTE) Group, University of Otago Christchurch, New Zealand

³ Graduate School of Biomedical Engineering, University of New South Wales, Australia

* Email: author: khoon.lim@otago.ac.nz

Introduction

The human vascular system consists of an intricate hierarchical network of blood vessels of different sizes, which operate in unison to ensure gas and nutrient exchange throughout the body (Figure 1A). Large blood vessels (≥ 6 mm in diameter) and capillaries (≤ 10 μm in diameter) represent the extremes of this hierarchical tree and play different roles in ensuring tissue homeostasis. The primary function of macro-vessels like arteries is to buffer the pressure associated with the intermittent left ventricular contraction and act as a conduit to deliver steady blood flow to the peripheral areas of the body. On the other hand, micro-vessels are responsible for the transmural exchange of gas, nutrients, and cellular waste (Figure 1B, C). The different functions of these blood vessels are also reflected in their anatomy. Specifically, there is a progressive decrease in the vessel diameter and wall thickness when moving from macro-vessels to micro-vessels. The cellular organization and structure of these vessels are also different, including having a different number of layers of vascular smooth muscle cells that surround the endothelium, with capillaries within the microcirculation composed only of a single layer of endothelial cells and supporting pericytes.¹

Considering the heterogeneity in structure and function of different types of blood vessels, it is not surprising that recapitulating the complexity of the vascular tree remains a significant challenge in the field of tissue engineering and regenerative medicine. Currently, several synthetic grafts and decellularized matrices are available for the replacement of large blood vessels to reconstruct or bypass vascular occlusions and aneurysms.^{1,2} On the contrary, there is an unmet clinical need for strategies to engineer small-diameter blood vessels to address occlusion in coronary and peripheral arteries and for the clinical translation of engineered

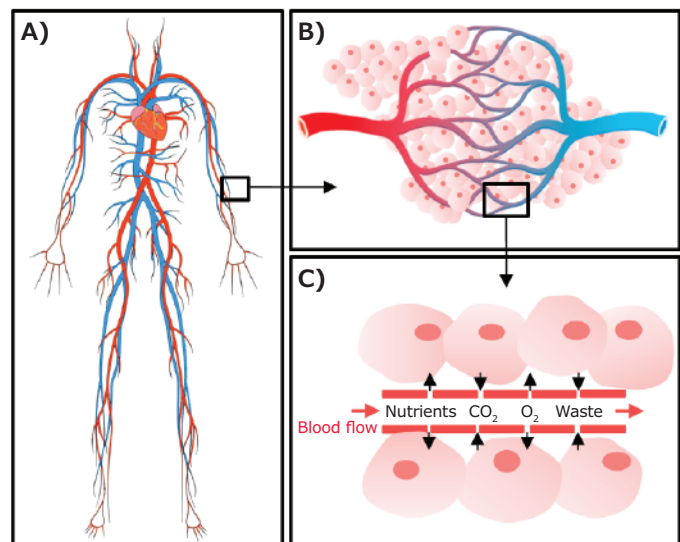


Figure 1. Schematic overview of the human vascular tree and vascular network function. **A)** Schematic representation of the main vessels that are part of the human cardiovascular system. **B)** Representation of the microcapillary network, which connects arterioles to venules. **C)** Gas and nutrient exchange that occurs at the capillary-tissue interface. While oxygen and nutrients are delivered by the arterioles into the capillaries, CO_2 and metabolic waste products are collected and transported by the venules. Reprinted with permission from reference 3, copyright 2019 Elsevier Ltd.

tissue analogs which require a healthy capillary supply to allow the exchange of gases, nutrients, and fluids.^{1,3} The formation of necrotic regions within engineered constructs is one of the leading causes of poor survival and integration with the host tissue, limiting their regenerative properties and clinical translation.^{3,4}

Over the past decade, various fabrication strategies to incorporate perfusable hollow microchannels/vessel-like structures into 3D scaffolds have been extensively studied, often using conventional templating and molding approaches. These approaches are often simplistic with limited spatial architecture and resolution. The rapid advancement in the biofabrication field has enabled the creation of more complex and sophisticated shapes that has vast potential to recapitulate the multiscale architecture of native vasculature.

Biofabrication is defined as *“the automated generation of biologically functional products with the structural organization from living cells, bioactive molecules, biomaterials, cell aggregates such as micro-tissues, or hybrid cell-material constructs, through Bioprinting or Bioassembly and subsequent tissue maturation processes.”*⁵ In this context, bioinks are further defined as *“a formulation of cells suitable for processing by an automated biofabrication technology that may also contain biologically active components and biomaterials.”*⁶ Thus, bioprinting is considered a subset technique of biofabrication, which involves automated processes where living cells are directly printed within bioinks. Therefore, it is important to note that printing approaches where structures are first printed then seeded with cells do not qualify as bioprinting, as cells were not included during the printing process.

This article outlines advances in biofabrication technologies used to construct the distinct hierarchical levels of the vascular system using seminal papers in the field. In addition, the extent to which engineered vessels recapitulate the physiological function of native vessels, current applications of biofabricated vessels, challenges, and future directions in the field will be discussed.

Biofabrication Approaches in Engineering Vasculature

In the past years, numerous technologies have been developed in the biofabrication field (i.e., ink-jet printing, laser-induced forward transfer, extrusion-based printing, and lithography-based printing),⁷ which have been applied to tissue engineering and regenerative medicine fields. To date, both extrusion-based and lithography-based biofabrication modalities are most commonly used to create vessel-like structures within 3D constructs.

Extrusion-based biofabrication technology involves precise deposition of materials in cylindrical filaments onto a receiver platform, according to computer-driven spatial instructions, allowing layer-by-layer formation of 3D constructs with predesigned structures.¹ Miller et al. demonstrated extrusion-printing of carbohydrate glass used as sacrificial templates in engineered tissues containing living cells.⁸ In general, the ‘sacrificial ink’ is first deposited and embedded in a hydrogel matrix. The printed template can be easily removed via dissolution in cell culture media, leaving open perfusable channels (diameter = 200 μm) that can be further lined with endothelial cells. The success of this technique led to the use of several other materials as sacrificial inks, such as poloxamer (Pluronic F127), gelatin, and alginate. For example, Kolesky et al. showed extrusion of

different sacrificial template designs with precise control over the resolution (diameter in the range of 45–1000 μm) and architecture (Figure 2A). Specifically, individual templates with varying channel diameter — largest channel (650 μm) to smallest channel (150 μm) in a hierarchical design — were successfully fabricated and embedded within cell-laden hydrogel constructs to mimic the bifurcating motifs present in native tissues where large channels often bifurcate into smaller channels for efficient blood flow and nutrient transport.⁹

Although the aforementioned studies are impressive and show proof-of-concept for vessel-like hollow channel fabrication, printing multi-scaled clinically relevant-sized heterogeneous constructs remains a challenge. Hence, to prevent deformation or collapse of the printed physiologically relevant sized structures, recent studies have investigated the extrusion of hydrogel-based materials into support baths. Noor et al. showed the possibility of fabricating heart analogs (height = 20 mm; diameter = 14 mm) with major blood vessels that are perfusable, by extruding cell-laden omentum hydrogels into an alginate/xanthan gum support bath (Figure 2B).¹⁰ More recently, Skylar-Scott et al. extruded gelatin-based sacrificial ink into a cell-laden supporting bath containing iPSCs aggregates to engineer perfusable cardiac embryoid bodies¹¹ (Figure 2C). After removing the gelatin sacrificial ink, the constructs were perfused with a hyper oxygenated medium (95% O₂, 5% CO₂) at a flow rate of 250 μm/min, which significantly improved cell viability and functionality. The functional performances of these constructs were further examined using perfusion of various cardiac-related drugs, where perfusion of isoproterenol through the embedded channel resulted in a doubling of the spontaneous beating frequency. In contrast, when 1-heptanol was perfused through the channels, a reduction in the overall tissue contractile amplitude was observed.

Another study by Soliman et al. showed that incorporating sacrificial templates of different designs into cell-laden hydrogels can affect cellular behavior.⁴ For example, sacrificial channels of different fiber orientations (30°, 60°, or 90° between adjacent layers) affected microcapillary formation driven by endothelial cells and stromal cells encapsulated in the surrounding hydrogel. It should be noted that most of these studies are not bioprinting, where cells are directly extruded with the sacrificial inks. However, as technology progresses, co-axial extrusion approaches are being explored for direct 3D bioprinting of vascular constructs. Cui et al. reported on the fabrication of blood vessels (diameter = 1 mm) with spatial localization of cells, where the inner chamber of the co-axial extrusion apparatus consists of endothelial cells in a fugitive crosslinking slurry. In contrast, the outer chamber is a catechol-functionalized gelatin-methacryloyl hydrogel containing smooth muscle cells.¹² This approach mimics the distinct cellular orientation and organization of native blood vessels, where the inner layer is often an endothelium (single layer of endothelial cells) surrounded by an outer layer consisting of smooth muscle cells.

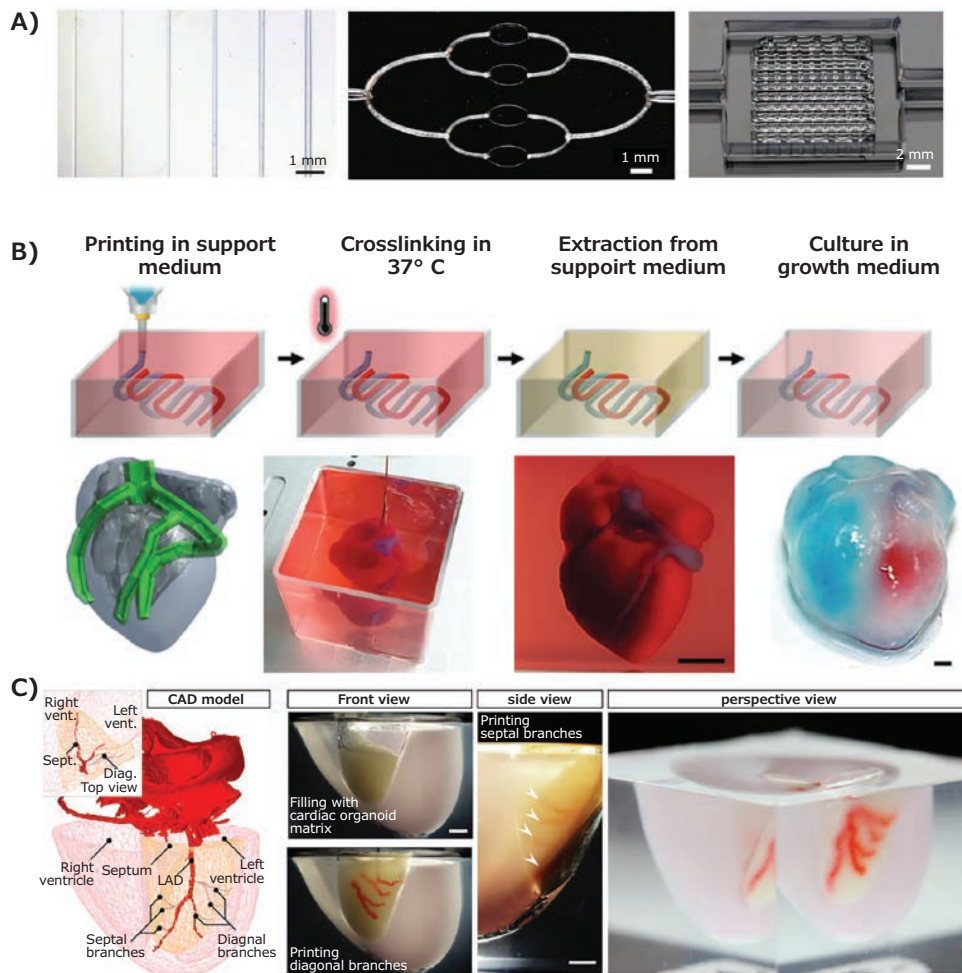


Figure 2. A) Pluronic F127 was used as fugitive ink by Kolesky et al. to print perfusable tubular vessel structures of different dimensions or hierarchical networks. Reproduced from reference 9 under terms of the CC-BY license, copyright 2014 John Wiley and Sons. B) Overview of the biofabrication workflow, starting from a human heart CAD model to its printing in a support bath and the extraction of the final product. Red and blue dyes indicated hollow chambers of the left and right ventricles, respectively. Reproduced with permission from 10 under the terms of the Creative Commons CC-BY-NC License. C) Overview of the biofabrication workflow to produce a perfusable cardiac tissue using sacrificial writing into a supporting bath containing iPSCs aggregates. Reprinted from reference 11, copyright The Authors, some rights reserved; exclusive licensee AAAS. Distributed under a CC BY-NC 4.0 license <http://creativecommons.org/licenses/by-nc/4.0/>.

Other common biofabrication technologies used to recapitulate the vessel architecture are light-based 3D-printing modalities. Light-based crosslinking processes allow control over the material spatiotemporal reaction, which can be leveraged to fabricate 3D structures of high resolution.⁷ Furthermore, light-based chemistries are known to be highly efficient while yielding minimal and non-toxic by-products, which is an essential requirement for the manufacturing of cell-laden constructs. Among the light-based biofabrication technologies, lithography-based techniques have been the most popular for vascularization applications, providing the highest accuracy and precision to pattern 3D constructs spatially.⁷ This technology is specifically dependent on the fundamental photo-polymerization principle — spatial control of light irradiation to facilitate the sol-gel transition of a photo-cross-linkable material. Light can be written (stereolithography, SLA) or projected (digital light processing, DLP) into a bath of photocrosslinkable material, crosslinking specific regions of the material onto a computer-driven build stage via light exposure (Figure 3A).⁷ By precise control over the voxel sizes,

lithography-based technologies allow significantly greater spatial resolutions (25–50 μ m) that cannot be achieved via extrusion-based biofabrication approaches. Grigoryan et al. recently showed the fabrication of a vascularized alveolar model using DLP technology (Figure 3B). The construct (height = 10 mm) was printed using poly(ethylene glycol)-diacrylate (PEGDA) hydrogels at a print time of 1 hour and voxel resolution of 5 pixels.¹³ Humidified oxygen gas was infused into the air sac, while deoxygenated red blood cells were perfused at the blood vessel inlet. In this study, intervascular oxygen transport between networks were successfully demonstrated by the collected red blood cells at the outlet having significantly higher oxygen saturation levels. Furthermore, the DLP-printed PEGDA hydrogels could withstand >10,000 ventilation cycles (at 24 kPa and a frequency of 0.5 Hz) over 6 hours. It is to be noted that although this model is acellular, the channels contain both convex and concave regions that are architecturally similar to native alveolar air sacs. A study by Levato et al. employed DLP technology to recreate the human cerebral arterial circle (Willis' circle) (Figure 3C).¹⁴ Convoluted and

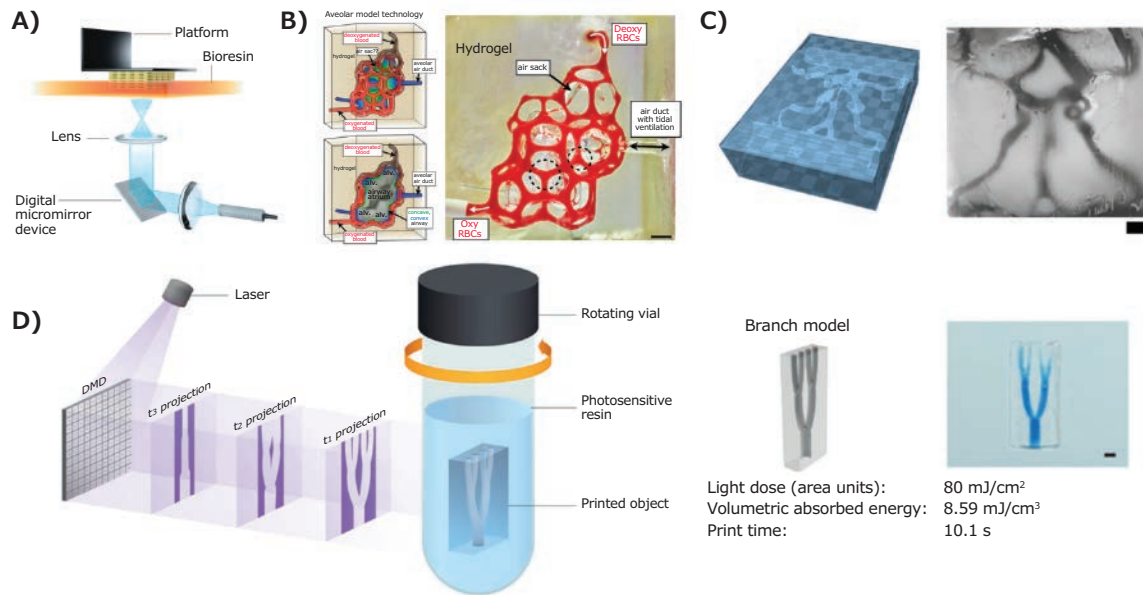


Figure 3. Vascular network fabricated with light-based biofabrication technologies. **A)** Schematic illustration of DLP technique that exploits light to control the spatial organization of biomaterials and cells. Adapted with permission from reference 7, copyright 2020 American Chemical Society. **B)** Vascularized alveolar model fabricated using DLP technology by Grigoryan et al. Republished with permission from reference 13, copyright 2019 The American Association for the Advancement of Science. **C)** Anatomical replica of a blood vessel present in the human Willis' circle were printed to prove the DLP printing capability of reproducing a convoluted and irregular vessel-like structure. Reproduced with permission from 14 under the terms of the Creative Commons CC-BY-NC License. **D)** Schematic overview of the volumetric printing principle of operation and the printed blood vessel structure. The obtained branches were perfused with blue-dextran. Adapted with permission from 15 under the terms of the Creative Commons CC-BY-NC License.

out-of-plane channel networks with irregular vessel-like channels were printed within gelatin-methacryloyl hydrogels, successfully recreating an anatomical replica of the Willis' circle based on 3D angiographic images. More recent breakthroughs to light-based biofabrication technologies have led to computed axial lithography (CAL) technology, where the principles of computed tomography process were adopted to produce an optical 3D dose distribution of light required to photo-crosslink a material by combining a series of 2D light patterns. Each image projection propagates through the material from a different angle, where the superposition of exposures from multiple angles results in sufficient 3D energy dose to facilitate sol-gel transition. The main advantage of this technology is the print speed, where Rizzo et al. demonstrated the successful fabrication of a branched perfusable vascular model (10 mm) within 10 seconds (Figure 3D).¹⁵

Functionality Requirements for Biofabricated Vessels

To ensure clinical translation of the developed vascularized constructs, it is essential that the engineered vessels also recapitulate the physiological function of the native ones. While vessels of different calibers have specific characteristics and functions, some general considerations apply to macro- and micro-vasculature. Firstly, the engineered vessels should possess perfusable lumens, which allow physiological blood flow without the formation of thrombi or occlusions.¹ Secondly, the blood vessels should possess adequate mechanical properties to withstand the pulsatile physiological pressure present at the different levels of the vascular tree without bursting or deforming.¹ Finally, the engineered blood vessels should integrate with the host vasculature once implanted, either through anastomosis or

sprouting and neo-angiogenesis.^{1,3} Thus, efforts have been made to go beyond the initial feasibility studies of using biofabrication approaches to fabricate acellular constructs containing vessel-like structures to 3D bioprinting of cell-laden constructs that dictate cell behavior and functionality.

Selecting the appropriate cell type and the source is also crucial as they directly affect the overall graft biofunctionality and *in vivo* performance, i.e., interaction with host tissue. So far, different types of endothelial cells have been used for vascularisation purposes. The most frequent are human umbilical vein endothelial cells (HUVECs) isolated from primary vein segments, as they have been proven suitable for fabricating vessels of multiple calibers.^{1,4,16-18} In addition to HUVECs, human microvascular endothelial cells (HMVECs) are derived from the microvessels of various tissues (e.g., adipose, liver, and cardiac tissues) have emerged as a promising source for engineering capillaries.¹ Ideally, these cells would be of autologous origin, as this would ensure immunological compatibility of the engineered vascularized construct and prevent its rejection. However, cell heterogeneity and limited expansion potential are shortcomings of using primary cell sources.¹ To overcome these limitations, current approaches focus on evaluating the feasibility of using induced pluripotent stem cell-derived endothelial cells (iPSC-ECs). iPSC-ECs are generated from reprogramming somatic cells, thus are of autologous origin. Furthermore, they have proven to have a great expansion potential while retaining their capability to differentiate into almost any cell type.^{1,11} Nevertheless, the ability of these cells to fully recapitulate endothelial cells mature phenotype and vessels functionality is still under investigation. In addition to endothelial cells, the presence of other cell types is required

to support the maturation of the vascular network and regulate blood vessel functions. Specifically looking at microcapillaries, pericytes can both stabilize and influence the permeability of the vessels network, as well as modulate endothelial cells behavior through paracrine signalling.^{1,4}

The field is rapidly progressing into the bioprinting space, where newer studies include the aforementioned vessel-forming cells (endothelial and pericytes) in the printing process to facilitate cell-mediated micro-capillary formation within 3D bioprinted constructs. Several studies have shown the presence of a vascular lumen and the expression of lineage-specific markers after 3D bioprinting of endothelial (e.g., CD31, von Willebrand factor, and VE-cadherin) and supporting cells (e.g., α -SMA and smooth muscles heavy chain).^{11,12,16} In addition, vessels functionality was evaluated *in vitro* by perfusing the printed networks, assessing their anti-thrombogenic properties by testing platelet activation, and investigating the vessels permeability and sprouting.^{12,15-19} Nevertheless, only a limited number of studies have investigated biocompatibility, long-term integration, and remodeling of the fabricated vessels *in vivo*.^{12,13,20} While this is understandable considering the rapid evolution and progress of biofabrication technologies and biopinks, collecting these data would pave the way for the clinical translation of 3D biofabricated vascular networks.

Conclusions and Future Directions

Currently, most vascular engineering strategies have focused on fabricating a single compartment/level of the vascular tree (macro- or micro-vessel only). Nevertheless, to ensure immediate connection to the host vasculature and perfusion of the engineered constructs, the recapitulation of vessels of different sizes and functions might be required. At this moment, although there have been numerous breakthroughs in biofabrication to create the shape and architecture of a multi-scalar vasculature network, the required functionality is still lacking. As the field is progressing from biofabrication to bioprinting technologies where the appropriate and essential cells are printed within the

3D constructs, we believe that these next generation bioprinting strategies might hold the potential to recapitulate both the complex architecture and functionality of the vascular system.

References

- (1) Fleischer, S.; Tavakol, D. N.; Vunjak-Novakovic, G. *Adv. Funct. Mater.* **2020**, *30* (37), 1910811.
- (2) Kirkton, R. D.; Santiago-Maysonet, M.; Lawson, J. H.; Tente, W. E.; Dahl, S. L. M.; Niklason, L. E.; Prichard, H. L. *Sci. Transl. Med.* **2019**, *11* (485), eaau6934.
- (3) Lim, K. S.; Baptista, M.; Moon, S.; Woodfield, T. B. F.; Rnjak-Kovacina, J. *Trends Biotechnol.* **2019**, *37* (11), 1189-1201.
- (4) Soliman, B. G.; Major, G. S.; Atienza-Roca, P.; Murphy, C. A.; Longoni, A.; Alcalá-Orozco, C. R.; Rnjak-Kovacina, J.; Gawlitta, D.; Woodfield, T. B. F.; Lim, K. S. *Adv. Healthc. Mater.* **2021**, *11* (2), e2101873.
- (5) Groll, J.; Boland, T.; Blunk, T.; Burdick, J. A.; Cho, D. W.; Dalton, P. D.; Derby, B.; Forgacs, G.; Li, Q.; Mironov, V. A.; et al. *Biofabrication* **2016**, *8* (1), 013001.
- (6) Groll, J.; Burdick, J. A.; Cho, D. W.; Derby, B.; Gelinsky, M.; Heilshorn, S. C.; Jüngst, T.; Malda, J.; Mironov, V. A.; Nakayama, K.; et al. *Biofabrication* **2018**, *11* (1), 013001.
- (7) Lim, K. S.; Galarraaga, J. H.; Cui, X.; Lindberg, G. C. J.; Burdick, J. A.; Woodfield, T. B. F. *Chem. Rev.* **2020**, *120* (19), 10662-10694.
- (8) Miller, J. S.; Stevens, K. R.; Yang, M. T.; Baker, B. M.; Nguyen, D.-H. T.; Cohen, D. M.; Toro, E.; Chen, A. A.; Galie, P. A.; Yu, X.; et al. *Nat. Mater.* **2012**, *11* (9), 768-774.
- (9) Kolesky, D. B.; Truby, R. L.; Gladman, A. S.; Busbee, T. A.; Homan, K. A.; Lewis, J. A. *Adv. Mater.* **2014**, *26* (19), 3124-3130.
- (10) Noor, N.; Shapira, A.; Edri, R.; Gal, I.; Wertheim, L.; Dvir, T. *Adv. Sci.* **2019**, *6* (11), 1900344.
- (11) Skylar-Scott Mark, A.; Uzel Sebastien, G. M.; Nam Lucy, L.; Ahrens John, H.; Truby Ryan, L.; Damaraju, S.; Lewis Jennifer, A. *Sci. Adv.*, **2019**, *5* (9), eaaw2459.
- (12) Cui, H.; Zhu, W.; Huang, Y.; Liu, C.; Yu, Z.-X.; Nowicki, M.; Miao, S.; Cheng, Y.; Zhou, X.; Lee, S.-J.; et al. *Biofabrication* **2019**, *12* (1), 015004-015004.
- (13) Grigoryan, B.; Paulsen, S. J.; Corbett, D. C.; Sazer, D. W.; Fortin, C. L.; Zaita, A. J.; Greenfield, P. T.; Calafat, N. J.; Gounley, J. P.; Ta, A. H.; et al. *Science* **2019**, *364* (6439), 458-464.
- (14) Levato, R.; Lim, K. S.; Li, W.; Asua, A. U.; Peña, L. B.; Wang, M.; Falandt, M.; Bernal, P. N.; Gawlitta, D.; Zhang, Y. S.; et al. *Materials Today Bio* **2021**, *12*, 100162.
- (15) Rizzo, R.; Ruetsche, D.; Liu, H.; Zenobi-Wong, M. *Adv. Mater.* **2021**, *33* (49), 2102900.
- (16) Kolesky, D. B.; Homan, K. A.; Skylar-Scott, M. A.; Lewis, J. A. *Proc. Natl. Acad. Sci. U. S. A.* **2016**, *113* (12), 3179-3184.
- (17) Lee, V. K.; Lanzi, A. M.; Haygan, N.; Yoo, S. S.; Vincent, P. A.; Dai, G. *Cell. Mol. Bioeng.* **2014**, *7* (3), 460-472.
- (18) Song, K. H.; Highley, C. B.; Rouff, A.; Burdick, J. A. *Adv. Funct. Mater.* **2018**, *28* (31), 1801331.
- (19) Rider, P.; Voronov, E.; Dinarello, C. A.; Apte, R. N.; Cohen, I. J. *Immunol.* **2017**, *198* (4), 1395-1402.
- (20) Zhu, W.; Qu, X.; Zhu, J.; Ma, X.; Patel, S.; Liu, J.; Wang, P.; Lai, C. S.; Gou, M.; Xu, Y.; Zhang, K.; Chen, S. *Biomaterials* **2017**, *124*, 106-115.

EVERYTHING BUT THE KITCHEN SINK

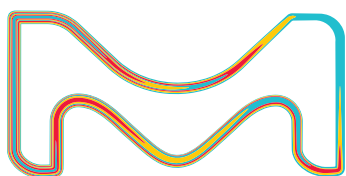
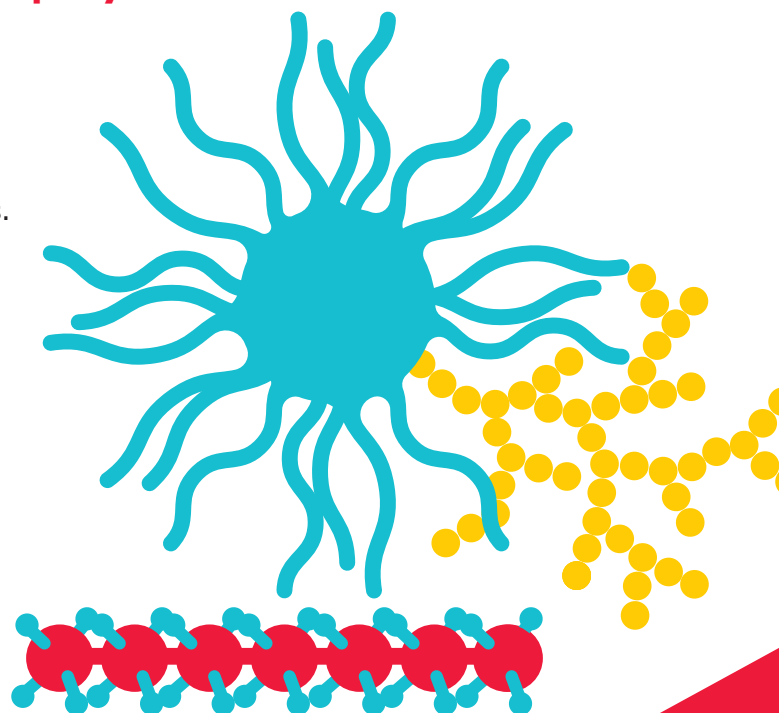
Comprehensive biodegradable polymers for biomedical research

Biodegradable polymers contain polymer chains that are hydrolytically or enzymatically cleavable, resulting in biocompatible or nontoxic by-products. They are widely used in drug delivery research to achieve controlled and targeted delivery of therapeutic agents (e.g. APIs, genetic material, peptides, vaccines, and antibiotics).

We now offer the following classes of high-purity biodegradable polymers:

- Poly (lactide-co-glycolide) copolymers (PLGA)
- Poly(lactic acid) (PLA)
- Poly(caprolactone) (PCL)
- Amphiphilic block copolymers
- End-functionalized biodegradable polymers

For more information, please visit:
[SigmaAldrich.com/biomedical](https://www.sigmaaldrich.com/biomedical)



The life science
business of Merck
operates as
MilliporeSigma in
the U.S. and Canada.

Sigma-Aldrich[®]
Lab & Production Materials

Bioprinting Protocol with Ready-to-use TissueFab® Bioinks

Introduction

TissueFab® bioinks are ready-to-use bioinks formulated for high cell viability and printability and are designed for extrusion-based 3D bioprinting. TissueFab® bioinks are biodegradable and compatible with human mesenchymal stem cells (hMSCs) and other diverse cell types. TissueFab® bioinks are compatible for use with most extrusion-based bioprinters. TissueFab® bioinks enable the precise fabrication of 3D cell models and tissue constructs for research in 3D cell biology, tissue engineering, *in vitro* tissue models, and regenerative medicine.

Disclaimer

TissueFab® bioinks are for research use only, not suitable for human, animal, or other use. Please consult the Safety Data Sheet for hazard information and safe handling practices.

Specifications

Storage: Store TissueFab® bioinks at 2–8 °C. Protect from light by storing the bottle in a foil bag or wrapping in aluminum foil.

Stability: Refer to the expiration date on the batch-specific Certificate of Analysis.

Materials

Materials supplied

TissueFab® bioinks are supplied as follows:

- 1 × 10 mL bottle (1 unit)

Materials required but not supplied

- Cultured cells (visit our website for an [up-to-date list of cell types](#))
- Appropriate cell culture medium
- PBS (Cat. No. [D8537](#))
- Sterile pipette tips for transferring bioink
- Sterile printing cartridge, piston, and nozzle/needle for 3D printing
- Extrusion-based 3D bioprinter
- Water bath or incubator
- Micropipettes
- Light source

Before you start: Important tips for optimal bioprinting results

Optimize printing conditions. Optimize printing conditions (e.g., nozzle diameter, printing speed, printing pressure, temperature, cell density) for the features of your 3D printer and for your application to ensure successful bioprinting. The suggestions below can guide you.

Reduce bubble formation. If the bioink has air bubbles, the bubbles may hamper bioprinting. Carefully handle the bioink when you mix and transfer to avoid bubble formation. Do not vortex or shake vigorously.

Aseptic techniques. Follow standard aseptic handling techniques when preparing and printing the bioink and during cell culture.

Cell density. Resuspend the cell pellet to the appropriate volume for the desired printed structure and cell density. Typical cell density for extrusion-based bioprinting is 1 to 5 × 10⁶ cells/mL.

Note: The number of prints obtained from each 10 mL bottle of bioink (a unit) varies depending on the printed structure. For example, each 10 mL bottle contains enough material to print a 30 µL structure in each well of three 96-well plates or a 100 µL structure in each well of four 24-well plates.

Procedure

Bioprint

Cool the bioink filled printing cartridge to the appropriate temperature indicated in the printing parameters table below using a “temperature-controlled printhead,” if available, or place the cartridge in a 4 °C refrigerator for 10–15 minutes to induce gelation.

TissueFab recommended printing temperature and pressures are listed in **table 1**. Please follow the printer guidelines as recommended by the manufacturer. Load the print cartridge onto the 3D printer and print directly onto a Petri dish or multi-well plates. Adjust the flow rate according to the nozzle diameter, printing speed, printing pressure, and temperature.

Table 1. Printing Parameters

Product #	Name		Recommended Print Temp (°C)	Recommended Print Pressure (kPa)	
905429	TissueFab® bioink	(Gel)ma -UV/365 nm	15	60–70	
918741		(Gel)ma -Vis/405nm	20	110–120	
920983		(GelAlg)ma -UV/365 nm	19	60–80	
921610		(GelAlg)ma -Vis/405 nm	19	70–90	
906905		Sacrificial	25	50–60	
919632		(GelHA)ma -UV/365 nm	18	80–100	
919624		(GelHA)ma -Vis/405 nm	18	80–100	
920975		(GelAlgHA)ma -UV/365 nm	17	50–70	
922862		(GelAlgHA)ma -Vis/405 nm	20	60–70	
905410		Alg(Gel)ma -UV/365 nm	20	70–80	
906913		Alg(Gel)ma -Vis/525 nm	20	70–80	
915033		TissueFab® bioink Bone	Vis/405 nm	20	70–80
915025			UV/365 nm	20	70–80
915637			support gel	80	120–130
915963	TissueFab® bioink Conductive	Vis/405 nm	20	70–80	
915726		UV/365 nm	20	70–80	

Troubleshooting

1. Bioink is incubated at 37°C for 30 minutes, but it is still gel.

Possible reasons: Malfunction of the incubator; or the bioink is crosslinked due to light exposure.

Solution: Ensure the temperature of the incubator/water bath is correct, and make sure the bioink bottle is evenly and adequately heated in the incubator/water bath. Do not expose the bioink to light before printing.

2. Air bubble is trapped in the middle of the bioink in the cartridge.

Possible reasons: Air bubble was created during transferred or when cells were dispersed in the bioink.

Solution: Warm the cartridge at 37°C for 5–10 minutes or until the bioink becomes fluid. Turn the cartridge so the tip faces up to allow any air bubbles to exit from the cartridge tip. Gently tap the cartridge to help air bubbles pass through the tip.

3. Printed structure spreads and does not hold its shape.

Possible reasons: Bioink was diluted with cell culture medium that remained in the cell pellet; bioink was not cooled sufficiently before printing, or the printing pressure was too high.

Solution: Do not dilute the bioink. Make sure the bioink has been cooled according to the instructions before printing. Adjust printing pressure to achieve sufficient flow of bioink.

4. Interrupted flow or no flow during printing.

Possible reasons: Insufficient printing pressure or nozzle is partially or fully clogged.

Solution: Adjust the printing pressure to achieve a sufficient flow of bioink. If the problem persists, change the nozzle.

Bioinks Preparation

This section includes basic protocols for bioink preparation for products from MilliporeSigma Partnerships; T&R Biofab, Advanced Biomatrix, and Rokit.

Three-dimensional (3D) gels allow for the study of the effects of the mechanical properties of the extracellular matrix (ECM), such as density and rigidity, on cell development, migration, and morphology. Unlike 2D systems, 3D environments allow cell extensions to simultaneously interact with integrins on all

cell surfaces, resulting in the activation of specific signaling pathways. Gel stiffness or rigidity also affects cell migration differently in 3D versus 2D environments. Furthermore, integrin-independent mechanical interactions resulting from the entanglement of matrix fibrils with cell extensions are possible in 3D systems but not in 2D systems where the cells are attached to a flat surface.

PhotoCol™ Methacrylated Collagen Bioink Preparation

Introduction

MilliporeSigma, in partnership with Advanced BioMatrix, offers PhotoCol™, a purified methacrylated Type I bovine collagen kit, which provides native-like 3D collagen gels with the unique attribute of being tunable when prepared at various concentrations and crosslinked with blue light.

The PhotoCol™ kit consists of purified methacrylated Type I bovine collagen as the core component with other support reagents in the kit. The methacrylated Type I collagen is produced from telo-peptide intact bovine collagen. The collagen has been modified by reacting the free amines, primarily the ϵ -amine groups of the lysine residues and the α -amines groups on the *N*-termini. Greater than 20% of the total lysine residues of the collagen molecule have been methacrylated. The collagen is extracted from bovine hide and contains a high monomer content. The collagen starting material was isolated from a closed herd and purified using controlled manufacturing processes.

The collagen is extracted from bovine hide and contains a high monomer content. The collagen starting material was isolated from a closed herd and purified using controlled manufacturing processes.

The 20 mM acetic acid solution is provided to solubilize the lyophilized methacrylated collagen at concentrations of 3 to 8 mg/ml.

The neutralization solution consists of an alkaline 10X phosphate-buffered saline (PBS) solution, which provides physiological salts and neutral pH in the final mixture.

Photoinitiator solution varies by kit

Each kit contains a unique photoinitiator that polymerizes under different conditions and in different solutions.

Product	Cat. No.	Photoinitiator	Light Source	Wave-length	Solution
PhotoCol™ -IRG	917575	Irgacure 2959	UV	365 nm	Methanol
PhotoCol™ -LAP	916293	LAP	Blue light	405 nm	1X PBS or cell culture media
PhotoCol™ -RUT	917834	Ruthenium and sodium persulfate	Visible light	400–450 nm	1X PBS or cell culture media

To sterilize, resuspend and filter each component **separately** through a 0.2 micron button filter.

Note: The PhotoCol™ kit is designed to provide collagen gels with varying gel stiffness based on collagen concentration and crosslinking. Light intensity, protein concentration, photoinitiator concentration, photocrosslinking time, and other variables will affect polymerization performance.

Specifications

Storage: Store PhotoCol™ Kits at 2–8 °C. The product ships on frozen gel packs. Store the neutralization solution at room temperature. Protect from light by storing the bottle in a foil bag or wrapping in aluminum foil.

Stability: Refer to the expiration date on the batch-specific Certificate of Analysis. After solubilizing the collagen with acetic acid, the collagen solution is stable for 2 months when stored at 2–8 °C.

Materials

Materials supplied

- Collagen, Type I, methacrylated, lyophilized 100 mg
- Acetic Acid, 20 mM solution 50 ml
- Neutralization solution 10 ml
- Photoinitiator (varies by kit)

Materials required but not supplied

- Cultured cells (visit our website for an [up-to-date list of cell types](#))
- Appropriate cell culture medium
- PBS (Cat. No. [D8537](#))
- Methanol (if using [917575](#))
- Sterile pipette tips for transferring bioink
- Sterile printing cartridge, piston, and nozzle/needle for 3D printing
- Extrusion-based 3D bioprinter
- Water bath or incubator
- Micropipettes
- Light source

Before you start: Important tips for optimal bioprinting results

Aseptic techniques. Employ aseptic practices to maintain the sterility of the product throughout the preparation and handling of the collagen and other solutions.

Handling. It is recommended that the collagen and other working solutions be chilled and kept on ice during collagen preparation.

Vortexing is not recommended unless expressly stated.

Procedure

1. Add volume of 20 mM acetic acid ([Table 1](#)) to the lyophilized methacrylated collagen to achieve the desired concentration.

Table 1: Recommend concentration(s) range from 3 to 8 mg/ml.

Desired PhotoCol™ Concentration	Volume of 20 mM Acetic Acid
3 mg/ml	33.3 ml
4 mg/ml	25.0 ml
6 mg/ml	16.7 ml
8 mg/ml	12.5 ml

Table 4: Photoinitiator Volumes

Cat. No	Photoinitiator	Calculation for Photoinitiator Volume
916293	LAP	Volume of LAP = (Volume of Collagen + Volume of NS) * 0.02
917834	Ruthenium and sodium persulfate	Volume of Ruthenium = (Volume of Collagen + Volume of NS) * 0.02 Volume of Sodium persulfate = (Volume of Collagen + Volume of NS) * 0.02 Note: Calculate the volume of <i>each</i> photoinitiator. For example, If the resulting number is 100 µl, you will add 100 µl of ruthenium and 100 µl of sodium persulfate
916575	I2959	Calculate Volume of I2959 Volume of I2959 = (Volume of Collagen + Volume of NS) * 0.01 Note: I2959 only has a 2-week shelf life upon solubilizing. If you need the I2959 to last longer, remove the required amount and solubilize a 10% solution

2. Mix on a shaker table or rotator plate at 2–10 °C until fully solubilized or overnight. Avoid the formation of air bubbles as possible.

Note: The higher concentrations of collagen will take longer to solubilize.

3. Determine the desired volume of collagen required based on printing requirements.
4. Determine the volume of the neutralization solution (NS) to mix with the collagen. To achieve a final pH of 7.0 to 7.4, follow the guidelines below in [Table 2](#) or [Table 3](#).

Note: Dispensing by weight versus volume varies due 1) to the different viscosity of the different collagen concentrations and 2) sample hold up in the pipet tip.

5. Transfer the required volume of the neutralization solution (NS) into a sterile vessel or tube and briefly chill.

Note: If the neutralization solution is chilled too long, the salts will come out of solution.

6. Calculate the volume of photoinitiator required for crosslinking following [Table 4](#).

Table 2: Collagen to Neutralization Solution by Weight

Solubilized Collagen Concentration	Weight of Collagen	Volume of NS
3 mg/ml	1.0 g	100 µl
4 mg/ml	1.0 g	114 µl
6 mg/ml	1.0 g	120 µl
8 mg/ml	1.0 g	128 µl

Table 3: Collagen to Neutralization Solution by Volume

Solubilized Collagen Concentration	Volume of Collagen	Volume of NS
3 mg/ml	1.0 ml	95 µl
4 mg/ml	1.0 ml	90 µl
6 mg/ml	1.0 ml	85 µl
8 mg/ml	1.0 ml	80 µl

7. Solubilize the photoinitiator with the recommended solvent in **Table 5**.
8. Add the calculated volume of chilled photoinitiator (**Table 4**) to the volume of chilled neutralization solution (NS) (From **Tables 2–3**) and mix thoroughly.
9. Transfer the total volume of the chilled collagen into the chilled neutralization solution (NS)/photoinitiator. Mix quickly and thoroughly by pipetting or rotating a vessel or tube. Do not vortex.

Note: Keep the collagen mixture chilled throughout this process.

Note: Check to ensure the pH is neutral. The high viscosity of this material can make it difficult to mix.

10. If desired, add dispersed chilled cells to the collagen mixture. Mix quickly and thoroughly by pipetting or rotating a vessel or tube.

Note: If air bubbles are a concern, allow to sit on ice until the bubbles come to the surface.

11. Load the mixture into a cartridge and dispense or print the collagen mixture in the desired sterile plates, culture vessels, or molds.

12. Incubate at 37 °C for > 30 minutes for gel formation.

13. To photocrosslink, place the gels directly under the recommended light source listed in **Table 6**.

Note: The consistency and fidelity of photocrosslinking are improved by printing gels on glass-bottom substrates with good optical properties that produce minimal light scattering.

References

- (1) Gaudet, I. D.; Shreiber, D. I. *Biointerphases* **2012**, 7 (1–4), 25.
- (2) Drzewiecki, K. E.; Parmar, A. S.; Gaudet, I. D.; Branch, J. R.; Pike, D. H.; Nanda, V.; Shreiber, D. I. *Langmuir* **2014**, 30 (37), 11204–11211.

Table 5: Photoinitiator Solutions

Cat. No.	Photoinitiator	Photoinitiator Volume	Final Concentration	Solvent
916293	LAP	From Step 6	17 mg/ml	1X PBS or cell culture media
917834	Ruthenium and sodium persulfate	From Step 6	1) Ruthenium: 37.4 mg/ml 2) Sodium persulfate: 119 mg/ml	1X PBS or cell culture media
916575	I2959	From Step 6	100 mg/ml (Add 1 mL of neat methanol to the amber vial containing 100 mg of I2959 and vortex)	100% Methanol

Table 6: Recommended Light Source

Cat. No.	Photoinitiator	Light Source	Wavelength	Exposure time	
916293	LAP	Blue light	405 nm		
917834	Ruthenium and sodium persulfate	Visible light	400–450 nm		
916575	I2959	UV	365 nm	Exposure correlates to gel stiffness*	
				40 sec	22% increase in stiffness
				90 sec	53% increase in stiffness
				10 min	75% increase in stiffness

* Longer exposure results in more crosslinking; however, exposure to UV and free radicals (generated by the photoinitiator) can affect cellular behavior and lead to cell death. The effects of exposure length depend on cell type.

PhotoHA™ Methacrylated Hyaluronic Acid Bioink Preparation

Introduction

Hyaluronic acid is the most abundant glycosaminoglycan in the body and an essential component of several tissues. While it is abundant in extracellular matrices, hyaluronan also contributes to tissue hydrodynamics, movement, and proliferation of cells and participates in several cell surface receptor interactions.

Hyaluronic acid is a polymer of disaccharides composed of D-glucuronic acid and N-acetyl-D-glucosamine, linked via alternating β -(1→4) and β -(1→3) glycosidic bonds. Hyaluronic acid can be 25,000 disaccharide repeats in length. Hyaluronic acid polymers can range from 5,000 to 20,000,000 Da *in vivo*. Hyaluronic acid is energetically stable, in part because of the stereochemistry of its component disaccharides. Bulky groups on each sugar molecule are in sterically favored positions, whereas the smaller hydrogens assume the less-favorable axial positions.

MilliporeSigma, in partnership with Advanced BioMatrix, offers PhotoHA™, a purified hyaluronic acid (HA) methacrylate kit, which provides native-like 3D HA gels with the unique attributes to be prepared at various concentrations and photocrosslinked to provide various gel stiffness.

Hyaluronic acid contains primary amino groups that react with methacrylic anhydride (MA) to add methacrylate pendant groups to the hyaluronic acid molecule. The method renders the hyaluronic acid into a product with unique properties. The PhotoHA™ UV-kit consists of HA methacrylate and a light-activated photoinitiator.

The photoinitiator solution will vary by kit

Each kit contains a unique photoinitiator that polymerizes under different conditions and in different solutions.

Product	Cat. No.	Photoinitiator	Light Source	Wavelength	Solution
PhotoHA™-IRG	917079	Irgacure 2959	UV	365 nm	Methanol
PhotoHA™-LAP	916471	LAP	Blue light	405 nm	1x PBS or cell culture media
PhotoHA™-RUT	917338	Ruthenium and sodium persulfate	Visible light	400-450 nm	1X PBS or cell culture media

Specifications

Storage: Store PhotoHA™ Kits at 2–8 °C. The product ships on frozen gel packs. The product and components are stable for a minimum of 1 year at receipt in powder form.

Stability: Refer to the expiration date on the batch-specific Certificate of Analysis.

Once solubilized, the PhotoHA™ can be stored at 2–10 °C for 1 month. The photoinitiator can be stored for no more than 2 weeks once solubilized.

Materials

Materials supplied

- Methacrylated Hyaluronic Acid, 100 mg
- Photoinitiator (varies by kit)

Materials required but not supplied

- Cultured cells (visit our website for an [up-to-date list of cell types](#))
- Appropriate cell culture medium

- PBS (Cat. No. [D8537](#))
- Methanol (if using [917079](#))
- Sterile pipette tips for transferring bioink
- Sterile printing cartridge, piston, and nozzle/needle for 3D printing
- Extrusion-based 3D bioprinter
- Water bath or incubator
- Micropipettes
- Light source

Before you start: Important tips for optimal bioprinting results

Aseptic techniques. Employ aseptic practices to maintain the sterility of the product throughout the preparation and handling of the collagen and other solutions.

Handling. It is recommended that the collagen and other working solutions be chilled and kept on ice during collagen preparation.

Procedure

The following recommended instructions are for a 1% hyaluronic acid (HA) methacrylate solution. Adjustments to this protocol may be required for various concentrations, recommended concentrations are 0.5–3.0% (5–30 mg/ml).

1. Add 10 ml of 1X phosphate buffer saline (PBS), water, or cell culture media to the 100 mg of lyophilized methacrylated HA powder.
2. Mix on a shaker table or rotator plate until fully solubilized (~30 to 60 minutes) at 2–10 °C.

Note: Solubilization times may vary depending on the desired concentration and volume of PBS, water or medium added.

3. Calculate the volume of the photoinitiator required following **Table 1**.

4. Solubilize the photoinitiator following **Table 2**.
5. Add the calculated volume of photoinitiator to the required volume of HA methacrylate solution and mix until homogeneous.
6. Resuspend your cell pellet with your HA/Photoinitiator solution
7. Dispense or print your HA methacrylate /photoinitiator/ cell solution into the desired cultureware (i.e., 6-well plate, 48-well plate), molds, or constructs.
8. To photocrosslink, place the gels directly under the recommended light source listed in **Table 3**.

Note: The consistency and fidelity of crosslinking are improved by printing gels on glass-bottom substrates with good optical properties that produce minimal light scattering.

Table 1: Photoinitiator Volumes

Cat. No.	Photoinitiator	Calculation for Photoinitiator Volume
916471	LAP	Volume of LAP = (Volume of HA solution) * 0.02
917338	Ruthenium and sodium persulfate	Volume of Ruthenium = (Volume of HA solution) * 0.02 Volume of Sodium persulfate = (Volume of HA solution) * 0.02 Note: Calculate the volume of each photoinitiator. For example, if the resulting number is 100 ul, you will add 100 ul of ruthenium and 100 ul of sodium persulfate in each vial
917079	I2959	Volume of I2959 = (Volume HA solution) * 0.01 Note: I2959 only has a 2-week shelf-life upon solubilizing. Only dissolve the required amount of photoinitiator. Store remaining photoinitiator (powder or solution) at 2–10 °C

Table 2. Photoinitiator solutions

Cat. No.	Photoinitiator	Photoinitiator Volume	Final Concentration	Solvent
916471	LAP	From Step 3	17 mg/ml	1X PBS or cell culture media
917338	Ruthenium and sodium persulfate	From Step 3	Ruthenium: 37.4 mg/ml Sodium persulfate: 119 mg/ml	1X PBS or cell culture media
917079	I2959	From Step 3	100 mg/ml (Add 1 mL of neat methanol to the amber vial containing 100 mg of I2959 and vortex	100% Methanol

Table 3: Recommended Light Source

Cat. No.	Photoinitiator	Light Source	Wavelength
916471	LAP	Blue light	405nm
917338	Ruthenium and sodium persulfate	Visible light	400-450 nm
917079	I2959	UV	365nm

* Longer exposure results in more crosslinking; however, exposure to UV and free radicals (generated by the photoinitiator) can affect cellular behavior and lead to cell death. The effects of exposure length depend on cell type.

Lifeink® Type I Collagen Bioink Preparation

Introduction

MilliporeSigma, in partnership with Advanced BioMatrix, offers two types of Lifeinks®.

Collagen Bioink	Cat. No.
Lifeink® 200, neutralized type I collagen bioink, 35 mg/ml	916226
Lifeink® 240, acidic type I collagen bioink, 35 mg/ml	915211

- Lifeink® 200, a bioink that is a highly concentrated type I collagen. Lifeink® 200 is pH-neutral collagen with physiological salt concentration. Lifeink® 200 needs to be printed at 2–8 °C into LifeSupport™ (FRESH Printing) for optimal results. For use in cellular bioprinting.
- Lifeink® 240 is a Type I collagen bioink at a 35 mg/ml concentration for extrusion-based 3D bioprinting. Lifeink® 240 is acidified collagen formulated in an acidic saline buffer solution. Lifeink® 240 needs to be printed at 2–8 °C into LifeSupport™ (FRESH Printing) for optimal results. After printing into LifeSupport™, the pH and salt concentration of the printed structure is at physiological levels. Other materials can be added to the Lifeink® 240 bioink in lieu of cells. Cells should NOT be added directly to this bioink.

Specifications

Storage: Store Lifeink® at 2–8 °C. The product ships on frozen gel packs.

Stability: Refer to the expiration date on the batch-specific Certificate of Analysis. The product is stable for a minimum of 1 year at receipt in powder form.

Materials

Materials supplied

- Lifeink® 200 or Lifeink® 240

Materials required but not supplied

- Cultured cells ([visit our website for an up-to-date list of cell types](#)) (for use with product [916226](#) only)
- Appropriate cell culture medium (for use with product [916226](#) only)

- PBS (Cat. No. [D8537](#))
- Sterile pipette tips for transferring bioink
- Sterile printing cartridge, piston, and nozzle/needle for 3D printing
- Extrusion-based 3D bioprinter
- Water bath or incubator
- Micropipettes

Before you start: Important tips for optimal results

Aseptic techniques. Employ aseptic practices to maintain the sterility of the product throughout the preparation and handling of the collagen and other solutions.

Handling. It is recommended that the collagen and other working solutions be chilled during the preparation of the bioink.

Vortexing of collagen is not recommended at any step.

Reduce bubble formation. Ensure that NO bubbles enter the system. The introduction of bubbles within the bioink during mixing will result in a foam-like material.

Optimize printing conditions. For pneumatic printers, transfer the collagen into an appropriate syringe using a syringe coupler. The new syringe should have the seal inserted, but the plunger removed. Centrifuge the syringe at 2000 RPM for 1 minute after transferring the collagen to remove any air bubbles.

Procedure – Preparing Bioink

1. Prepare cell suspension or additives solution ([Table 1](#)) for in a separate sterile syringe (Syringe 1) to be mixed with the bioink before printing.
2. Place sterile coupler on the end of Syringe 1 (containing cell suspension or additive solution)
3. Slowly push plunger until solution forms a slight external meniscus above the end of the coupler on the syringe.
4. Remove cap from the syringe with collagen (Syringe 2) and slowly push plunger until collagen forms a slight external meniscus above the end of the syringe.

Table 1: Suspension or additives preparation

Cat. No.	Lifeink®	Applications	Recommended final concentration	Volume of cell suspension or additive solution
916226	Lifeink® 200	Cell encapsulation	5x10 ⁶ cells/mL**	2 mL of cell suspension per 5 mL Lifeink® 200*
915211	Lifeink® 240	Additives compatible with acidic pH conditions	N/A	5 mL of additives per 5 mL Lifeink® 240*

* For smaller volumes, use a similar ratio.

**Cell culture media is recommended for cell suspension.

- Couple the Syringe 1 (containing the cell suspension or additive solution) to the Syringe 2 (collagen).

Note: Ensure that there are no air bubbles in the system. The “external meniscus” on both syringes helps prevent air bubbles formation.

- Slowly push plungers back and forth ~40 times to ensure thorough mixing. End with all of the material in the syringe to be used for printing.
- The bioink with other components is now ready for extrusion 3D bioprinters.

General Printing Notes

To use a smaller volume of collagen, transfer the desired amount of collagen to another syringe using the provided sterile coupler. To remove the air from the new syringe, you can do either of the following:

- Centrifuge the syringe (capped) with the cap pointing up to cause the air to accumulate at the cap. Evacuate the air.
- Centrifuge the syringe (capped) with the cap pointing down, and then use a hemostat to squeeze the syringe while pushing the plunger to allow the air to escape.

When printing with FRESH gelatin slurry, allow the final printed structure to incubate at 37 °C for 30 to 60 minutes, and then replace the gelatin with media.

Lifesupport™ Support Slurry Preparation

Introduction

FRESH 3D bioprinting is performed by extruding bioinks and other materials within the hydrated, compacted LifeSupport™ bath, specially formulated to prevent constructs from collapsing and deforming during printing. A wide range of polymer crosslinking chemistries and gelation mechanisms can be supported within LifeSupport™ by incorporating ions, enzymes, pH buffers, and more into the support bath during the rehydration process. LifeSupport™ allows for FRESH 3D bioprinting of soft hydrogel bioinks in complex geometries without the need for sacrificial support inks (e.g., Pluronic® F-127, polycaprolactone, gelatin) or ink modifiers to increase mechanical stability (e.g., gelatin methacrylate, cellulose, alginate).

LifeSupport™ can be rehydrated in a range of buffers and cell culture media to support multiple cell types and specific bioinks. LifeSupport™ can also be rehydrated to support the cross-linking and/or gelation of multiple types of bioinks within the same container of support bath. Bioinks that can be printed into the support bath include collagen, alginate, fibrin, decellularized extracellular matrix, methacrylated gelatin, methacrylated hyaluronic acid, and more. The specific bioinks that can be printed will also depend on the hardware capabilities of the 3D bioprinter that you are using.

MilliporeSigma, in partnership with Advanced BioMatrix, offers two types of Lifeinks® that are formulated to print into LifeSupport™ as discussed in the previous protocol.

Description	Cat. No.
LifeSupport™, support slurry for FRESH bioprinting	915467

Specifications

Storage: Store LifeSupport™ at room temperature. Limit exposure to air, LifeSupport™ is highly hygroscopic.

Stability: Refer to the expiration date on the batch-specific Certificate of Analysis. Rehydrated LifeSupport™ can be stored in the noncompacted state (i.e., before centrifugation) for 7 days under refrigeration to avoid degradation.

Once compacted, LifeSupport™ should be used within 12 hours, and the temperature should not exceed 32 °C during handling or printing.

Materials

Materials supplied

Each LifeSupport™ printing kit comes with 5 individual 2 g units of sterile, dried, LifeSupport™ powder, composed of gelatin microparticles of defined size and shape. Each unit rehydrates to approximately 20 mL of support bath.

Materials required but not supplied

- Cultured cells ([visit our website for an up-to-date list of cell types](#)) (for use with product [916226](#) only)
- Appropriate cell culture medium (for use with product [916226](#) only)
- PBS ([Cat. No. D8537](#))
- Sterile pipette tips for transferring bioink
- Sterile printing cartridge, piston, and nozzle/needle for 3D printing
- Extrusion-based 3D bioprinter
- Water bath or incubator
- Micropipettes

Before you start: Important tips for optimal bioprinting results

Aseptic techniques. Employ aseptic practices to maintain the sterility of the product throughout the preparation and handling of the collagen and other solutions.

Handling. To prevent premature melting of LifeSupport™, all suspension media should be refrigerated before use.

Reduce bubble formation. Ensure that NO bubbles enter the system. The introduction of bubbles within the bioink during mixing will result in a foam-like material.

Optimize printing conditions. For pneumatic printers, transfer the collagen into an appropriate syringe using the coupler. The new syringe should have the seal inserted, but the plunger removed. Centrifuge the syringe at 2000 RPM for 1 minute after transferring the collagen to remove any air bubbles.

Procedure

1. For best preparation results, we strongly recommend splitting the 2g unit of LifeSupport™ into 1g aliquots. Add 35 mL of cold (4 °C) suspension media to a 1g aliquot of LifeSupport™.
2. Vortex (Figure A) and shake vigorously for 1 min to ensure all powder is fully resuspended (top right) and not stuck to tube walls / tip (bottom right).
3. Let stand for 10 minutes at 4 °C to allow LifeSupport™ to rehydrate fully.

OPTIONAL: Degas the support bath in a vacuum chamber for 30 min to remove dissolved gases and prevent the formation of bubbles during printing.

4. After rehydration, shake LifeSupport™ for 10 seconds. Centrifuge the rehydrated LifeSupport™ at 600x g for 5 min.
5. The LifeSupport™ should now be compacted at the bottom of the centrifuge tube (Figure B). Gently pour off or aspirate the liquid supernatant to leave only the compacted LifeSupport™ in the bottom of the centrifuge tube (Figure C). Cap the tube containing the compacted LifeSupport™.

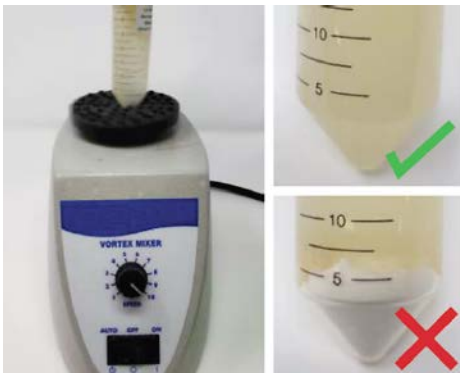


Figure A. Proper vortexing

6. Dislodge the compacted LifeSupport™ slurry by holding horizontally, and gently tapping the body of the tube against the edge of a hard surface 15 times (Figure D).
7. Shake the tube containing dislodged LifeSupport™ vigorously for 10 seconds. Shake along the length of the tube (Figure D). *User should feel LifeSupport™ moving and hitting the cap and inner surfaces of the tube during shaking.*

Note: Hold tube by the cap during shaking and avoid handling the body of the tube to reduce warming.



Figure B. LifeSupport™ compacted at the bottom of the centrifuge tube with liquid supernatant on top.



Figure C. LifeSupport™ compacted at the bottom of the centrifuge tube with liquid supernatant removed.

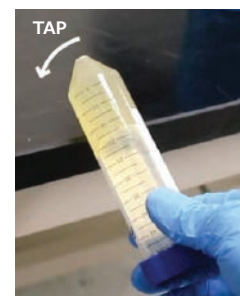


Figure D. Demonstrating the tapping process.

- Centrifuge well-shaken LifeSupport™ at 1000x g for 5 min to compact it. If resuspended in serum-based growth media, centrifuge at 2000 x g for 5 min until compacted. To ensure the LifeSupport™ bath is compacted the material should stay in place when the tube is slowly turned on its side (**Figure E**).

Note: Use a temperature-controlled centrifuge if possible. If this is not available, carefully monitor LifeSupport™ behavior after centrifugation. If your centrifuge warms up significantly during the centrifugation cycle, it may affect the performance of LifeSupport™.

- The LifeSupport™ should now be compacted at the bottom of the centrifuge tube. Gently pour off or aspirate any remaining liquid supernatant to leave only the compacted LifeSupport™ in the bottom of the centrifuge tube. LifeSupport™ has been appropriately prepared if the LifeSupport™ stays in place when the tube is slowly placed horizontally (**Figure E**). A small amount of flow is acceptable.

WARNING If the LifeSupport™ flows easily in the tube (**Figure E**), stop and resuspend in cold media, and repeat steps 4-10. In this case, it may be necessary to increase the “2nd Centrifugation” speed in step 9 in 200X g increments until LifeSupport™ is adequately compacted.

- Aseptically remove the compacted LifeSupport™ using a sterile spatula into the desired printing container.
- Tap the container against a surface to settle and evenly distribute the bath in the container.



Figure E. Demonstrating properly compacted LifeSupport™.



Figure F. Removing compacted LifeSupport™.

- The bath should be as bubble-free as possible. Tapping firmly against the table can force large bubbles to the surface. The bath should not move easily if the container is tilted. Be gentle when tapping glass dishes. It is recommended that you use a print container that provides a minimum of 1 mm clearance on the bottom and a minimum of 3 mm clearance on all sides as well as the top of the construct to be printed. Additional clearance is fine but requires using more LifeSupport™.

Printing Recommendations

Note: LifeSupport™ can be used as a scaffold support for a variety of bioinks, including Lifeink® 200, Lifeink® 240, collagen, alginate, fibrinogen, and other inks with cells. For recommended printing guidelines for Lifeink®, please refer to the protocols within this guide.

- Ensure the print container is large enough to avoid the needle running into the walls during printing.
- Place the LifeSupport™ bath on your 3D bioprinting platform. **OPTIONAL** Vacuum grease (Dow Corning, 1597418) can be added to the bottom of the print container to prevent sliding during printing.
- Position your needle ~1 mm off the bottom of the container, then move the needle to the middle of the container. Unlike typical printing, the needle does not have to start out touching or even be close to the bottom of the container. The support bath will trap your print in place no matter where you start. Ensure that your printer begins printing from this position. You may need to disable homing procedures to prevent the printer from traveling outside the container.
- Begin printing.

Print Release Recommendations

- After printing, incubate at 37 °C for at least 30 min to release your print.
- After 30 min of incubation, the LifeSupport™ bath should be fully melted, and your printed structure will be released. Large volumes may require longer times to completely melt.
- Carefully transfer released prints into warm (37 °C) suspension media according to your ink.

NOTE: Melted LifeSupport™ can be serially replaced with suspension media to avoid handling the printed construct. For example, if you printed into a 6-wellplate, carefully aspirate 2 mL of melted LifeSupport™ out and add 2 mL of warm media. Repeat this process until most of the gelatin has been replaced by media.

- If culturing tissues, continue standard media exchange in accordance with your cell culture protocol.

Decellularized ECM Bioink Precursor Preparation

Introduction

MilliporeSigma, in partnership with T&R Biofab, offers a decellularized ECM bioink precursor. The decellularized ECM (dECM) is a biomaterial consisting of both structural and functional biomolecules, such as collagen, glycosaminoglycans, and glycoproteins. Decellularized ECM bioink precursors have different characteristics depending on the origin of tissues (skin, bone, cartilage), thus providing optimized environments for cellular activities that are tissue-specific.

Decellularized Bioink	Cat. No.
Decellularized ECM bioink precursor from porcine bone, suitable for 3D bioprinting applications	906883
Decellularized ECM bioink precursor from porcine skin, suitable for 3D bioprinting applications	906867
Decellularized ECM bioink precursor, from porcine cartilage, suitable for 3D bioprinting applications	906875

Specifications

Storage: Store decellularized ECM bioink precursor at -20 °C for up to 12 months.

Stability: Refer to the expiration date on the batch-specific Certificate of Analysis.

Materials

Materials supplied

- Decellularized ECM bioink precursor lyophilized solid 100 mg

Materials required but not supplied

- 0.5M acetic acid
- 10x Minimum Essential Medium (MEM) (Cat. No. [M0275](#))
- HEPES (Cat. No. H4034)
- Sodium bicarbonate (NaHCO₃)
- Deionized or Distilled water
- Sodium hydroxide (NaOH)
- Cultured cells ([visit our website for an up-to-date list of cell types](#))
- Appropriate cell culture medium
- PBS
- Sterile tube for reagent preparation
- Positive displacement pipette is recommended
- Sterile pipette tips for transferring bioink
- Sterile printing cartridge, piston, and nozzle/needle for 3D printing
- Extrusion-based 3D bioprinter
- Petri-dish
- Scraper
- pH indicator

Before you start: Important tips for optimal bioprinting results

Aseptic techniques. Employ aseptic practices to maintain the sterility of the product throughout the preparation and handling of the collagen and other solutions.

Handling. All processes should be completed at 2–8 °C to prevent gelation of the solubilized bioink precursor.

The solubilized bioink should be prepared and used immediately

Procedure

Bioink Solubilization process

- Prepare 0.5M acetic acid and decellularized ECM bioink precursor on ice.
- Place the decellularized ECM bioink precursor in a glass vial and add 0.5M acetic acid to the desired concentration. A 3% ink (30 mg/ml) is recommended for printing. (i.e. 1 ml final sample; 24 mg precursor in 800µl of acetic acid)
- Keep the sample at 2–8 °C for 72 hours to ensure solubilization. ([Figure 1 and 2](#))

Note: It is recommended to Vortex ink every 24 hours during the solubilization process.

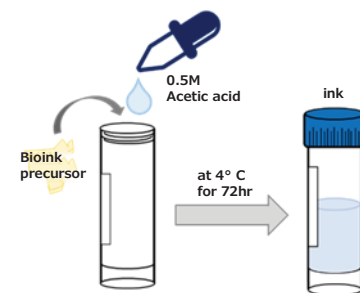


Figure 1. Bioink Solubilization process

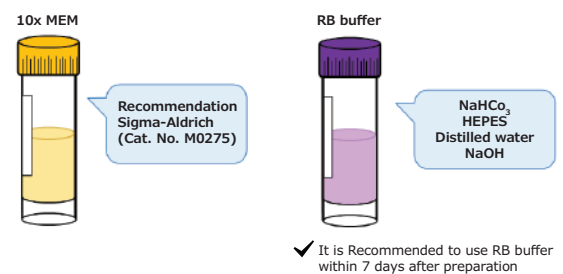


Figure 2. Reagent preparation

Reagent preparation

- Prepare resuspension buffer (RB) by mixing the components as mentioned in **Table 1**.

Bioink preparation procedure

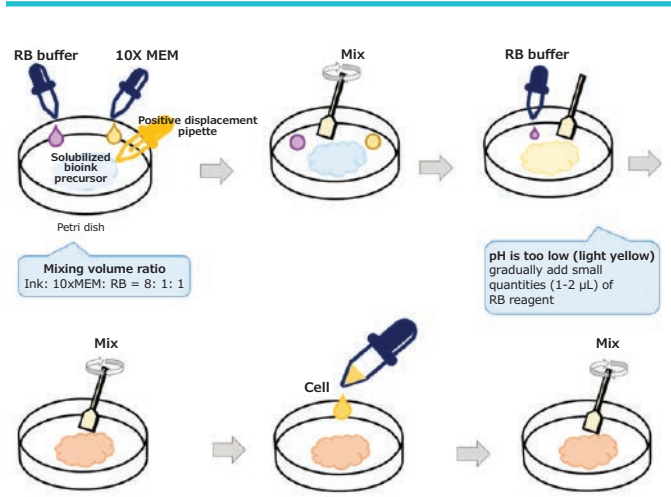
Note: This procedure can be done using either a petri dish or a 50 mL tube (**Options 1 and 2**).

Table 1. RB composition

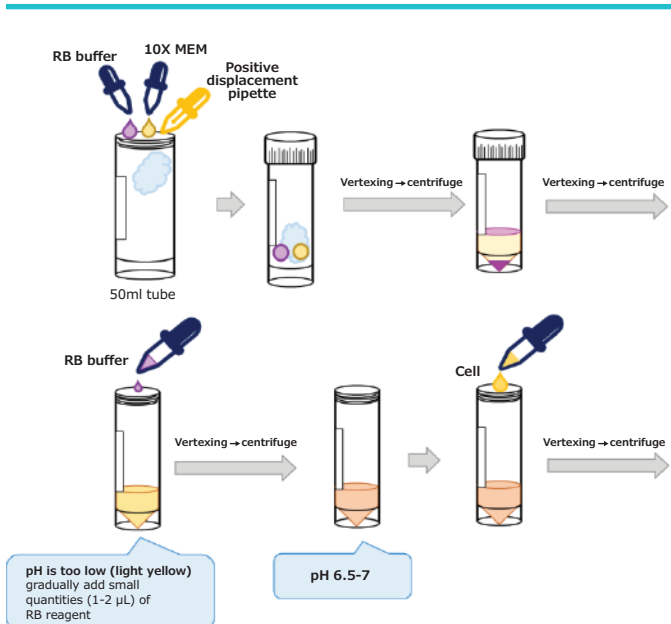
		NaHCO ₃ (g)	HEPES (g)	Distilled water (ml)	NaOH (g)
Skin	906867	0.22	0.48	10	1.4
Bone	906883	0.22	0.48	10	1.7
Cartilage	906875	0.22	0.48	10	1.7

Note: Use RB buffer within 7 days after preparation.

Option 1: Prepare in a petri dish



Option 2: Prepare in a 50mL tube



- Place RB, 10xMEM (Minimum Essential Medium, **Cat. No. M0275**) and solubilized bioink precursor on ice to cool for ~10 mins
- Mix together 10 MEM, RB, and ink (mixing volume ratio - ink:10MEM:RB = 8:1:1) (i.e. 800 µl ink, 100 µl 10X MEM, 100 µl RB).
- Adjust ink pH to 6.5-7.0. See Options for mixing in following sections.

Note: The color of the final bioink should be light orange (**Figure 1**). If the pH of the bioink is too low (pH <6.5, and indicated by light yellow or yellow color), add small quantities (1-2 µl) of RB reagent and gradually adjust it to the ideal pH range.

- Resuspend the cell pellet at the desired cell density with the bioink solution by gently pipetting up and down. Maximum 100 µl cell suspension can be mixed with 1 ml of bioink solution; we recommend a starting cell density of 1×10^7 cells/ml media, although this will vary depending on the cell type used.

Printing procedure

- Transfer solubilized bioink precursor to a printing cartridge (**Figure 2**).

Note: Centrifugation can be used for removing residual bubbles (Recommended condition: 2,000 RPM for 30 s at 4 °C)

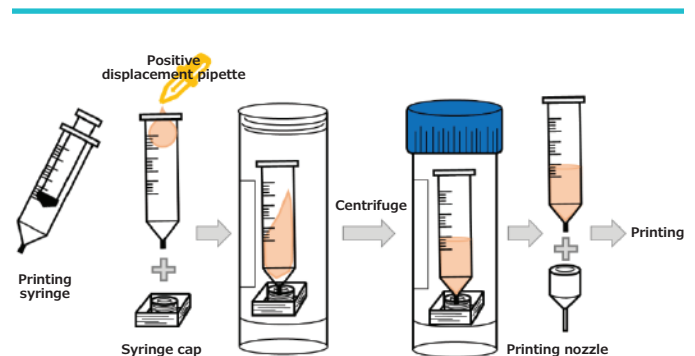
- Start printing process using bioink, and then incubate the printed construct for 40-60 minutes without any solutions (ex. culture medium) in an incubator (at 37 °C in a humidified atmosphere with 5% CO₂) for gelation.

Note: Recommending printing temperature: For prints < 30 minutes: room temperature printing, for prints >30mins <3 hours: 15 °C.


Figure 1. Mixing to correct pH adjusted color.



Figure 2. Printing Procedure



Example of printing conditions; printing conditions may vary from user to user.

Contents	Skin	Bone	Cartilage
Ink concentration (w/v %)		3%	
Nozzle Diameter (µm)		500	
Minimum pneumatic pressure (kPa)		10	
Feed rate (mm/min)		500	
Strut width (µm)	700	730	950
Representative images			

Example

Printer: Cellink BIO X™ or Cellink INKREDIBLE™ printer

Temperature: 15 °C

Flow rate (speed): 10 mm/s

Nozzle: 22G TT tapered needle

Pressure: 50–60 kPa for Cartilage and Bone bioinks

Culture cells

After the printed construct has been incubated, add the appropriate cell culture medium and culture the bioprinted tissue with the appropriate cell culture medium following standard tissue culture procedures.

INVIVO-Gel Preparation

Introduction

The INVIVO GEL product is made from gelatin methacrylate (GelMA) created to mimic the extracellular environment. INVIVO GEL bioink series has two distinct advantages compared to other commercially available GELMA based bioink products. First, INVIVO GEL provides a degree of freedom to tune the elastic modulus (or stiffness) according to user's specific needs by changing the concentration of INVIVO GEL (GELMA) and Gel-linker, a photo-initiator. Also, by changing the UV light (365 nm) exposure time, the degree of cross-linking can be adjusted. The INVIVO GEL formulation mimics extracellular environment with a choice of growth factors (VEGF A, TGF-β1, BMP-2, or GF), allowing precise control of the extracellular environment in your research.

MilliporeSigma in partnership with ROKIT now offers newly and uniquely formulated GELMA based bioinks.

Name	Cat. No.
INVIVO GEL BMP-2 bioink	923745
INVIVO GEL essential bioink	923796
INVIVO GEL TGF-β bioink	923753
INVIVO GEL VEGF bioink	923737

Specifications

Storage: Store INVIVO GEL at 2–8 °C. The product ships on frozen gel packs.

Stability: Refer to the expiration date on the batch-specific Certificate of Analysis. The product is stable for a minimum of 1 year at receipt in powder form.

Materials

Materials supplied

- INVIVO-Gel (5 ml x 2 ea)
- mixing tube (1 ea)
- 0.22 µm filter (1 ea)
- photo-initiator agent (powder form)

Materials required, but not supplied

- Cultured cells ([visit our website for an up-to-date list of cell types](#))
- Appropriate cell culture medium
- PBS (Cat. No. [D8537](#))
- Sterile pipette tips for transferring bioink
- Sterile printing cartridge, piston, and nozzle/needle for 3D printing
- Extrusion-based 3D bioprinter
- Water bath or incubator
- Micropipettes

Before you start: Important tips for optimal results

Aseptic techniques. Employ aseptic practices to maintain the sterility of the product throughout the preparation and handling of the collagen and other solutions.

Handling. It is recommended that working solutions be chilled during the preparation of the collagen.

Procedure – Photoinitiator Solution Preparation (in a dark room).

1. Add 500 μ l of room temperature sterile distilled water to the photo-initiator vial.
2. Close the vial cap and mix well to dissolve.
3. Sterilize the photoinitiator solution by filtering through the 0.22 μ m filter (included).
4. Aliquot the photoinitiator solution into covered or opaque tubes and store at -20 °C or -80 °C until use.
5. Use 35 μ l of photo-initiator solution per 1 ml of INVIVO-Gel. For 5 ml INVIVO-Gel, 175 μ l of photoinitiator is required.

Warming INVIVO-Gel

6. Warm the INVIVO GEL in a 37 °C water bath for about 10 min until it turns into a clear yellowish color liquid

Combining INVIVO-Gel with the Photoinitiator Agent (in a dark room)

7. After warming INVIVO-GEL, spray 70% ethanol to the INVIVO-Gel syringe and wipe before proceeding.
8. Remove the cap from the INVIVO-Gel syringe and connect a mixing tube.
9. Take 175 μ l of the sterilized photoinitiator solution. While carefully pulling the piston of the INVIVO-Gel syringe down and removing air inside the mixing tube, add the photoinitiator solution into the tube by careful pipetting.
10. Connect an empty syringe to the other side of the mixing tube. Mix carefully by moving back and forth between the syringes.

Note: After adding photo initiator, pull the plunger until the photoinitiator-added INVIVO-Gel solution comes to the edge of the mixing tube so you can minimize air bubble formation during mixing.

Cell Preparation

11. Prepare a cell pellet and remove the supernatant as much as possible.
12. Recommended cell density is 1×10^6 cells/ml
13. Add 1 ml of the INVIVO-Gel solution.
14. Resuspend the cell pellet with INVIVO-Gel. (If possible, cut the tip of a sterile 1000 μ l micropipette tip while keeping sterility before cell resuspension to reduce stress on the cells.)
15. Mix together the 1 ml cell mixed INVIVO-GEL back to the 4ml INVIVO-Gel in the syringe (a mixing tube is recommended).
16. Incubate the final cell-laden INVIVO-Gel at 4 °C for 10 minutes before starting the printing process.
17. Install the INVIVO-GEL to the printer with the following setting and rest for 10 minutes before start of printing.

Printing

Recommended ROKIT Dr. 4D2 Bioprinter parameter setting.

Note: *Parameters with other printers may need to be optimized.*

- *Syringe holder:* 10 °C
- *Bed:* 8 °C
- *Average printing speed:* 3 mm/s
- *Max printing speed:* 5 mm/s
- *Nozzle size:* 0.2 mm
- *Height per layer:* 0.15 mm
- *Printing feature diameter:* 10-15 mm

Cell-bioink Mixing Protocol with TissueFab[®] Bioinks

Introduction

Bioinks are generally provided in an acellular form, but researchers may be interested in incorporating their specific viable cells of interest to create a cell-laden printed construct. This is usually carried out in one of two methods outlined below, depending on the material properties of the bioink. If the bioink can be liquified through temperature or other means, Protocol A will be suitable through pipetting the cell pellet with the bioink in its low viscosity state. If the bioink is highly viscous or preloaded into a sterile syringe cartridge, Protocol B is recommended using a cellmixer. The final cell density will depend on the application; however, $1-10 \times 10^6$ cells/mL bioink is recommended.

Disclaimer

TissueFab[®] bioinks are for research use only, not suitable for human, animal, or other use. Please consult the Safety Data Sheet for information regarding hazards and safe handling practices.

Specifications

Storage: Store TissueFab[®] bioinks at 2–8 °C. Protect from light by storing the bottle in a foil bag or wrapping in aluminum foil.

Stability: Refer to the expiration date on the batch-specific Certificate of Analysis.

Materials

Materials supplied

TissueFab[®] bioinks are supplied as follows:

- 1 × 10 mL bottle (1 unit)

Materials required but not supplied

- Cultured cells (visit our website for [an up-to-date list of cell types](#))
- Appropriate cell culture medium
- PBS (Cat. No. [D8537](#))
- Sterile pipette tips for transferring bioink
- Sterile printing cartridge, piston, and nozzle/needle for 3D printing
- Extrusion-based 3D bioprinter
- Water bath or incubator
- Cell mixing unit (for mixing large amounts of bioinks)
- Female/female Luer lock adaptors
- Micropipettes
- Light source

Protocol A: For Pipetting or Low Viscosity Bioinks

Prepare bioink

Warm the 10 mL bottle of TissueFab[®] bioink in a water bath or incubator set to 37 °C for 30 minutes or until the bioink becomes fluid and easy to pipette.

Prepare bioink-cell solution

1. Centrifuge the cell suspension to obtain a cell pellet. Remove the supernatant carefully so that the cell pellet is not disrupted.
2. Resuspend the cell pellet at the desired cell density with the bioink solution by gently and slowly pipetting up and down several times.
 - a. Ensure the cells are evenly distributed in the bioink solution by gently and slowly pipetting up and down several more times. Avoid creating air bubbles. DO NOT vortex or shake vigorously. Be careful not to dilute the bioink solution with the cell culture medium because it may interfere with the printability of the bioink.
3. Pipette the bioink-cell solution into the desired printing cartridge. This step creates a filled printing cartridge.
4. Place the remaining bioink in a foil bag or wrap in aluminum foil and store at 4 °C to protect from heat and light.

Protocol B: For Preloaded Syringe or High Viscosity Bioinks

Prepare bioink

Warm the 10 mL bottle of TissueFab® bioink in a water bath or incubator set to 37 °C for 30 minutes or until the bioink becomes fluid and easy to pipette.

To Prepare 1-2 ml using female/female Luer lock adaptors

1. Prepare the cell suspension – Resuspend 10 million cells per 100 µL cell culture medium.
 - a. Recommend 100ul of cells per 1 ml of bioink.
2. Use a 10:1 bioink:cell suspension, taking care not to introduce air bubbles to the mixture. Transfer bioink and cell suspension into separate female/female Luer lock adaptors. Attach the bioink syringe to the syringe with cell suspension.
3. Carefully mix the bioink with the cell suspension by gently pushing the bioink back and forth between the syringes. Transfer the cell containing bioink back to the cartridge and cap it.

Note: To avoid an air gap when mixing, pre-fill the Luer lock adaptor with a small amount of bioink of choice before attaching the syringe with the cell suspension.

To Prepare 3+ ml using a cell mixer

1. Prepare the cell suspension – Resuspend 10 million cells per 100 µL cell culture medium.
 - a. Recommend 100ul of cells per 1 ml of bioink.
2. Use a 10:1 bioink:cell suspension, taking care not to introduce air bubbles to the mixture. Transfer bioink and cell suspension into separate female/female Luer lock adaptors. Attach syringes to a cell mixing dispensing unit.
3. Connect the bioink and cell suspension syringes to a mixing unit, then connect the empty cartridge to the other side of the mixing unit.
4. Apply gentle pressure onto the dispensing unit to mix the content of both syringes into the empty cartridge.

General Guide to Photo, Ionic, and Enzymatic Crosslinking

Introduction

Bioinks are mainly composed of hydrogels or soft materials. In the process of 3D bioprinting, bioinks are constructed into 3D structures. To keep the integrity of the printed structure, crosslinking is utilized during or post printing. Crosslinking significantly increases the mechanical strength of the bioprinted constructs, preventing them from collapsing or dissolving due to environmental changes such as temperatures or the addition of media. It also affects the physicochemical properties of the bioprinted constructs and the cellular behavior of encapsulated cells.

Photocrosslinking is widely used in 3D bioprinting for its ease in preparation and operation. The choice of photoinitiator determines the wavelength of light needed to crosslink the bioink. During photocrosslinking, the light wavelength and exposure time can impact cell viability and other cellular behaviors.

Disclaimer

TissueFab® bioinks are for research use only, not suitable for human, animal, or other use. Please consult the Safety Data Sheet for information regarding hazards and safe handling practices.

Specifications

Storage: Store TissueFab® bioinks at 2–8 °C. Protect from light by storing the bottle in a foil bag or wrapping in aluminum foil.

Stability: Refer to the expiration date on the batch-specific Certificate of Analysis.

Materials

Materials supplied

TissueFab® bioinks are supplied as follows:

- 1 × 10 mL bottle (1 unit)

Materials required but not supplied

- Cultured cells (visit our website for an [up-to-date list of cell types](#))
- Appropriate cell culture medium
- PBS (Cat. No. [D8537](#))
- Sterile pipette tips for transferring bioink
- Sterile printing cartridge, piston, and nozzle/needle for 3D printing
- Extrusion-based 3D bioprinter
- Water bath or incubator
- Micropipettes
- Light source

Before you start: Important tips for optimal bioprinting results

Optimize printing conditions. Optimize printing conditions (e.g., nozzle diameter, printing speed, printing pressure, temperature, cell density) for the features of your 3D printer and for your application to ensure successful bioprinting. The suggestions below can guide you.

Reduce bubble formation. If the bioink has air bubbles, the bubbles may hamper bioprinting. Carefully handle the bioink when you mix and transfer to avoid bubble formation. Do not vortex or shake vigorously.

Aseptic techniques. Follow standard aseptic handling techniques when preparing and printing the bioink and during cell culture.

Cell density. Resuspend the cell pellet to the appropriate volume for the desired printed structure and cell density. Typical cell density for extrusion-based bioprinting is 1 to 5×10^6 cells/mL.

Note: The number of prints obtained from each 10 mL bottle of bioink (a unit) varies depending on the printed structure. For example, each 10 mL bottle contains enough material to print a 30 µL structure in each well of three 96-well plates or a 100 µL structure in each well of four 24-well plates.

Procedure

UV Light Crosslinking

1. Calibrate the irradiance of light if needed.
2. Place the UV light source directly above the 3D-bioprinted structure and expose the structure to the UV light.
3. Use the appropriate distance and exposure time based on your light source. For low-intensity light sources commonly available in desktop bioprinters, such as Cellink™ bioprinters (Bio X™ and INKREDIBLE™ printers), distances of 3 cm or less and exposure times of 60 s or more are recommended.

Note: Recommended settings for bioinks:

wavelength – 365 nm; irradiance – 10 mW/cm²; exposure – 90s

4. The 3D-bioprinted structure is ready for culture or analysis immediately after crosslinking.

TissueFab® Inks for UV Crosslinking

Cat. No.	Product Name	
905410	TissueFab® bioink	Alg(Gel) _{ma} -UV/365 nm
905429	TissueFab® bioink	(Gel) _{ma} -UV/365 nm
919632	TissueFab® bioink	(GelHA) _{ma} -UV/365 nm
920983	TissueFab® bioink	(GelAlg) _{ma} -UV/365 nm
920975	TissueFab® bioink	(GelAlgHA) _{ma} -UV/365 nm
915025	TissueFab® bioink Bone	UV/365 nm
915726	TissueFab® bioink Conductive	UV/365 nm

Visible light crosslinking

1. Calibrate the irradiance of light if needed.
2. Place the light source directly above the 3D-bioprinted structure and expose the structure to the specific wavelength of light.

Note: Use the appropriate distance and exposure time based on your light source. For 405 nm light sources commonly available in desktop bioprinters, such as Cellink™ bioprinters (Bio X™ and INKREDIBLE™ printers), distances of 3 cm or less and exposure times of 30–40 s or more are recommended.

Note: Recommended settings for inks:

wavelength – 405 nm; irradiance – 10 mW/cm²; exposure – 30s.

Wavelength – 525 nm or white light; power – 800 mW/cm²; distance – 8 cm; exposure – 60s

3. The 3D-bioprinted structure is ready for culture or analysis immediately after crosslinking.

405 nm TissueFab® Inks for UV Crosslinking

Cat. No.	Product Name	
919624	TissueFab® bioink	(GelHA) _{ma} -Vis/405 nm
918741	TissueFab® bioink	(Gel) _{ma} -Vis/405nm
921610	TissueFab® bioink	(GelAlg) _{ma} -Vis/405 nm
922862	TissueFab® bioink	(GelAlgHA) _{ma} -Vis/405 nm
915033	TissueFab® bioink Bone	Vis/405 nm
915963	TissueFab® bioink Conductive	Vis/405 nm

525 nm TissueFab® Inks for UV Crosslinking

Cat. No.	Product Name	
906913	TissueFab® bioink	Alg(Gel) _{ma} -Vis/525 nm

Ionic crosslinking

Ionic crosslinking is one of the most common crosslinking methods used in 3D bioprinting, and it is commonly used for alginate and its derivatives. Alginate is a water-soluble polysaccharide composed of linked units of β-D-galuronate (G) and α-D-mannuronate (M). In the presence of multivalent cations (such as Ca²⁺), carboxylic groups of adjacent alginate polymer chains are bonded in exchange of sodium ions to form crosslinked networks.

1. Gently pipette the crosslinking solution on the 3D-bioprinted construct. Ensure the entire structure is covered by the solution. The crosslinking time may vary depending on the structure size.

Note: Recommended settings for crosslinking solution: 200mM CaCl₂ (available as 919926 TissueFab® crosslinking solution; crosslinking time: 1 min).

2. Remove the crosslinking solution by washing twice with PBS.
3. Add cell culture media and incubate.
4. The 3D-bioprinted structure is ready for culture or analysis immediately after crosslinking.

Cat. No.	Product Name	
906913	TissueFab® bioink	Alg(Gel) _{ma} -Vis/525 nm
905410	TissueFab® bioink	Alg(Gel) _{ma} -UV/365 nm

Enzymatic crosslinking -Thrombin crosslinking

Enzymes such as microbial transglutaminase, tyrosinase, and thrombin are commonly used as catalysts for crosslinking in 3D bioprinting due to their biocompatibility. Thrombin plays a vital role in regulating the conversion of fibrinogen to fibrin monomer and further polymerizing to form insoluble fibrin clots. It is used as an enzymatic crosslinker in 3D bioprinting bioinks containing fibrinogen. Fibrinogen promotes cell adhesion, proliferation and migration, and therefore, has been widely utilized in tissue engineering for wound healing, neural regeneration, bone generation and vascularization, fibrinogen containing gels, and more.

1. Prepare 1 unit/uL thrombin stock solution by adding 100 uL DPBS to 100 units lyophilized thrombin. The stock solution is recommended to be stored at -80 °C.
2. Prepare 10units/ml thrombin solution in cell culture media by diluting 1 unit/uL thrombin stock solution 100 times with cell culture media (e.g., 10 uL thrombin stock solution + 990 uL cell culture media).
4. Gently pipette the diluted thrombin solution on the 3D-bioprinted construct. Ensure the entire structure is covered by solution.
5. Change the media after overnight incubation or until the next standard media change time.
6. The 3D-bioprinted structure is ready for culture or analysis immediately after crosslinking is complete.

References

- GhavamiNejad, A.; Ashammakhi, N.; Wu, X. Y.; Khademhosseini, A. *Small* **2020**, *16* (35), 2002931.
- (Khoon, L. S.; Galarraga, J. H.; Xaiolin, C.; Lindberg, G. C. J.; Burdick, J. A.; Woodfield, T. B. F. *Chem. Rev.* **2020**, *120* (19), 10662–10694.
- Xiaolin, C.; Li, J.; Hartanto, Y.; Durham, M. *Adv. Healthc. Mater.* **2020**, *9* (15), 1901648.
- Teixeira, L.S. M.; Feijen, J.; van Blitterswijk, C. A.; Dijkstra, P. J.; Katerien, K. *Biomaterials* **2012**, *33* (5), 1281–1290.

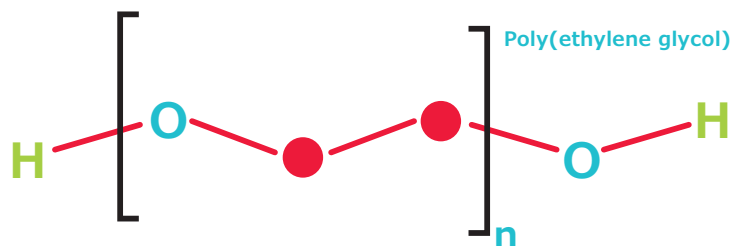
POLYMERS with possibilities

Functionalized Poly(ethylene glycol)s for Drug Delivery

Polymer of choice for optimal and reproducible results.

When it comes to drug delivery technologies and solutions, poly(ethylene glycol)s or PEGs are the polymer of choice for optimal and reproducible results. With excellent pharmacokinetic properties, they are ideal materials for bioconjugation, pegylation, crosslinking, and hydrogel formation.

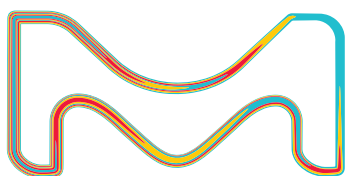
Let us help you transform your work into new therapeutic discoveries with our diverse PEG selection.



Features

- Well characterized, high-purity materials with a wide variety of functional groups
- High biocompatibility, with little to no immunogenicity
- M_n ranging from 1-40 kDa
- Reactivity
 - For amine, N-terminal amine, and thiol pegylation
 - For click chemistry and photochemistry
 - Heterobifunctional and multi-arm PEG crosslinkers
- Narrow polydispersity

For a complete list of available materials, visit: [SigmaAldrich.com/PEG](https://www.sigmaaldrich.com/PEG)



The life science business of Merck operates as MilliporeSigma in the U.S. and Canada.

Sigma-Aldrich[®]
Lab & Production Materials

Natural Polymers

Cellulose Precursors

Name	Structure	Molecular Weight	Extent Of Labeling	Cat. No.
2-Hydroxyethyl cellulose		Average $M_v \sim 90,000$	2.5 mol per 1 mol (M.S.)	434965-250G 434965-1KG
		Average $M_w \sim 380,000$	2.0 mol per 1 mol (M.S.) 1.0 mol per 1 mol (D.S.)	308633-25G 308633-500G
		Average $M_v \sim 720,000$	2.5 mol per 1 mol (M.S.)	434973-250G 434973-1KG
		Average $M_v \sim 1,300,000$	2.5 mol per 1 mol (M.S.)	434981-250G 434981-1KG
Hydroxyethylcellulose ethoxylate, quaternized		-	-	525944-50G
Hydroxypropyl cellulose		Average $M_n \sim 10,000$ Average $M_w \sim 80,000$	-	435007-5G 435007-100G 435007-250G
		Average $M_w \sim 100,000$	-	191884-5G 191884-100G 191884-250G
		Average $M_w \sim 370,000$	-	191892-5G 191892-100G 191892-250G
		Average $M_w \sim 1,000,000$	-	191906-5G 191906-100G 191906-250G
		(Hydroxypropyl)methyl cellulose		Average $M_n \sim 10,000$
Average $M_n \sim 86,000$	Methoxy 1.8–2.0 mol per 1 mol (D.S.) Propylene oxide 0.2 mol per 1 mol (M.S.) methoxy 29 wt. % propylene oxide 7 wt. %			423203-100G
Average $M_n \sim 90,000$	Methoxy 1.1–1.6 mol per 1 mol (D.S.) Propylene oxide 0.1–0.3 mol per 1 mol (M.S.) Methoxy 21 wt. % Propylene oxide 5 wt. %			423181-100G
Average $M_n \sim 120,000$	Methoxy 1.1–1.6 mol per 1 mol (D.S.) Propylene oxide 0.1–0.3 mol per 1 mol (M.S.) Methoxy 21 wt. % Propylene oxide 5 wt. %			423173-100G
Methyl 2-hydroxyethyl cellulose				-
		Sodium carboxymethyl cellulose		Average $M_w \sim 250,000$
Average $M_w \sim 250,000$	Carboxymethyl groups 0.9	419303-100G 419303-1KG		
Average $M_w \sim 250,000$	Carboxymethyl groups 1.2	419281-100G 419281-1KG		
Average $M_w \sim 700,000$	Carboxymethyl groups 0.9	419338-100G 419338-1KG		

Chitosans

Name	Molecular Weight	Description	Cat. No.
Chitosan	50–190 kDa	Low molecular weight	448869-50G 448869-250G
	190–375 kDa	-	417963-25G 417963-100G
	-	Medium molecular weight	448877-50G 448877-250G
	310–375 kDa	High molecular weight	419419-50G 419419-250G
	Average M_w 50 kDa	Biological source: Fungal fermentation High purity Non-animal derived	900341-2G
	Average M_w 100 kDa	High purity Non-animal derived	900342-2G
	Chitosan-mPEG 1k	Medium M_w	40–70% PEGylation
Chitosan oligosaccharide lactate	Average M_n 5,000	-	523682-1G 523682-10G
Trimethyl chitosan	Low molecular weight	Degree of quaternization >70%	912700-1G
	Medium molecular weight	Degree of quaternization: 40–60%	912123-1G
	High molecular weight	Degree of quaternization >70%	912034-1G

Lignins

Name	Molecular Weight	Solubility	Cat. No.
Lignin, alkali	Average M_w ~10,000	-	471003-100G 471003-500G
	-	Ethylene glycol soluble NaOH 0.05 % (warm 5% aqueous) Benzene insoluble Methanol partially soluble Dioxane soluble Hexane insoluble MEK partially soluble	370959-100G 370959-500G
Lignosulfonic acid calcium salt	Average M_n ~2,500 Average M_w ~18,000	H ₂ O soluble	471054-100G
Lignosulfonic acid sodium salt	Average M_n ~7,000 Average M_w ~52,000	H ₂ O soluble	471038-100G 471038-500G

Hyaluronic Acid

Name	M_w	Description	Cat. No.
Hyaluronic acid methacrylate	20,000–30,000	NMR: Conforms to structure degree of substitution 20–50%	914568-500MG
	50,000–70,000	NMR: Conforms to structure degree of substitution 20–50%	914304-500MG
	120,000–150,000	NMR: Conforms to structure degree of substitution: 20–50%	914800-500MG

Bioinks

TissueFab®

Name	Description	Composition	Low Endo	Bioburden	Cat. No.
TissueFab® bioink	Crosslinking solution, low endotoxin	CaCl ₂	Yes	Yes	919926-1EA
	(Gel)ma -UV/365 nm	GeIMA	-	Yes	905429-1EA
	(Gel)ma -Vis/405 nm, low endotoxin	GeIMA	Yes	Yes	918741-1EA
	Alg(Gel)ma -UV/365 nm	GeIMA, Alginate	-	Yes	905410-10ML
	Alg(Gel)ma -Vis/525 nm	GeIMA, Alginate	-	Yes	906913-1EA
	(GelAlg)ma -UV/365 nm	GeIMA, AlgMA	-	Yes	920983-1EA
	(GelAlg)ma -Vis/405 nm	GeIMA, AlgMA	-	Yes	921610-1EA
	(GelHA)ma -UV/365 nm	GeIMA, HAMA	-	Yes	919632-1EA
	(GelHA)ma -Vis/405 nm	GeIMA, HAMA	-	Yes	919624-1EA
	(GelAlgHA)ma -UV/365 nm	GeIMA, AlgMA, HAMA	-	Yes	920975-1EA
	(GelAlgHA)ma -Vis/405 nm	GeIMA, AlgMA, HAMA	-	Yes	922862-1EA
	Sacrificial	Pluronic	-	Yes	906905-1EA
	TissueFab® bioink Bone	UV/365 nm	GeIMA, Hydroxyapatite	-	Yes
Vis/405 nm		GeIMA, Hydroxyapatite	-	Yes	915033-1EA
Support gel		PCL, Hydroxyapatite	-	-	915637-5G
TissueFab® bioink Conductive	UV/365 nm	GeIMA, CNTs	-	Yes	915726-1EA
	Vis/405 nm	GeIMA, CNTs	-	Yes	915963-1EA

Gelatin Methacryloyl (GelMA)

Name	Gel Strength (g Bloom)	Degree Of Functionalization	Cat. No.
Gelatin methacryloyl	90-110	Degree of substitution: 60%	900628-1G
	170-195	Degree of substitution: 60%	900741-1G
	300	Degree of substitution: 40%	900629-1G 900629-5G
	300	Degree of substitution: 60%	900622-1G
	300	Degree of substitution: 80%	900496-1G

Modified Gelatins

Name	Gel Strength (g Bloom)	Degree Of Functionalization	Cat. No.
Allyl-modified gelatin	300	Degree of substitution: 70% by TNBS method	901553-1G
Azide functionalized gelatin	-	Degree of substitution: greater than 80% by TNBS method NMR: Conforms to structure Degree of substitution >80%	907723-1G
Gelatin-Rhodamine B	300	1-10 µmol Rhodamine B per g gelatin	923869-1G
mPEG functionalized gelatin	300	50% PEGylation	920444-1G
Thiol functionalized gelatin	-	NMR: Conforms to structure Thiol content 200-300 µmol/g	904643-1G

Low Endotoxins

Name	Description	Form	Impurities	Cat. No.
Low endotoxin alginate	Medium viscosity	Lyophilized powder	Bioburden <10 CFU/g Endotoxin <100 EU/g	919373-1EA
Low endotoxin alginate solution	Medium viscosity	Viscous liquid	Bioburden <5 CFU/g Total Aerobic Bioburden <5 CFU/g Fungal Endotoxin <10 EU/g	918652-1EA
Low endotoxin gelatin from bovine bone	-	Powder	Endotoxin ≤10 EU/g	920037-1G
Low endotoxin gelatin from porcine skin	-	Powder	Endotoxin <10 EU/g Total viable aerobic count <300 g total impurities <10 EU/g	901757-1G 901757-5G
	-	Powder	Endotoxin <10 EU/g Total viable aerobic count <300 g	901756-1G 901756-5G
	-	Powder	Endotoxin ≤10 EU/g	920010-1G
	-	Viscous liquid	Bioburden <5 cfu/mL Endotoxin <25 EU/mL	918644-1EA
Low endotoxin GelMA	Degree of substitution 80%	Powder, chunks, or fibers	Bioburden <10 CFU/g Endotoxin <125 EU/g	918628-1EA
	Degree of substitution 60%	Powder	Endotoxin ≤10 EU/g	920045-1G

Name	Description	Form	Impurities	Cat. No.
Low endotoxin GelMA solution	Degree of substitution 80%	Viscous liquid	Bioburden <5 cfu/mL Endotoxin <25 EU/mL	918636-1EA
Low endotoxin non-gelling gelatin from porcine skin	-	Powder	Endotoxin ≤10 EU/g	920029-1G

Alginate-Based Bioinks

Name	Form	Impurities	pH	Cat. No.
Alginate bioink	Viscous liquid	Endotoxin <25 EU/mL	6.5-7	901953-1EA
Alginate-RGD bioink	Viscous liquid	Endotoxin <25 EU/mL	6.5-7	901950-1EA
Cellulose-Alginate bioink	Viscous liquid	Endotoxin <25 EU/mL	6.5-7	901960-1EA
Cellulose-Alginate-Calcium Phosphate bioink	Viscous liquid	Endotoxin <25 EU/mL	6.5-7	901958-1EA
Cellulose-Alginate-RGD bioink	Viscous liquid	Endotoxin <25 EU/mL	6.5-7	901955-1EA

Decellularized Bioinks

Name	Description (µg/mg)	Form	Cat. No.
Decellularized ECM bioink precursor from porcine skin	GAG (bicolor) 0.4-0.8 Collagen (hydroxyproline) 90-125	Semisolid	906867-1EA
Decellularized ECM bioink precursor from porcine bone	GAG (bicolor) 1.5-5.0 Collagen (hydroxyproline) 60-120	Semisolid	906883-1EA
Decellularized ECM bioink precursor from porcine cartilage	GAG (bicolor) 2.0-6.0 Collagen (hydroxyproline) 60-120	Semisolid	906875-1EA

Collagen Bioinks

Name	Description	Kit Components	Endotoxin (EU/mL)	Cat. No.
Lifeink® 200	Neutralized type I collagen bioink	Sterile-filtered yes	≤10	916226-1EA
Lifeink® 240	Acidic type I collagen bioink	Sterile-filtered yes	≤10	915211-1EA
LifeSupport™	Support slurry for FRESH bioprinting	Irradiated yes	-	915467-1EA
PhotoCol™-IRG, methacrylated collagen bioink kit, with Irgacure	Methacrylated collagen: Degree of methacrylation ≥ 20%	Sterile-filtered yes Methacrylated collagen (100 mg) 20 mM acetic acid (50 mL) Neutralization solution (10 mL) Irgacure photoinitiator (100 mg)	≤10	917575-1EA
PhotoCol™-LAP	Methacrylated collagen: Degree of methacrylation ≥ 20%	Sterile-filtered yes Methacrylated collagen (100 mg) 20 mM acetic acid (50 mL) Neutralization solution (10 mL) LAP photoinitiator (100 mg) Methacrylated collagen bioink kit, with LAP	≤10	916293-1EA
PhotoCol™-RUT, methacrylated collagen bioink kit, with ruthenium	Methacrylated collagen: Degree of methacrylation ≥ 20%	Sterile-filtered yes Methacrylated collagen (100 mg) 20 mM acetic acid (50 mL) Neutralization solution (10 mL) Ruthenium (100 mg) Sodium persulfate photoinitiator (500 mg)	≤10	917834-1EA

HA Bioinks

Name	M _w (kDa)	Degree of Methacrylation	Kit Components	Cat. No.
PhotoHA™-IRG, methacrylated hyaluronic acid bioink kit, with Irgacure	100-150	≥ 45-65%	Methacrylated hyaluronic acid (100 mg) Irgacure photoinitiator (100 mg)	917079-1EA
PhotoHA™-LAP, methacrylated hyaluronic acid bioink kit, with LAP	100-150	≥45-65%	Methacrylated hyaluronic acid (100 mg) LAP photoinitiator (100 mg)	916471-1EA
PhotoHA™-RUT	100-150	≥ 45-65%	Methacrylated hyaluronic acid (100 mg) Ruthenium (100 mg) Sodium persulfate photoinitiator (500 mg) Methacrylated hyaluronic acid bioink kit, with ruthenium	917338-1EA

Ready-Made Bioinks

Name	pH	Viscosity	Form	Impurities (LB Broth)	Cat. No.
INVIVO-GEL BMP2 bioink	8-9	>30K cP	Opaque gel	ND CFU/mL	923745-1EA
INVIVO-GEL essential bioink	8-9	>30K cP	Opaque gel	ND CFU/mL	923796-1EA
INVIVO-GEL TGF-β bioink	8-9	>30K cP	Opaque gel	ND CFU/mL	923753-1EA
INVIVO-GEL VEGF bioink	8-9	>30K cP	Opaque gel	ND CFU/mL	923737-1EA

Biodegradable Polymers

Name	Structure	Molecular Weight	Cat. No.
Bio-based Polyether Polyol		M_w 400-600 Da	923990-500G 923990-1KG
		M_w 900-1100 Da	923974-1KG 923974-500G
		M_w 1900-2100 Da	923966-500G 923966-1KG
		2600-2800 Da	923982-500G 923982-1KG
Polycaprolactone		Average M_n ~10,000 by GPC Average M_w ~14,000	440752-5G 440752-250G 440752-500G
Polycaprolactone diacrylate		Average M_n 5,000	914495-1G
		Average M_n 10,000	914509-1G
Polycaprolactone dimethacrylate		Average M_n 3,000	802158-2G
		Average M_n 5,000	914762-1G
		Average M_n 10,000	915106-1G
Poly(lactic acid)		M_n ~30,000 M_w ~60,000	38534-1G 38534-5G
Poly(L-lactide), acrylate terminated		Average M_n 5,500	775983-1G
Poly(D,L-lactide-co-caprolactone)		-	457647-5G
Poly(L-lactide) dimethacrylate		Average M_n 10,000	916102-1G
		Average M_n 5,000	915009-1G
Resomer® R 202 H, Poly(D,L-lactide)		M_w 10,000-18,000	719978-1G 719978-5G
Resomer® RG 502 H, Poly(D,L-lactide-co-glycolide)		M_w 7,000-17,000	719897-1G 719897-5G

Poly(ethylene glycol) and Poly(ethylene oxide)

Name	Structure	Avg. M_n (Da)	Cat. No.
4-Arm-PEG20K-acrylate		Average M_n 20,000	JKA7034-1G
8-Arm-PEG10K-acrylate, tripentaerythritol core		Average M_n 10,000	JKA10021-1G

R = tripentaerythritol core structure



Merck KGaA
Frankfurter Strasse 250
64293 Darmstadt, Germany

SigmaAldrich.com

© 2022 Merck KGaA, Darmstadt, Germany and/or its affiliates. All Rights Reserved. Merck and the vibrant M are trademarks of Merck KGaA, Darmstadt, Germany or its affiliates. All other trademarks are the property of their respective owners. Detailed information on trademarks is available via publicly accessible resources.

MK_BR9101EN
37475
04/2022